CALIBRATION OF WIND TUNNEL FLOW QUALITY

By

Ayman Said Abu-Mostafa

Bachelor of Mechanical Engineering
Cairo University
Giza, Egypt
1976

Master of Science
Oklahoma State University
Stillwater, Oklahoma
1980

Submitted to the Faculty of the Graduate College
of the Oklahoma State University
in partial fulfillment of the requirements
for the Degree of
DOCTOR OF PHILOSOPHY
May, 1984

CALIBRATION OF WIND TUNNEL FLOW QUALITY

Thesis Approved:

Troy D. Reed
Thesis Adviser

Dean of the Graduate College

PREFACE

This study deals with the calibration of environmental effects in transonic wind tunnels which cause tunnel tests on models to give different results than those obtained in free flight. It was generously sponsored by the NASA Ames Research Center.

I wish to acknowledge the assistance I received from my adviser, Dr. Troy D. Reed. I am particularly indebted to Dr. Peter M. Moretti for selecting me to do this project.

I would also like to thank the members of my advisory committee, Drs. David G. Lilley, John A. Wiebelt and Donald W. Grace; Mrs. Neisa Locke and Carol Grondzik for typing services and Mr. Eldon Hardy for doing the figures.

I dedicate this thesis to my father, mother, brother and sister for their continuous love and support.

And, above all, I am thankful to Allah for surrounding me with these good people and for making it possible for me to receive this advanced degree.

TABLE OF CONTENTS

LIST OF TABLES

LIST OF FIGURES

NONMEMCLATURE

A^+	Effective sublayer thickness, Equation (43)
A, B, C	General correlation coefficients, Equation (23)
A_1, B_1, D_1	Correlation coefficients for flight data, Equation (25a)
A_2, B_2, D_2	Correlation coefficients for wind tunnel data, Equation (25b)
C	Constant of Equation (52)
C_f	Skin friction coefficient, $\tau_w/(\frac{1}{2}\rho_{eUe}{}^2)$
$\overline{C}_f$	$= (C_{f,fit} - C_{f,\ theoretical})/C_{f,\ theoretical}$
$\overline{C}_{f,rms}$	R.M.S. error in C_f
$C_{P,rms}$	R.M.S. fluctuating freestream pressure coefficient, $\sqrt{\overline{P'^2}}/q_\infty$
$C_{P_P,rms}$	R.M.S. fluctuating Preston-tube pressure coefficient, $\sqrt{\overline{P_P'^2}}/q_\infty$
D	Pipe internal diameter, or Van Driest damping coefficient, Equation (41)
d	Outer diameter of circular Preston tube
F	Function defined in Equation (27)
h	Preston-tube height
K_{eff}	Normalized, effective Preston-tube height, $2\ Y_{eff}/h$
L	Characteristic length of a pipe, or cone length
M	Mach number

P	Static pressure
P'	R.M.S. fluctuating freestream static pressure
P_P	Preston-tube pressure
P_P'	R.M.S. fluctuating Preston-tube pressure
q_∞	Freestream dynamic pressure, $\frac{1}{2}\rho_\infty U_\infty^2$
R	Gas constant, = 53.34 Btu/lbm ^oR for air
R_τ	$= U_\tau h/\nu_w$
Re_D	Reynolds number based on pipe internal diameter
Re_{ft}	Freestream unit Reynolds number, U_∞/ν_∞
$Re_{ft,eff}$	Effective freestream unit Reynolds number
Re_x	Length Reynolds number, $U_e X/\nu_e$
Re_θ	Momentum-thickness Reynolds number, $U_e\theta_e/\rho_e$
S	Compressibility factor, $(\rho_e/\rho')^{.5}$
T	Static temperature
T_o	Total temperature
T^*	Dimensionless group, Equation (24c)
TF	Turbulence factor, $Re_{ft,eff}/Re_{ft}$
U_e	Velocity at edge of boundary layer
U_P	Velocity at Y_{eff}
U^+	$= U/U_\tau$
U_τ	Shear velocity, $(\tau_w/\rho_w)^{0.5}$
X	Local surface distance from cone apex
X^*	Dimensionless parameter, $\log_{10}(\frac{U_P Y_{eff}}{\nu_w})^2$
X_1^*	Dimensionless parameter, Equation (6a)
X_2^*	Dimensionless parameter, Equation (15a)
Y	Distance normal to cone surface
Y^+	$= Y U_\tau/\nu_w$

Y_{eff}	Effective Preston-tube height
Y^*	Dimensionless parameter, $\log_{10} \left(\frac{\tau_w Y_{eff}^2}{\rho_w \nu_w^2}\right)$
Y_1^*	Dimensionless parameter, Equation (6b)
Y_2^*	Dimensionless parameter, Equation (15a)

Greek Letters:

α	Angle of attack
β	Angle of yaw
γ	Dhawan-Narasimha's intermittency function, Equation (19), or ratio of specific heats (= 1.4 for air)
δ	Boundary layer thickness
ΔP_P	Pressure increment used to correct experimental data
ΔR_{eff}	$= (Re_{ft,eff} - Re_{ft})/Re_{ft}$
ΔX	Location of virtual origin of turbulent boundary layer
ε	Turbulent eddy diffusivity
θ	Momentum thickness
κ	Von Karman's constant, = 0.41
λ	Dhawan-Narasimha's fit factor, Equation (21)
μ	Molecular viscosity
ν	Kinematic viscosity
ρ	Density
ξ	$= (X - X_B)/\lambda$
τ	Shear stress

Subscripts:

B	Beginning of boundary layer transition
E	End of boundary layer transition

e	At the edge of the boundary layer
eff	At the effective Preston-tube height
FD	Flight data
g	At the geometric center of the probe
i	At the edge of Couette-flow region
ℓ	Fully laminar flow, or end of Preston-tube pressure trace
P	Associated with the Preston-tube measurement
ref	At the reference point used for transition calculations
T	Position of maximum transitional Preston-tube pressure, or fully turbulent flow
t	Position of minimum Preston-tube pressure during laminar traverse
v	Measured from the virtual origin of turbulent boundary layer
WT	Wind-tunnel data
w	At the wall (cone surface)
o	Total property
∞	Freestream property

Superscripts:

'	At Summer and Short's reference temperature

CHAPTER I

DEFINITION OF THE PROBLEM

Since the transonic wind tunnel became operational at NASA Langley Research Center in the late 1940's, there has been a need for a procedure to calibrate the effects of wall-generated noise on the tunnel flow quality. As noted by Dougherty and Steinle (32), the primary indicators of flow quality in a wind tunnel are variations of: (1) Mach number, (2) flow angularity within the empty test section, and (3) the Reynolds number at which transition from laminar to turbulent flow occurs on models. Variations in Mach number and flow angularity can be calibrated with conventional Pitot-static probes and yaw meters, e.g. see Reed et al., (85). And in the case of low-speed wind tunnels, the Reynolds number at which the drag coefficient of a sphere equals 0.30 can be used to define a turbulence factor (TF), as described by Pope and Harper (76). An "effective" unit Reynolds number for a given low-speed tunnel can then be defined by

$$Re_{ft,eff} = (TF)\ Re_{ft}$$

However, when Mach number exceeds about 0.35, compressibility effects cause the classical turbulence factor to become increasingly erroneous and therefore not useful. Recently, Miller and Bailey (64) have reviewed the status of knowledge concerning the drag of a sphere at transonic speeds. Even today, the precise variation of sphere drag with Mach number and Reynolds number is not well defined. Thus, the

classical turbulence-sphere method is not applicable to the calibration of transonic wind tunnels.

In recognition of the non-applicability of a sphere for defining a turbulence factor for tests in transonic wind tunnels, NASA, as part of the C-5A wind tunnel correlation program (Treon et al., (94)) employed what is now known as the AEDC 10° Transition Cone as a means of defining an adjustment to Reynolds numbers on a tunnel-to-tunnel basis. The cone was initially developed in the mid-sixties by engineers at Arnold Engineering Development Center (AEDC). It had a traversing Pitot probe resting on its surface to directly detect boundary-layer transition.[1] The cone geometry has the advantage that no shock is generated along the surface at transonic speeds, and thereby avoids shock/boundary-layer interactions such as occur on airfoils, wings and blunt-nose bodies. A schematic of this cone and some of the associated instrumentation are shown in Figure 1. Since the cone was designed to calibrate the effects of tunnel noise on boundary-layer transition, it also has two miniature microphones imbedded in the surface at 18 and 26 inches aft of the nose for noise measurements. Additional description of this cone can be found in the papers by Dougherty and Steinle (32) and Dougherty and Fisher (30).

The need for such a calibration device was emphasized when discrepancies between numerous transonic wind-tunnel tests of models at ostensibly identical flow conditions were observed. A particularly well-documented study of differences in static aerodynamic data has been

---

[1]This, of course, is not a new measurement technique. In fact, the first Wright brothers' lecture by Jones (49) in 1937 describes the utility of this technique for flight tests.

NOTE: CS = Cone Station = Distance in inches aft of the nose

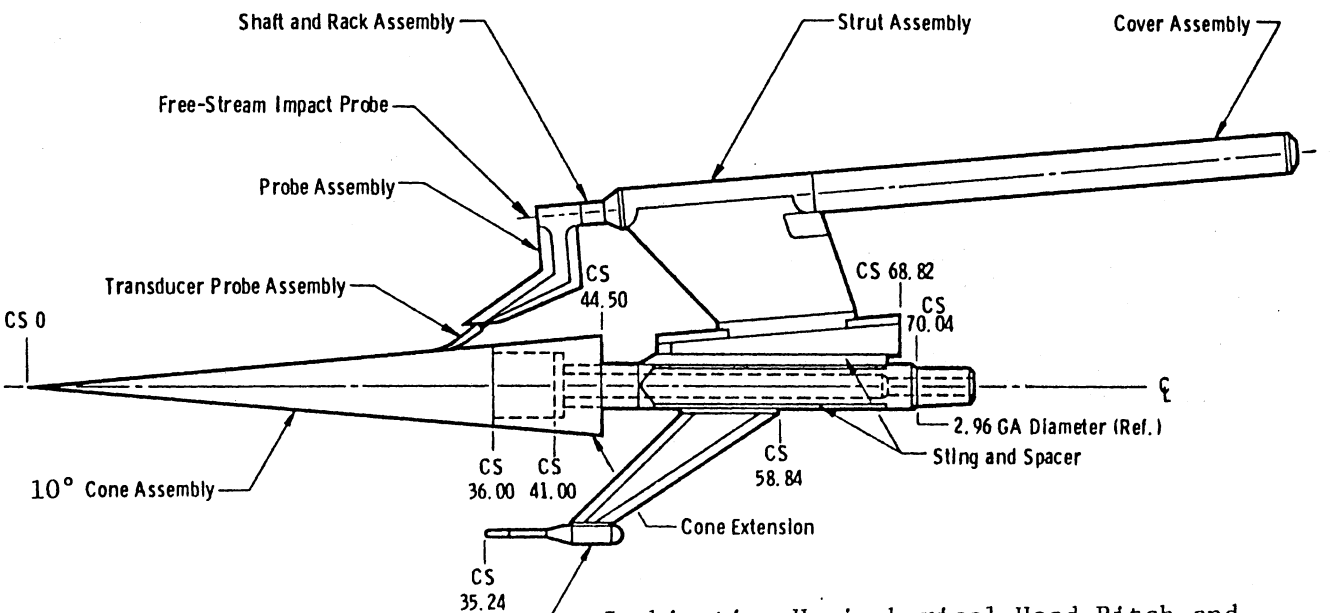

Figure 1. AEDC Boundary Layer Transition Cone

obtained with the same model of a Lockheed C-5A transport aircraft in the three major transonic wind tunnels. The results have been reported by Treon et al. (94). The differences between the three different sets of wind-tunnel data were reduced by accounting for "relative" Reynolds number effects between facilities. The AEDC Transition Cone was used to define the differences in "relative" Reynolds number.

As observed by Dougherty and Steinle (32), these results substantiated the need for developing a method for predicting these corrections to Reynolds number to improve extrapolation of wind-tunnel test results to full-scale conditions, i.e., a "turbulence factor for transonic tunnels."

Subsequent to the C-5A correlation program, the cone was tested in transonic wind tunnels both in the U.S. and in Europe. At the completion of the wind tunnel tour, the cone was tested in flight, Dougherty and Fisher (31). Parallel with the planning of the flight program, NASA focused on using the data from the cone in flight, in conjunction with the wind tunnel data, to develop a means for defining an adjustment (transonic turbulence fator) to Reynolds number on a tunnel-to-flight basis.

Such a Reynolds number will calibrate noise effects on the onset of transition, so that by increasing the flight Reynolds number to that value, transition will occur at the same location as in the tunnel. However, matching of transition onset is of little practical use since other useful parameters like Preston-tube pressure and skin friction measurements are not necessarily matched by that procedure.

The objective of this work, on the other hand, is to infer skin friction along the AEDC cone using the Preston-tube impact pressure

measurements in both wind-tunnel and flight tests and, in analogy with the turbulence sphere method, define a procedure whereby an "effective" freestream unit Reynolds number can be calculated for a given tunnel setting, but this number now represents the freestream unit Reynolds number at which the model tested in the tunnel will experience the same average, theoretical skin friction as in flight, or, equivalently, will give the same measured average values of Preston-tube pressure.

The importance of this work lies not only in the calibration of wind tunnel flow quality, but also in the general and systematic way of relating wind-tunnel flow conditions to actual flight. Thus, the prediction of flight level drag will be improved and the results obtained from wind tunnel tests can be directly applied towards the design and development of prototypes.

The basic approach used in this study to achieve the above-mentioned objective is as follows:

1. Preston-tube measurements are correlated with theoretical skin friction along the surface of the AEDC Cone in laminar, transitional and turbulent portions of the boundary-layer flow. This is done for the wind tunnel tests as well as the flight tests.
2. With the two sets of correlations (one set of three correlations for the wind tunnel tests, and a second set for the flight tests), the skin friction coefficient is equated as well as all other variables and parameters, <u>except</u> the freestream unit Reynolds number, Re_{ft}. The two sets of correlations are expected to have different empirical coefficients since noise and freestream turbulence effects, which are not modeled in the theoretical computations, are different. This means that substituting wind tunnel data, which includes C_f but <u>excludes</u> Re_{ft},

into the flight correlation results in a freestream unit Reynolds number that is different from the measured one in the tunnel. This derived Reynolds number is therefore the noise-free "effective" Reynolds number the tunnel should operate at to get the same average P_p measurements as in flight.

3. Since correlations for the laminar portion of the boundary layer are expected to be different from those in the transitional and turbulent portions, the resulting $Re_{ft,eff}$'s may be different in general for each portion. Analysis of these results should reveal the best measure of tunnel flow quality.

CHAPTER II

SURVEY OF RELATED LITERATURE

Since Preston-tube pressures are by definition total pressures near the wall, the classical law-of-the-wall can be used to relate these pressures to wall shear stress. The law-of-the-wall can be expressed in the following general form:

$$U^+ = F_1(Y^+). \tag{1}$$

Using the definitions of U^+ and Y^+, Equation (1) can be written as

$$\frac{U}{U_\tau} = F_1\left(\frac{U_\tau Y}{\nu_w}\right), \tag{2}$$

where U is the velocity parallel to the wall at the normal distance Y. Associated with the Preston-tube measurement of total pressure, P_p, is a velocity, U_p, at a height Y_{eff}. In other words, there exists a streamline entering the probe face, Y_{eff} units above the wall, at which the theoretical total pressure in the undisturbed boundary layer flow equals the total pressure measured by the probe, P_p, Figure 2. This "effective" probe center or height concept was introduced by Preston (78) in 1953. The corresponding theoretical velocity at this height is denoted by U_p.

Thus, at the effective height, Equation (2) is written as follows

$$\frac{U_p}{U_\tau} = F_1\left(\frac{U_\tau\ Y_{eff}}{\nu_w}\right) \tag{3}$$

Multiplying both sides by $U_\tau Y_{eff}/\nu_w$ gives

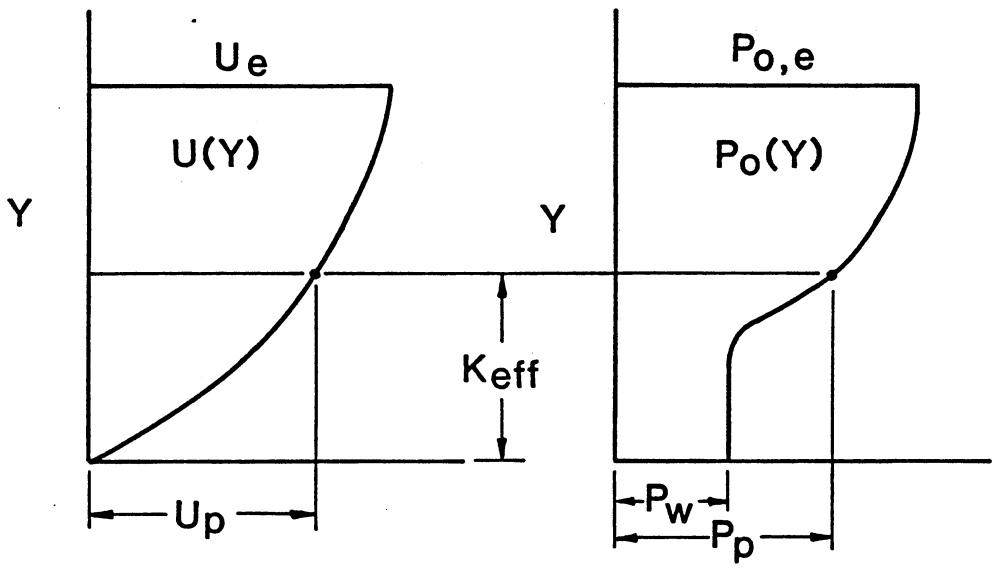

Figure 2. Definition of the Effective Probe Center

$$\frac{U_P Y_{eff}}{\nu_w} = \frac{U_\tau Y_{eff}}{\nu_w} F_1 \left(\frac{U_\tau Y_{eff}}{\nu_w}\right) = F_2 \left(\frac{U_\tau Y_{eff}}{\nu_w}\right),$$

or alternatively,

$$\frac{U_\tau Y_{eff}}{\nu_w} = F_3 \left(\frac{U_P Y_{eff}}{\nu_w}\right). \tag{4}$$

Equation (4) is the general form of the correlation between Preston-tube measurements and skin friction.

2.1 Incompressible-Flow Correlations

According to Preston (78), the British engineers Stephens and Haslam (92) suggested in 1938 that it should be possible to use the data from a Pitot tube traversed along a surface to infer skin friction. Apparently, this idea was not pursued until Preston's work during the early 1950's. He developed a correlation between turbulent skin friction and the total pressure as measured with circular Pitot tubes resting on the inside wall of a pipe. In order to develop his correlation, Preston used a simplified version of Equation (4) by making two assumptions:

1. The flow is incompressible and Bernoulli's equation is valid, thus U_P can be easily related to P_P as follows:

$$P_P = P_w + \frac{1}{2}\rho_w U_P^2.$$

2. The effective center of the circular tube is fixed and coincides with its geometric center, i.e. $Y_{eff} = d/2$.

These two assumptions lead to the following relation.

$$\frac{\tau_w d^2}{4\rho_w \nu_w^2} = F\left[\frac{(P_P - P_w)d^2}{4\rho_w \nu_w^2}\right] \tag{5}$$

Using Equation (5) as a guide, Preston obtained measurements inside a

pipe flow with circular Pitot tubes having four different external diameters but a nearly constant ratio of internal to external diameter of 0.6. Pipe Reynolds number was varied over the range $10^4 < Re_D < 10^5$. Skin friction was determined via measurements of pressure drop over a known length of constant diameter pipe, viz., $\tau_w = (P_1 - P_2)D/4L$. An empirical fit of the data led to the following correlation.

$$Y_1^* = -1.396 + 0.875\ X_1^* \tag{6}$$

Where the variables are defined as

$$X_1^* = \log_{10} \left[\frac{(P_P - P_w)\ d^2}{4\rho\ \nu^2}\right], \tag{6a}$$

$$Y_1^* = \log_{10} \left[\frac{\tau_w d^2}{4\rho\nu^2}\right]. \tag{6b}$$

In 1964, Patel (73) published the results of an extensive set of tests with fourteen circular Pitot probes and three different pipe diameters. He obtained a more accurate calibration for Preston tubes and established limits on the pressure gradient conditions within which his calibration can be used with prescribed accuracy. Patel obtained empirical equations for $Y_1^* = f(X_1^*)$ over three regions of Y_1^*. These regions correspond to the fully-turbulent, the buffer or transition zone, and the viscous-sublayer regions of the classical law-of-the-wall. The normal Reynolds number range of Preston-tube measurements in incompressible flow correspond to the buffer zone, and for this region Patel obtained

$$Y_1^* = 0.8287 - 0.1381X_1^* + 0.1437(X_1^*)^2 - 0.0060(X_1^*)^3, \tag{7}$$

where $1.5 < Y_1^* < 3.5$ or $5.6 < U_\tau d/\nu_w < 55$. Patel reported this correlates his data to within $\pm$ 1.5% of τ_w.

In the viscous sublayer region, Patel found his data were correlated by

$$Y_1^* = 0.5\ X_1^* + 0.037, \tag{8}$$

when $Y_1^* < 1.5$ or $U_\tau\ d/\nu_w < 5.6$. In this near-wall region, the classical law-of-the-wall exhibits the linear relation

$$U^+ = Y^+. \tag{9}$$

In order to relate (8) and (9), Patel introduced K_{eff} as the normalized effective center of a round Pitot tube defined by

$$K_{eff} = 2\ Y_{eff}/d. \tag{10}$$

Substituting into (9) and using the definitions of X_1^* and Y_1^* result in the following equation.

$$Y_1^* = 0.5X_1^* - 0.5\ \log_{10}\ (0.5\ K_{eff}{}^2) \tag{11}$$

When this equation is equated with Equation (8) and solved for K_{eff}, the result is $K_{eff} = 1.3$.

The traversing Pitot probes, used during wind-tunnel tests with the AEDC transition Cone, are of the flattened or oval-shaped type. Since Patel's correlations are for circular Preston tubes, they cannot be applied directly to the AEDC Cone tests. In addition, these tests were conducted at transonic speeds, and compressibility effects are expected. With regard to the flattened Preston tubes, Quarmby and Das (80) conducted an experimental study and calibration of six oval-shaped Preston tubes. When $X_1^* > 4.6$, they found these probes gave exactly the same calibration relation between Y_1^* and X_1^* as was obtained by Patel (Equation 7) if the external height of the probe face is used in place of d. At Lower values of X_1^*, the negative displacement of effective center caused by wall promimity was larger (≈5%) for the flattened

probes with aspect ratios between 1.5 and 1.9[1]. The following calibration equation correlated the measurements of Quarmby and Das within 1.5% of τ_w.

$$Y_1^* = 0.5152 + 0.1693X_1^* + 0.0651(X_1^*)^2,$$
$$3.38 < X_1^* < 6. \qquad (12)$$

The two correlations, Equations (11) and (12) make the assumption that the effective center of the probe is fixed. Preston showed that it is a function of $U_\tau d/\nu_w$ but did not attempt to define this function.

McMillan (62) pursued this point and found for circular tubes that the displacement of the effective center is 0.15d (K_{eff} = 1.3) when the probe is more than two diameters away from the wall, and is affected by shear flow alone. As the probe gets closer to the wall, K_{eff} decreases. McMillan confirmed, therefore, that K_{eff} is a function of $U_\tau h/\nu_w$. One can understand this wall proximity effect by considering that a greater portion of the flow, blocked by the probe, will have to lift upward and move over and around the probe face as less passes underneath between the probe and the wall. McMillan proposed a single curve, independent of Reynolds number, to correct for wall proximity effects on the measured velocity.

The work done by Patel (73), McMillan (62) and Quarmby and Das (80) leads to the conclusion that, in general, K_{eff} is a function of $U_\tau h/\nu_w$, Y_g/h and w/h (aspect ratio). Since the Pitot tube used in the tests for this study was resting on the wall, Y_g/h = 0.5, and for a given probe

---

[1]This is consistent with the idea that flow about the face becomes more two-dimensional as aspect ratio increases and more of the flow passes up and over the face rather than around the sides.

w/h is constant. Therefore, the relation

$$K_{eff} = Fn. \left(\frac{U_\tau h}{\nu_w}\right) \tag{13}$$

seems to describe the actual variation in K_{eff} for incompressible-flow conditions. If this relation is incorporated in Equation (4), it can be shown that K_{eff} can be eliminated while Equation (4) remains in the same form. This explains why the assumption of fixed effective probe height has worked well for incompressible-flow correlations.

For compressible-flow correlations, however, Equation (13) is expected to be different. It will perhaps have the form

$$K_{eff} = Fn. \left(\frac{U_\tau h}{\nu_w}, M_\infty\right). \tag{14}$$

In this case, any attempt to neglect the variation of K_{eff} must show up in a greater scatter of data about the developed correlation.

2.2 Compressible-Flow Correlations

Allen (4,5) has performed a comprehensive analysis of Preston tubes in supersonic boundary layers. He developed a correlation using three independent sets of simultaneous measurements of Preston-tube pressures and skin friction via floating-element force balance. These data were obtained within flat-plate, turbulent boundary layers and with freestream Mach numbers in the range: $1.6 < M_\infty < 4.6$. Allen selected the same basic parameters as Patel; except, he chose to evaluate the fluid properties at a reference temperature developed by Sommer and

Short (89), and the velocity U_P was calculated from P_P and the wall pressure P_w ($=P_e$) using standard compressible flow relations[2].

$$X_2^* = \log_{10} \left(\frac{U_P d}{\nu'}\right)$$

$$Y_2^* = \log_{10} \left(\sqrt{2}\,\frac{U_\tau d}{\nu'}\right) \tag{15a}$$

The primes denote properties evaluated at the Sommer and Short reference temperature, viz.,

$$\frac{T'}{T_e} = 0.55 + 0.035\, M_e^2 + 0.45\, \frac{T_w}{T_e}. \tag{16}$$

The correlation derived by Allen is

$$Y_2^* = -0.4723 + 0.74814\, X_2^* + 0.01239\, (X_2^*)^2. \tag{17}$$

Allen found that the majority of the skin-friction-coefficient data were within +15% to -12% of Equation (17). This rather large scatter, compared to the incompressible pipe-flow calibrations of Patel and Quarmby and Das, is at least partly associated with the much greater sensitivity and vulnerability of floating-element balances to extraneous errors.[3]

Obviously, the parameters used by Allen are logical candidates in any attempt to correlate the transonic cone data. However, the basic purpose of a reference temperature is to permit use of skin-friction formulas for incompressible flow to estimate compressible skin friction by evaluating fluid properties at the reference temperature. Thus, the

---

[2]The details can be found in a report by Allen (8).

[3]Allen (7) discussed the various error sources in floating-element balances. He has recently suggested an improved design for this type of instrumentation, Allen (9).

resulting reference properties represent "average" values across a boundary layer. Whereas, small Preston tubes encounter only the flow near the wall. Therefore, the author decided that properties based simply on the wall temperature were more appropriate.

2.3 Laminar Preston-Tube Correlations

A survey of the literature uncovered only one paper, published by Prozorov (79) which addresses the problem of using Preston-tube measurements to deduce skin friction in a laminar boundary layer. He obtained surface Pitot-probe measurements within low-speed, flat-plate, laminar boundary layers. He used several circular and rectangular probes with different aspect ratios. Though his data exhibited considerable scatter, he concluded that K_{eff} is a function of Upd/ν_w for both laminar and turbulent portions of the boundary layer irrespective of the aspect ratio, which is inconsistent with the results of McMillan (62) and Quarmby and Das (80). He also found $\tau_w d^2/\rho_w \nu_w^2$ (the square of $U_\tau d/\nu_w$) to be a different function of Upd/ν_w compared to what Preston (78) found.

His deduction of the laminar correlation is based on a McLaurin series expansion of U_p near the wall (since the probe height was small relative to the boundary layer thickness) and the conservation equations of mass and momentum for steady, two-dimensional, incompressible flow. The result is the following equation.

$$\tau_w = \frac{\mu_w U_p}{Y_{eff}} - \frac{1}{2}\frac{dP_e}{dX} Y_{eff} \qquad (18)$$

Prozorov's correlation takes into account the pressure gradient. The theoretical calculations of inviscid static-pressure distribution by Wu

and Lock (104) for the wind tunnel cases, and the measurements of surface pressures in the flight tests show that the pressure gradient in this study is negligible. Prozorov claims that his correlation is valid in laminar, transitional and turbulent flows provided that the probe is always within the viscous sublayer; a condition which was found to be invalid in this study.

It can be shown that Prozorov's correlation is equivalent to the calibration model used in this study when $dP_e/dX = 0$ and K_{eff} is small.

2.4 Boundary-Layer Transition Computation

Dhawan and Narasimha (29) developed a method of calculating the properties of a boundary layer undergoing transition by preserving the essential intermittency of the flow. Narasimha (68) modified Emmons's (33) original function to obtain an intermittency function described by

$$\gamma(X) = 1 - e^{-A\xi^2(X)}, \quad A = 0.41, \tag{19}$$

$$\xi(X) = \frac{X - X_B}{\lambda}. \tag{20}$$

Here X_B is the transition point defined as the location where the Pitot-tube measurements depart from the laminar ones and is defined by

$$\lambda \equiv X_{\gamma = .75} - X_{\gamma = .25} \tag{21}$$

By comparison with numerous other data, including supersonic data, Equation (19) was shown to be a good approximation to a universal intermittency function for boundary layer transition, and its use is as will be described in detail in Chapter IV. Figure 3 illustrates a typical distribution and how it changes with λ.

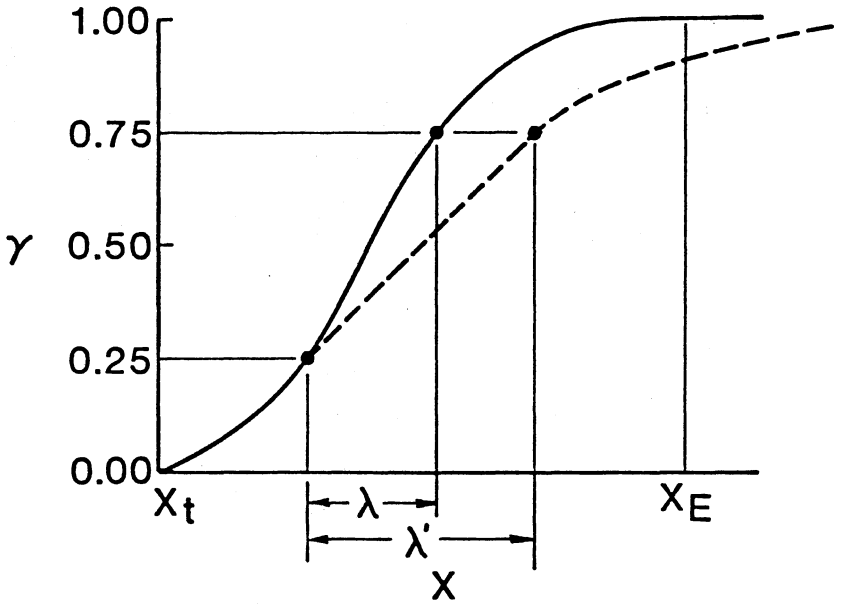

Figure 3. Distribution of γ-Intermittency Function

2.5 Calibration of Wind-Tunnel Flow Quality

With the establishment of the fact that freestream disturbances can significantly affect transonic wind-tunnel data, an extensive test program was begun at the NASA Ames research center in 1971. The AEDC Cone was tested in twenty-three tunnels between 1971 and 1977. Finally in 1978, it was flight-tested on the nose of a McDonnel-Douglas F-15 aircraft. A summary of the resulting noise and transition data has been reported by Dougherty and Fisher (31). In this concluding report, Dougherty and Fisher found, for the range of $C_{p,rms}$ observed, that the data for transition Reynolds number, based on the product of local unit transition Reynolds number, and distance from the nose to end of transition, X_T,[4] appear to correlate with $C_{p,rms}$ by the following equation.

$$Re_T \sim (C_{p,rms})^{-.25} \tag{22}$$

This relation, with the value of the proportionality constant suggested by Whitfield and Dougherty (100), is compared in Figure 4 with some transition data obtained with the AEDC Cone in seven different tunnels (Dougherty and Steinle (32) and Mabey (57)) and a flight test at $M_\infty = 0.80$.

The Dougherty-Fisher correlation indicates that the end-of-transition location, X_T, is decreased by either increasing the tunnel noise or <u>increasing</u> the freestream unit Reynold number. In other words, the effects of noise and Re_{ft} on X_T are equivalent. However, their effects on measurements of C_f or P_p are not equivalent. Becker and

---

[4]As will be shown in this study, the end-of-transition location is actually different from X_T, the location of maximum P_p in transition.

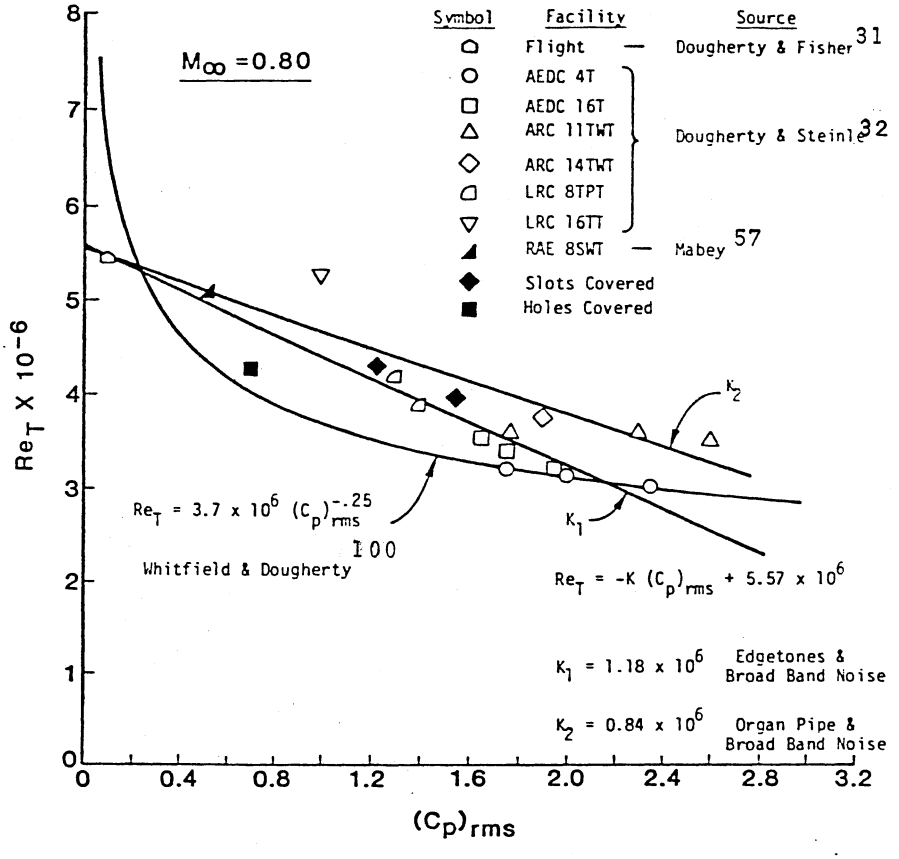

Figure 4. Effect of Noise on Boundary Layer Transition

Brown (12) have discussed the effects of turbulence on time averaged pressures measured with Pitot probes. Since turbulence causes fluctuations in the direction of the flow with respect to the probe's axis, the time-averaged pressure is reduced below the true total pressure.[5] Similarly, the author has found that tunnel noise, in the case of laminar boundary layers, also causes P_p fluctuations and reduces P_p measurements. This is equivalent to <u>decreasing</u> Re_{ft}. It is important to distinguish between the effects of noise on X_T (which is the purpose of Dougherty, Steinle and Fisher's work) and noise effects on theoretical C_f, or measured P_p (which is the purpose of this work.) The two effects are actually opposite, Figure 5.

---

[5]This effect decreases as a wall is approached, since turbulence is damped at an impermeable wall.

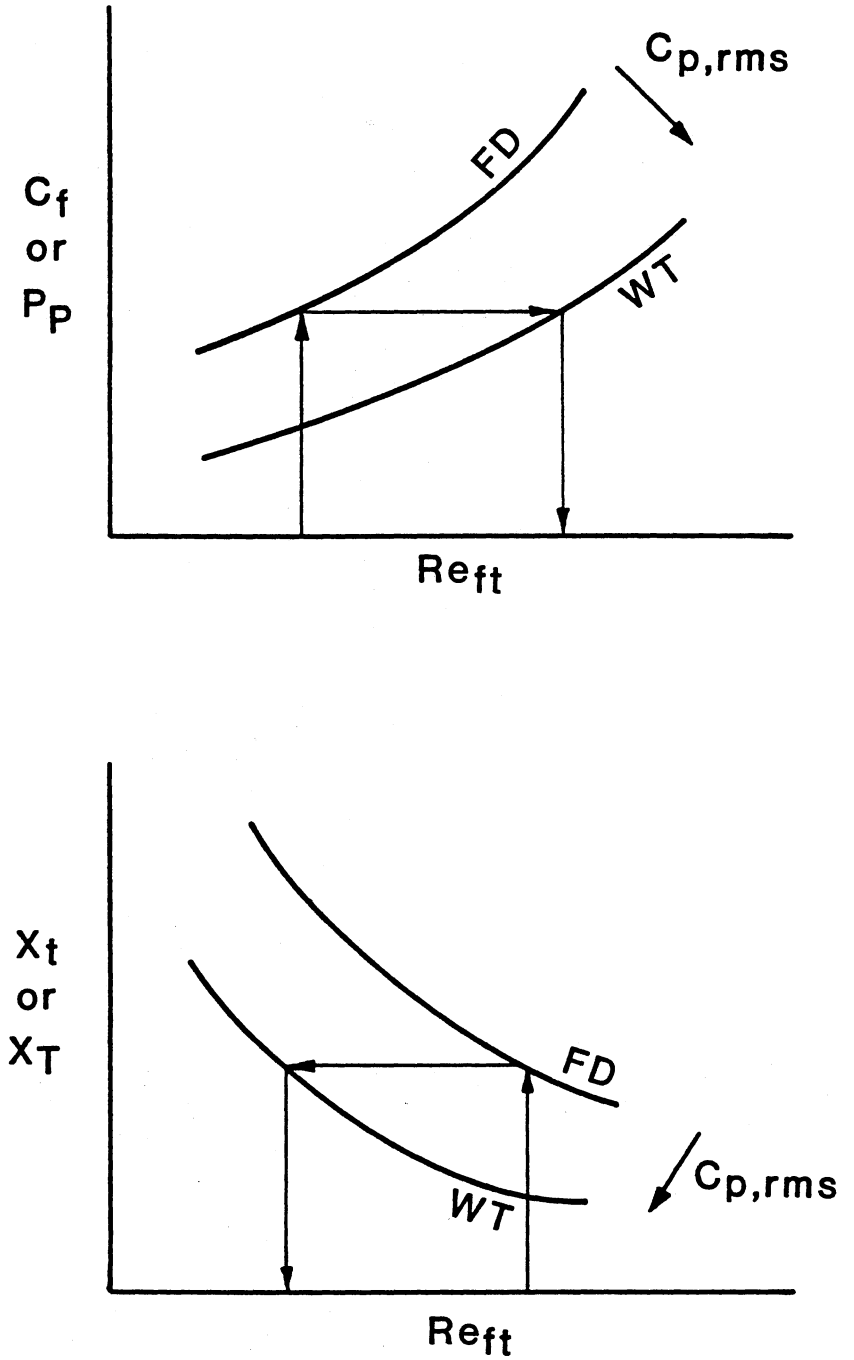

Figure 5. Effect of Tunnel Noise on Preston-Tube Measurements and Transition Onset

CHAPTER III

ANALYSIS PROCEDURE

3.1 Experimental Data

Although the AEDC Cone was tested in Twenty-three different tunnels, only the data from the NASA Ames 11-Ft Transonic Wind Tunnel (67), 11-TWT for brevity, was considered for analysis in this study. Table I lists nineteen subsonic wind-tunnel tests, and Table II lists nine subsonic flight tests which were selected for analysis in this study. The criteria for choosing a case for analysis are:

1. The Preston-tube survey covers all three portions of the boundary layer.
2. The flow angles α, β are very small.[1]
3. The freestream Mach number is less than unity.

The distribution of static pressure along the surface of the sharp cone was measured only in flight. For wind-tunnel analysis, this pressure distribution is assumed to be defined by the inviscid-flow theory of Wu and Lock (104). Wu and Lock's predictions for the pressure coefficient along the surface of a 10-degree cone are shown in Figure 6 as a function of freestream Mach number. Measurements of pressure

---

[1]This criterion is necessary since the boundary-layer code used in this study, STAN-5 (25), was found to be insensitive to changes in α, β. Also, values of $\alpha > 0.5^{o}$ and/or $\beta > 0.25^{o}$ have been shown to affect the beginning of transition, X_B. Notice that the values tabulated in Table II for α and β have an experimental uncertainty of $\sim \pm 0.25^{o}$.

TABLE I

WIND TUNNEL TEST CASES

Run Number	M_∞	$Re_{ft} \times 10^{-6}$	q_∞ (psf)	α^o	β^o
15.231	0.95	4.0	693	-0.05	0.02
19.289	0.8	4.0	617	-0.00	-0.02
21.318	0.7	4.0	548	-0.01	-0.03
23.346	0.6	4.0	477	-0.00	-0.03
29.440	0.3	4.0	230	-0.01	-0.03
40.547	0.6	5.0	586	0.02	0.02
41.548	0.7	5.0	680	0.02	0.02
42.549	0.8	5.0	761	0.01	0.02
43.550	0.9	5.0	842	0.01	0.02
44.551	0.95	5.0	873	0.01	0.02
56.631	0.9	3.0	492	0.06	0.01
57.632	0.8	3.0	453	0.07	0.01
58.633	0.7	3.0	408	0.07	0.02
59.634	0.6	3.0	357	0.08	0.01
60.635	0.5	3.0	302	0.07	0.01
61.636	0.4	3.0	246	0.07	0.01
70.726	0.7	4.0	538	0.04	0.02
72.748	0.8	4.0	605	0.03	0.02

coefficients together with linear curve fits from two typical flights are shown in Figures 7 and 8. With this information and the known freestream conditions, the flow conditions at the outer edge of the boundary layer can be calculated. (For details see Reference 1).

TABLE II

FLIGHT TEST CASES

Flight Number	M_∞	$Re_{ft} \times 10^{-6}$	q_∞ (psf)	α°	β°
327.0907	0.86	2.2	304	-0.03	0.30
327.0918	0.66	2.4	299	0.04	0.48
329.1028	0.85	2.1	289	-0.16	0.30
329.1036	0.74	2.2	277	0.19	0.25
329.1042	0.67	2.5	306	-0.05	0.47
332.1020	0.93	2.8	451	-0.44	-0.20
333.1020	0.94	2.8	457	-0.50	-0.16
333.1351	0.88	2.8	438	-0.04	0.30
349.1400	0.75	2.3	284	0.17	0.27

Note: α and β are time-averaged during a traverse.

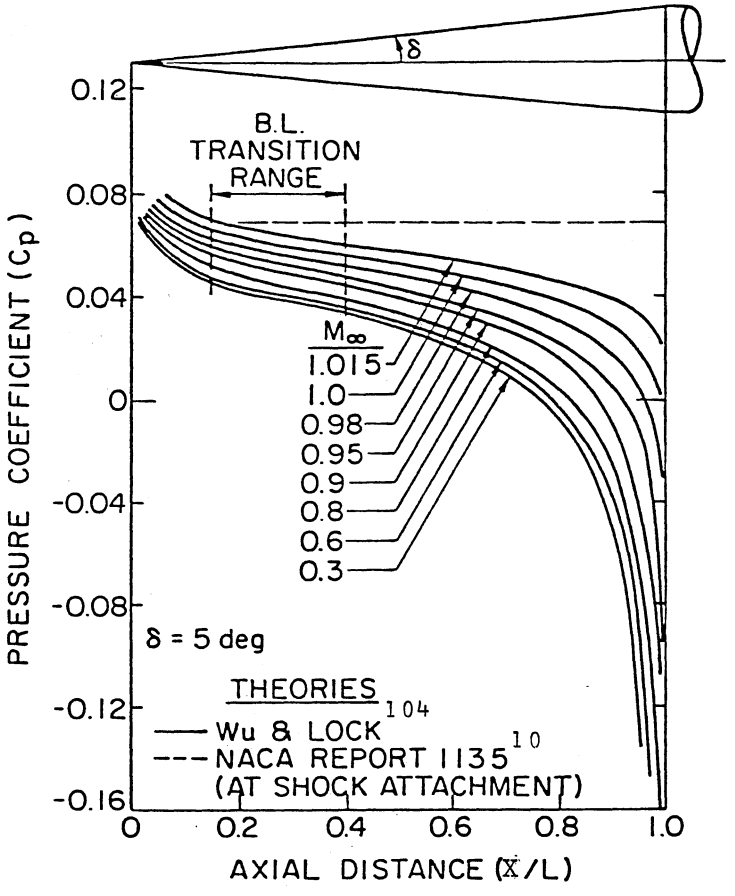

Figure 6. Inviscid Pressure Distribution on a 10° Cone (Wu & Lock)

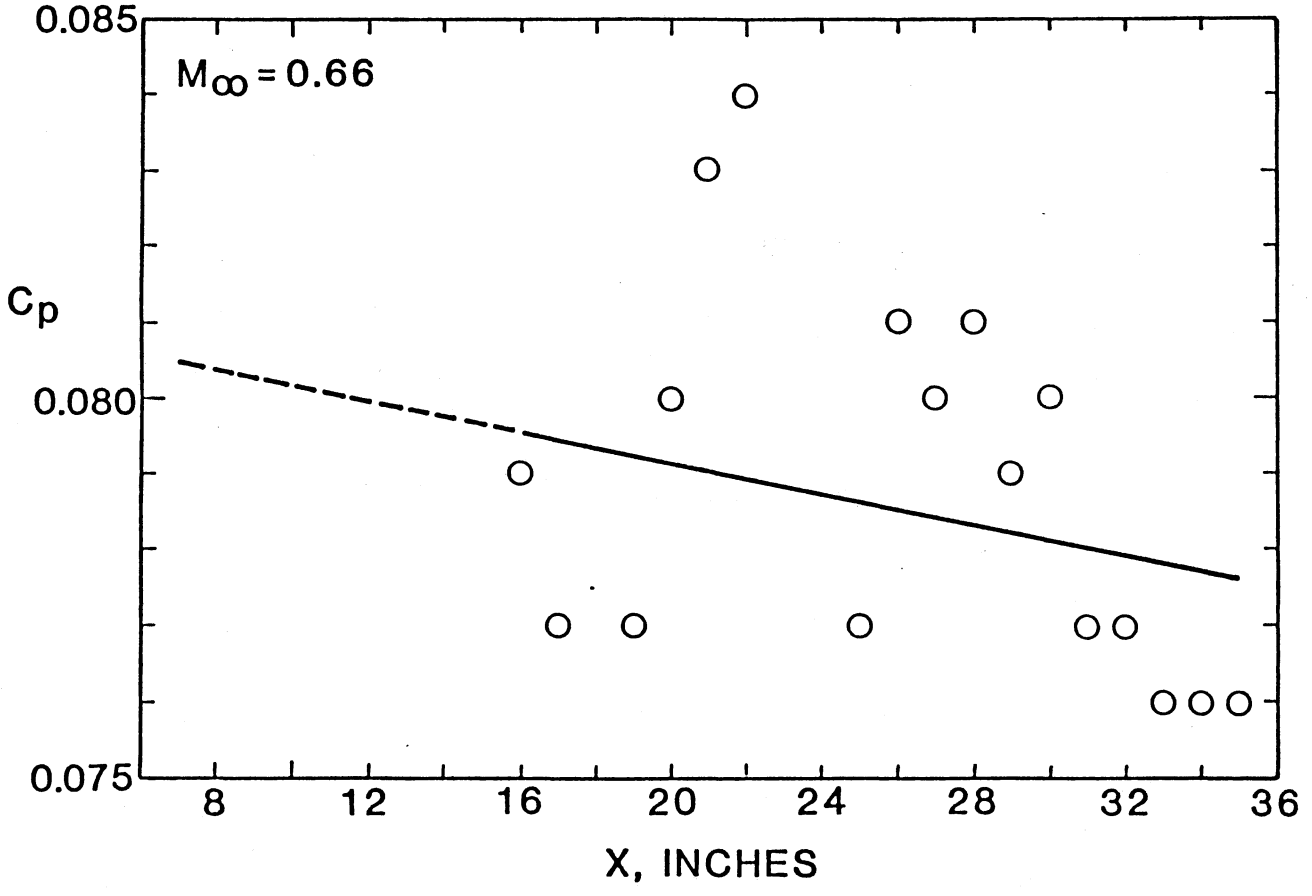

Figure 7. A Favorable Surface Pressure Distribution Measured During Flight

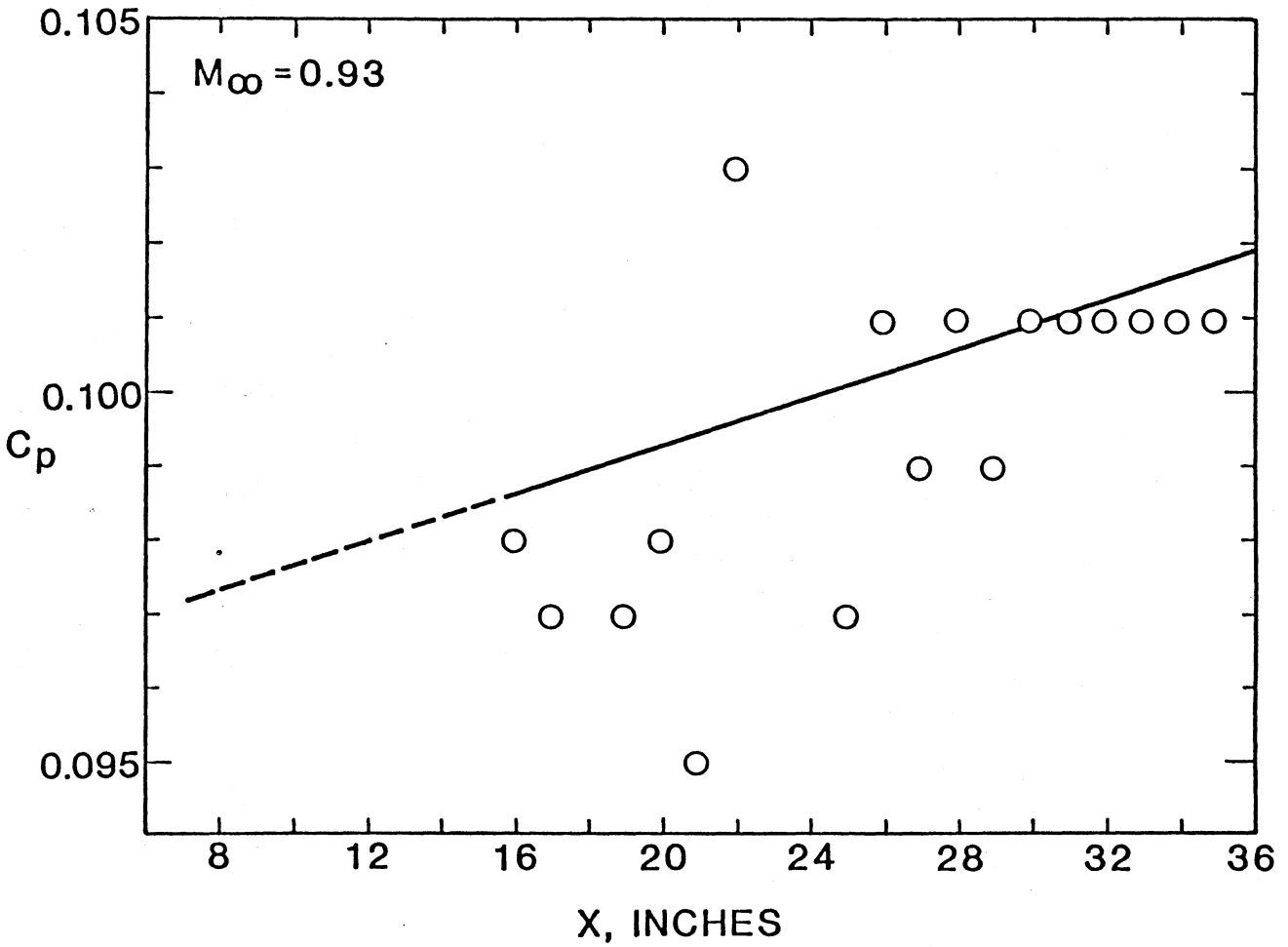

Figure 8. An Adverse Surface Pressure Distribution Measured During Flight

3.2 Correlation of the Data

The fully-laminar and fully-turbulent boundary layer computations are done using a computer program developed by Crawford and Kays (25) which they labeled STAN-5. The resulting distribution of skin friction and boundary layer properties are then correlated with the Preston-tube pressures.

The form of the correlation equation is derived from Equation (4) using the parameters of Patel (73) and Quarmby and Das (80) but allowing the effective center of the probe to vary, i.e.,

$$Y^* = A(X^*)^2 + BX^* + C \tag{23}$$

where

$$X^* = \log_{10} (U_P \, Y_{eff}/\nu_w)^2 \tag{24a}$$

and

$$Y^* = \log_{10} (U_\tau \, Y_{eff}/\nu_w)^2. \tag{24b}$$

In order to account for small variations of properties at Y_{eff} from those at the wall, a third dimensionless parameter, T^*, is introduced. It is defined as follows.

$$T^* \equiv \log_{10} \left(\frac{T'}{T_e}\right) \tag{24c}$$

It was observed that $T' \simeq T$ at Y_{eff} for all the cases. It was also noticed that the term containing T^* in the correlation equation was so much smaller than the other terms, the author decided to drop it. A T^*-term is necessary in the analysis of supersonic flow or flows with significant heat transfer. U_P and Y_{eff} are defined as the longitudinal velocity and the height at which the theoretical total pressure (calculated by STAN-5) is equal to the measured Preston-tube pressure at a given location on the cone surface. The coefficients A, B, and C are

determined by a least-squares curve fit of the data. The results are presented and discussed in the next chapter. Figure 9 outlines the steps followed in the data analysis to obtain Preston-tube correlations.

3.3 Effective Reynolds Number Derivation

Given the flight correlation in the form

$$Y^* = A_1(X^*)^2 + B_1 X^* + C_1, \tag{25a}$$

and the wind-tunnel correlation in the form

$$Y^* = A_2(X^*)^2 + B_2 X^* + C_2, \tag{25b}$$

it is desired to derive an expression for the freestream unit Reynolds number in the wind tunnel when all other properties and parameters are equated between the two Equations (25a) and (25b) and the skin-friction coefficient predicted by the flight correlation is used. In other words, substitute the wind tunnel data into the flight correlation, solve for C_f in flight, then use this value of C_f together with the same wind tunnel data, except Re_{ft} to solve for Re_{ft} which is therefore the effective wind-tunnel unit Reynolds number, $Re_{ft,eff}$, required to match the flight values of Preston-tube pressures.

The following identity relates the freestream conditions and can be derived using simple algebra, Abu-Mostafa (1).

$$\frac{0.5564 \times 10^{-6} M_\infty Re_{ft}}{q_\infty} T_\infty^2 - T_\infty - 198.6 = 0 \tag{26}$$

Thus, if only M_∞ and q_∞ are to be equated between wind-tunnel and flight correlations, then T_∞ must be allowed to change. This means that T_o also will change. Since it is desired to equate the values of the local Mach number, M_e, between the two correlations so that the static pressure may also be equated, T_e must therefore be allowed to change,

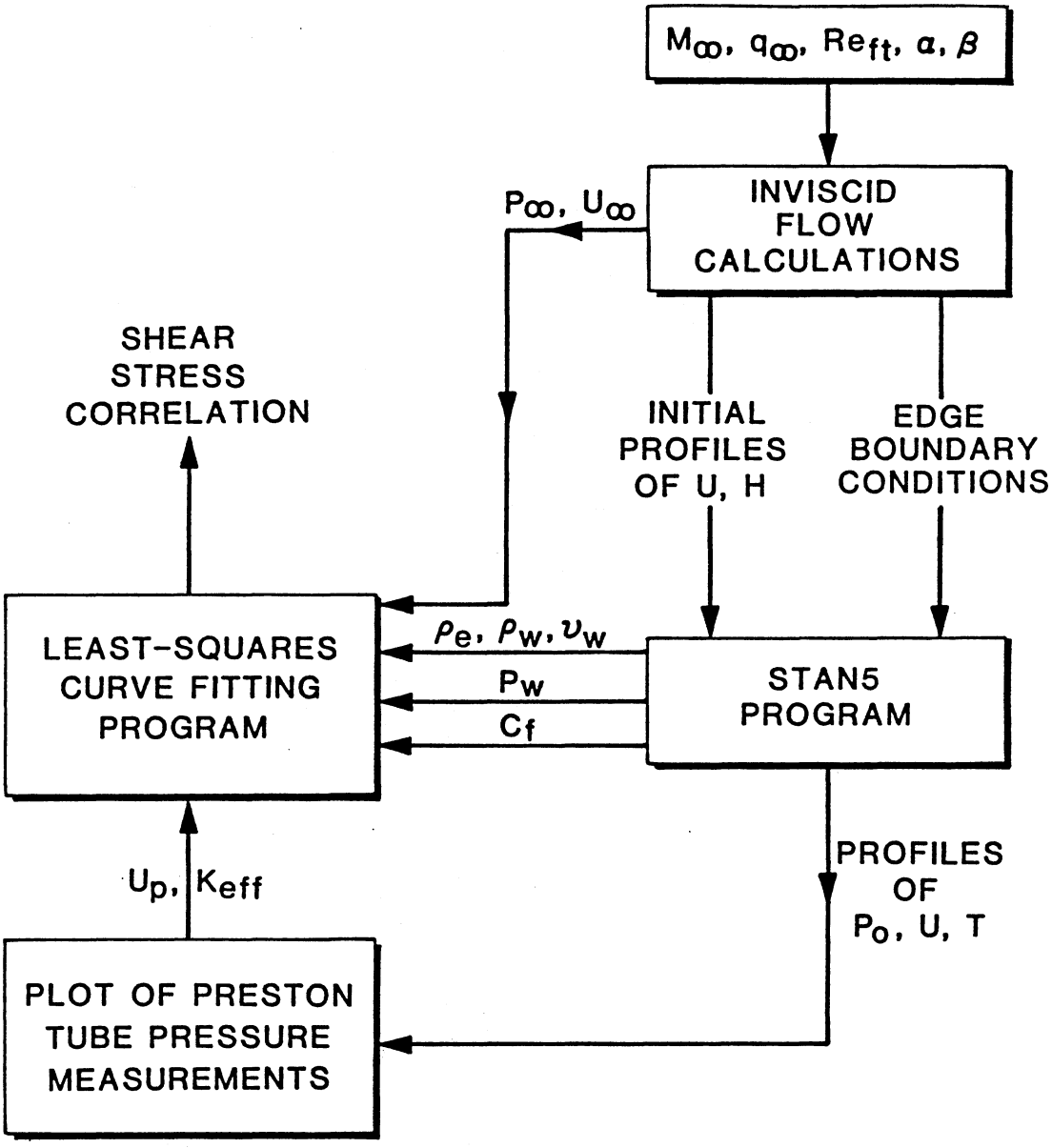

Figure 9. Flow Chart for the Analysis Procedure

and hence, U_e, ρ_e, T' and U_p. It can be shown that all variables other than T_∞, T_o, T_e, ρ_e, T', U_p and U_e can be kept unchanged without fixing Re_{ft}. Notice that T_o is assumed constant, $T_{o,2}$, along the cone for a given wind-tunnel case, but equals a different constant, $T_{o,1}$, for the flight case.

Now, by substituting the definition of X^* and Y^* into Equations (25a,b) and subtracting one from the other to eliminate C_f, the following equation is obtained.

$$A_2 \log_{10}^2 T'_2 + (4 A_2 + B_2) \log_{10} T'_2 - [4 F^2 (A_1 - A_2 + 2F (B_1 - B_2) + (D_1 - D_2 + A_1 \log_{10}^2 T'_1 + (4 FA_1 + B_1)\log_{10}T'_1] = 0,$$

where $$F = \log_{10}(M_P \sqrt{\gamma R}\ Y_{eff}/\nu_w). \qquad (27)$$

This is a quadratic equation that can be solved for $\log_{10}(T'_2)$, hence T'_2, the effective local reference temperature in the wind tunnel. $T_{e,2}$ follows from the definition of reference temperature by Sommer and Short (89):

$$\frac{T'_2}{T_{e,2}} = 0.55 + 0.035M_e^2 + 0.45 \frac{T_w}{T_{e,2}}. \qquad (28)$$

Then $T_{\infty,2}$ can be evaluated using the isentropic relation

$$\frac{T_{\infty,2}}{T_{e,2}} = \frac{1 + 0.2\ M_e^2}{1 + 0.2M_\infty^2}.$$

And finally $Re_{ft,2}$ ($=Re_{ft,eff}$) can be calculated using Equation (26).

This procedure is graphically outlined in Figure 10, and the results of its application are shown in the next chapter.

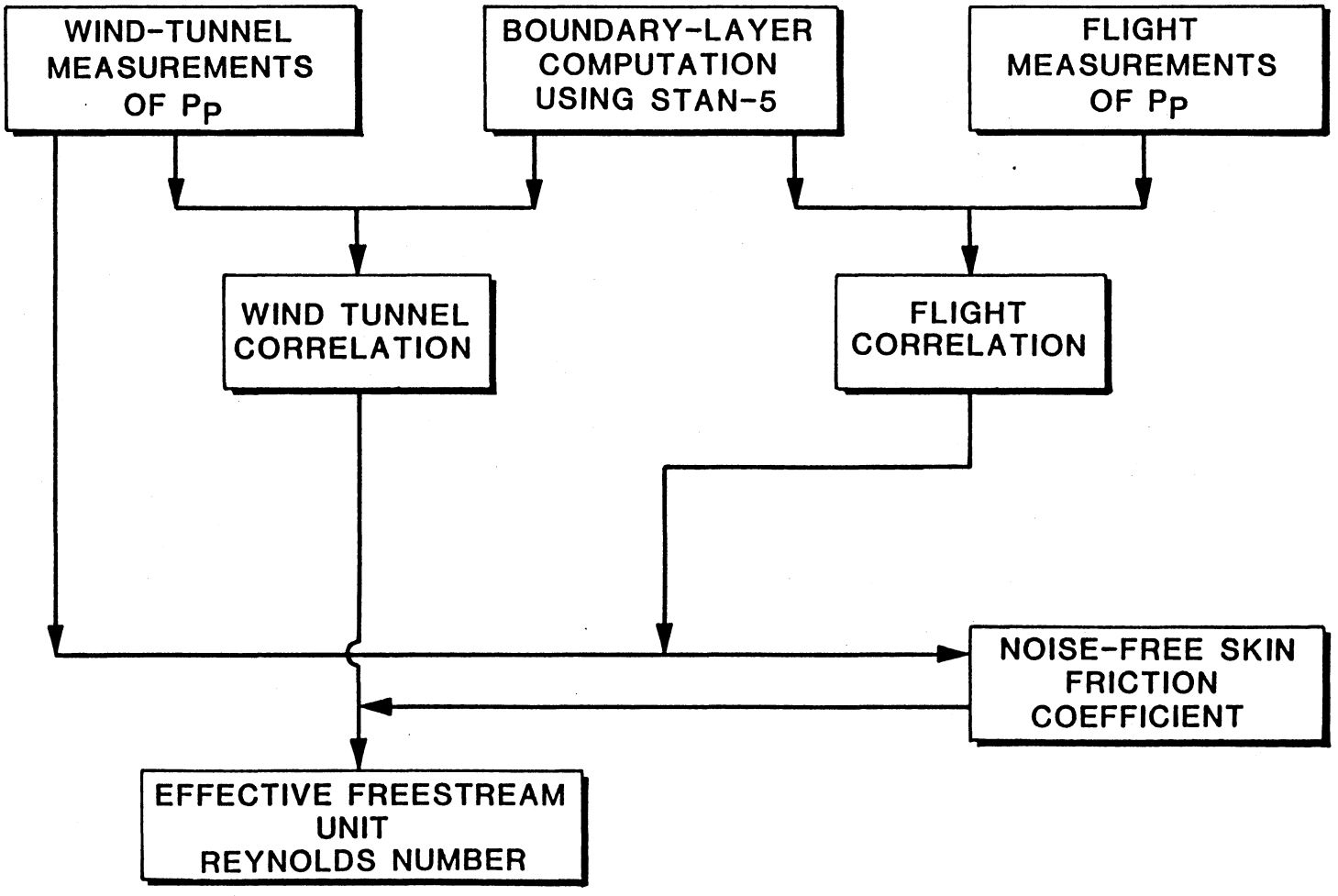

Figure 10. Flow Chart for Effective Reynold Number Calculation

CHAPTER IV

RESULTS AND DISCUSSION

4.1 Laminar Wind-Tunnel Correlation

In the process of developing the Preston-tube correlation, values of K_{eff} are needed. These values are obtained, as explained earlier, by linear interpolation of measured Preston-tube pressures in the theoretical total pressure profiles. It would be very useful if an empirical equation is developed in the form of Equation (14). In an earlier work by the author (82), the variation in K_{eff} was ignored, which led to a correlation that suffered a relatively large scatter of the data ($\overline{C}_{f,rms}$ = 4.93%).

For this purpose, the K_{eff} values for the laminar wind tunnel data were plotted versus R_τ ($=U_\tau h/\nu_w$) with M_∞ a parameter. The plot is shown in Figure 11. All attempts to curve-fit these data were unsuccessful. Since it is expected that the $K_{eff} - R_\tau$ curves be continuous, Figure 11 is an indication that probably the Re_{ft} = 3 x 10^6 group of data is in error. Re-examination of the data sheets (67) revealed that, for runs #56 through 72, the scaling factor of the plotter (Gain factor) which recorded the Preston-tube pressure signals was in error. Corrections were made upon NASA's directions (91) using run #21.318 (M_∞ = 0.70, Re_{ft} = 4 x 10^6) as a reference. The new $K_{eff} - R_\tau$ plot is shown in Figure 12. The correction procedure is outlined in section 4.1.1.

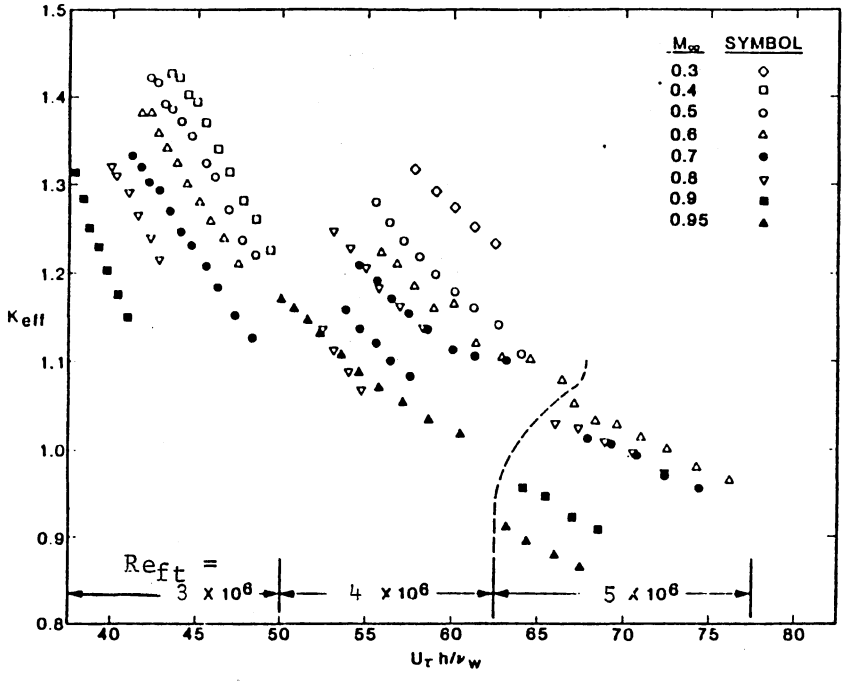

Figure 11. Distribution of Effective Probe Height as Determined from the Original Laminar Wind Tunnel Data

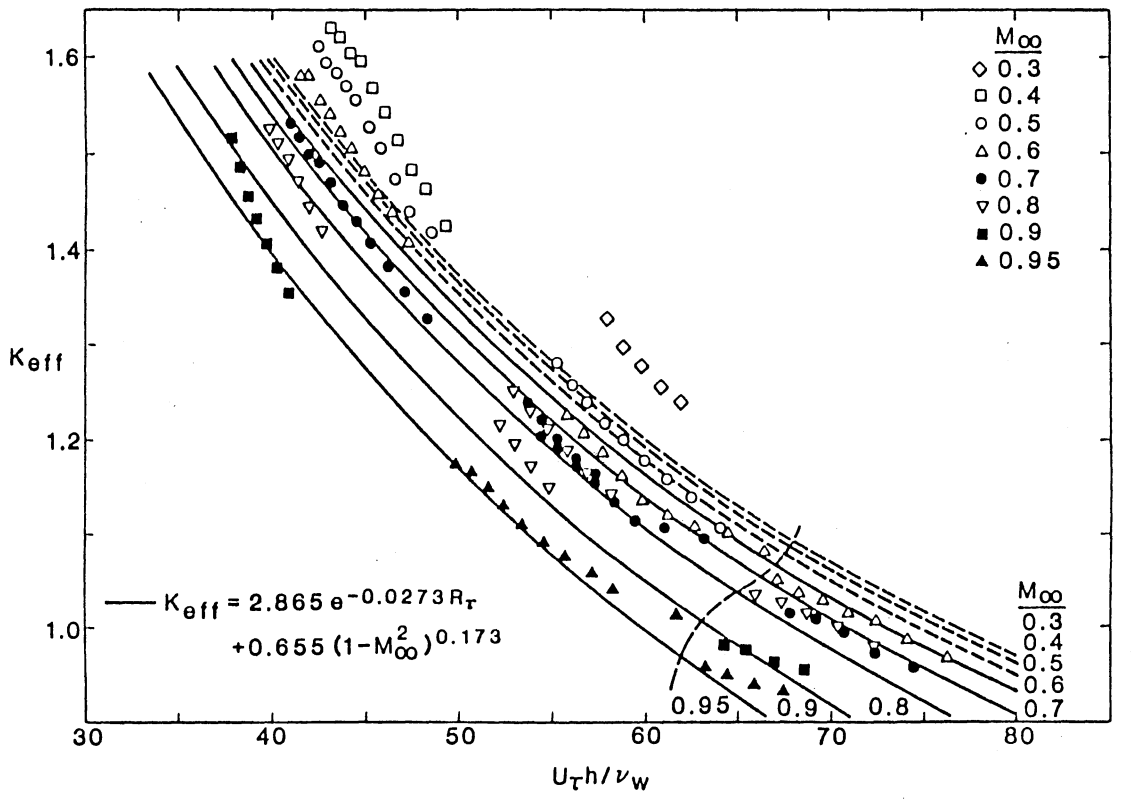

Figure 12. Distribution of Effective Probe Height as Determined from the Shifted Wind Tunnel Laminar Data

It is worth mentioning that this kind of plot (K_{eff} versus R_T) proved to be a powerful way of detecting possible errors in the data which could otherwise go unnoticed.

The data in Figure 12 could only be curve-fitted when the low-Mach-number data (M_∞= 0.30 - 0.50) were deleted. The fitted equation follows.

$$K_{eff} = 2.865\, e^{-0.273\, R_T} + 0.655\, (1 - M_\infty{}^2)^{0.173} \qquad (29)$$

This equation applies to laminar-boundary-layer flows in the 11-TWT for Mach numbers in the range $0.60 < M_\infty < 0.95$. The associated r.m.s. scatter in the predicted values of K_{eff} is 1.96%. Equation (29) will be called "the wind-tunnel asymptotic equation" for reasons that will become clear later.

In the development of the laminar wind-tunnel correlation, the author used the actual K_{eff} values rather than those predicted by Equation (29) for two reasons:

a. Equation (29) does not apply to the data for $M_\infty < 0.60$ which should be included in the analysis. It is always better to collect more data for curve fitting.

b. The r.m.s. error in K_{eff} is considered to be high.

Even though Equation (29) was not used in the development of the laminar wind-tunnel correlation, it proved to be very useful in the flight analysis as will be shown later.

Using the interpolated values of K_{eff} (and U_P), defining the dimensionless parameters X^*, Y^* and T^* as in Equations (24a,b,c) and doing a least-squares curve fit on the data results in the following correlation.

$$Y^* = -0.0136\ (X^*)^2 + 0.6977\ X^* + 0.1051\ T^* + 0.6669,$$

$$\overline{C}_{f,rms} = 0.97\%,$$

$$5.7 < X^* < 6.3, \quad -0.01 < T^* < -0.10, \tag{30a}$$

And, after dropping T^*,

$$Y^* = -0.0103\ (X^*)^2 + 0.6653\ X^* + 0.5946,$$

$$5.7 < X^* < 6.3, \qquad 0.30 \leq M_\infty \leq 0.95,$$

$$3 \times 10^6 \leq Re_{ft} \leq 5 \times 10^6. \tag{30b}$$

The associated r.m.s. scatter of C_f is only 0.98%. This very low scatter is comparable to the scatter obtained with pipe-flow correlations. It demonstrates how important it is to include the variation of K_{eff} in the analysis. Equation (30b) will be called "the wind-tunnel shifted correlation" due to the fact that a subset of the data was shifted as decribed above. A graph of Equation (30a) and the corresponding data scatter are shown in Figures 13 and 14.

It is here emphasized that the coefficients in Equation (30b) are valid only for the NASA Ames 11-TWT and the particular probe used during the tests. The coefficients are expected to be different for different wind-tunnel environments and for probes with significantly different aspect ratios and/or face geometries. This is because the coefficients in Equation (30b) contain information about the freestream disturbance levels and noise which are peculiar to the 11-TWT.

Thus, Equation (30b) is not presented as a universal correlation applicable to all wind tunnels, Preston tubes and models with arbitrary pressure gradients. Rather the described procedure for developing a correlation is applicable to the data obtained with the AEDC Cone in other wind tunnels (see Dougherty and Fisher (30)). In fact, no

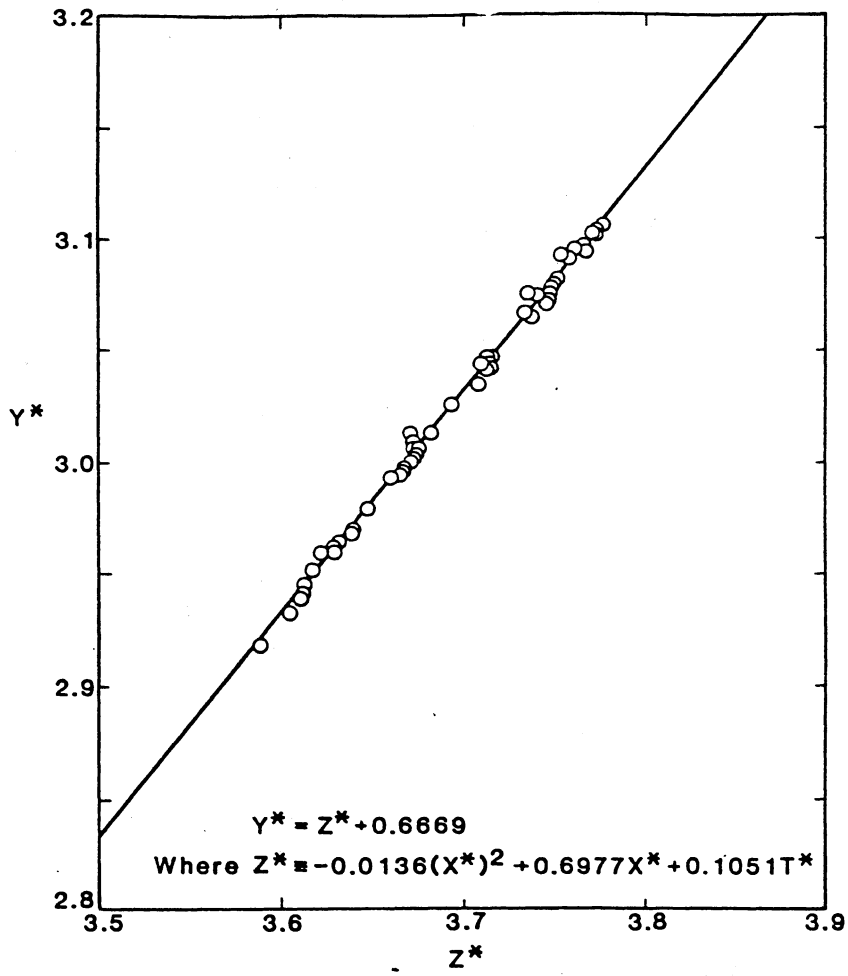

Figure 13. Laminar Correlation for Shifted Wind Tunnel Data

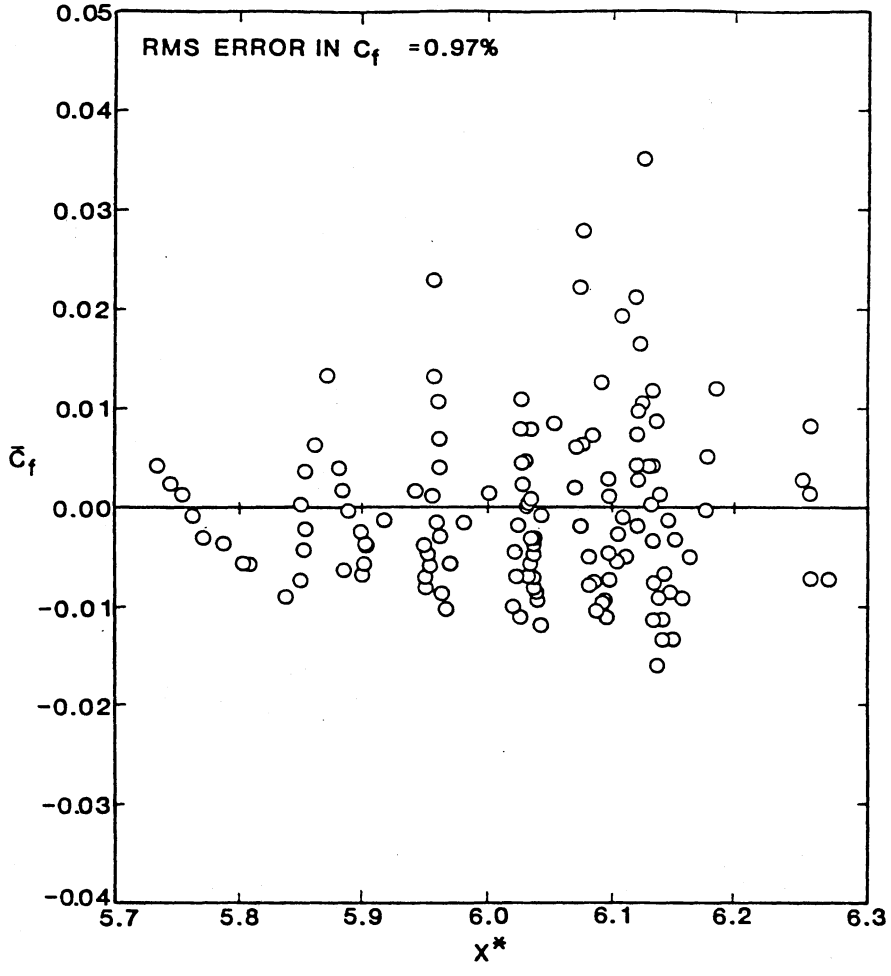

Figure 14. Scatter of Laminar Skin Friction Coefficient About Correlation for Shifted Wind Tunnel Data

Preston-tube correlation is universal unless it properly models the wind-tunnel environmental effects.

4.1.1 Procedure for Correcting Laminar Wind-Tunnel Data

The first objective is to align case 58.633 ($M_\infty = 0.7$, $Re_{ft} = 3 \times 10^6$) with case 21.318 ($M_\infty = 0.7$, $Re_{ft} = 4 \times 10^6$, $q_\infty = 548$ psf) which is considered the reference. Then shift all the cases whose $Re_{ft} = 3 \times 10^6$ accordingly. Refer to Figure 11.

The second objective is to coincide case 70.726 ($M_\infty = 0.7$, $Re_{ft} = 4 \times 10^6$, $q_\infty = 538$ psf) with case 21.318, then shift case 72.748 ($M_\infty = 0.7$, $Re_{ft} = 4 \times 10^6$, $q_\infty = 605$ psf) accordingly.

a. Evaluate $\overline{R}_\tau$ of case 58.633 as the average of all R_τ values in this case. Denote it by $\overline{R}_{\tau,58}$.

b. Extrapolate the data in case 21.318 up to $\overline{R}_{\tau,58}$. Use a French curve or do a least-squares curve fit of the data in case 21.318.

c. Evaluate K_{eff} at $\overline{R}_{\tau,58}$ given by the extrapolated curve; denote it by $K_{eff,21}$. Also read K_{eff} at $\overline{R}_{\tau,58}$ given by case 58.633 (the original value). Call this value $K_{eff,58}$.

d. Compute $\Delta K_{eff,58} = K_{eff,21} - K_{eff,58}$. This is the incremental adjustment of K_{eff} for the $Re_{ft} = 3 \times 10^6$ cases.

e. Find $\Delta P_{o,58}$ = corresponding total pressure adjustment (from theoretical STAN-5 profiles). Add this increment, algebraically, to all P_p measured values in case 58.633.

f. Find ΔP_o's for other cases in the $Re_{ft} = 3 \times 10^6$ group which correspond to the same value of $\Delta K_{eff,58}$ above and shift these cases by the proper increment of total pressure.

g. The procedure for shifting cases 70.726 and 72.748 is similar to steps a-f above.

4.2 Laminar Flight Correlation

Since a plot of K_{eff} versus R_τ is important to pinpoint possible errors in the data, it was logical to start the flight analysis with such a plot. The theoretical boundary layer computations were done by the STAN-5 program and K_{eff} values were interpolated just like in the wind tunnel analysis. The K_{eff} - R_τ plot appears in Figure 15. From Figure 12 for the wind tunnel data, at least three things are expected in this kind of plot:

1. The curve for a given M_∞ should be continuous.
2. K_{eff} should decrease with increasing M_∞ at a given R_τ.
3. The curves should be orderly spaced with M_∞.

As can be seen from Figure 15, none of these conditions is satisfied. Besides, some of the K_{eff} values are actually larger than 2.0. All this clearly indicates that the flight data are erroneous. The source of these errors is unknown. One explanation is the possible twisting of the probe in all three directions. Twisting in the α-plane will force the probe face to see a higher pressure region of the boundary layer, and therefore measure a higher-than-desired total pressure. Also, Y_g/h becomes a variable and is no longer equal to 0.5 and that affects K_{eff}. Still, the pitch angle becomes largely different from zero which is a requirement in this study. Twisting in the β-plane is equivalent to a non-negligible yaw angle and that makes the theoretical computations inaccurate. Finally, twisting in the θ-plane

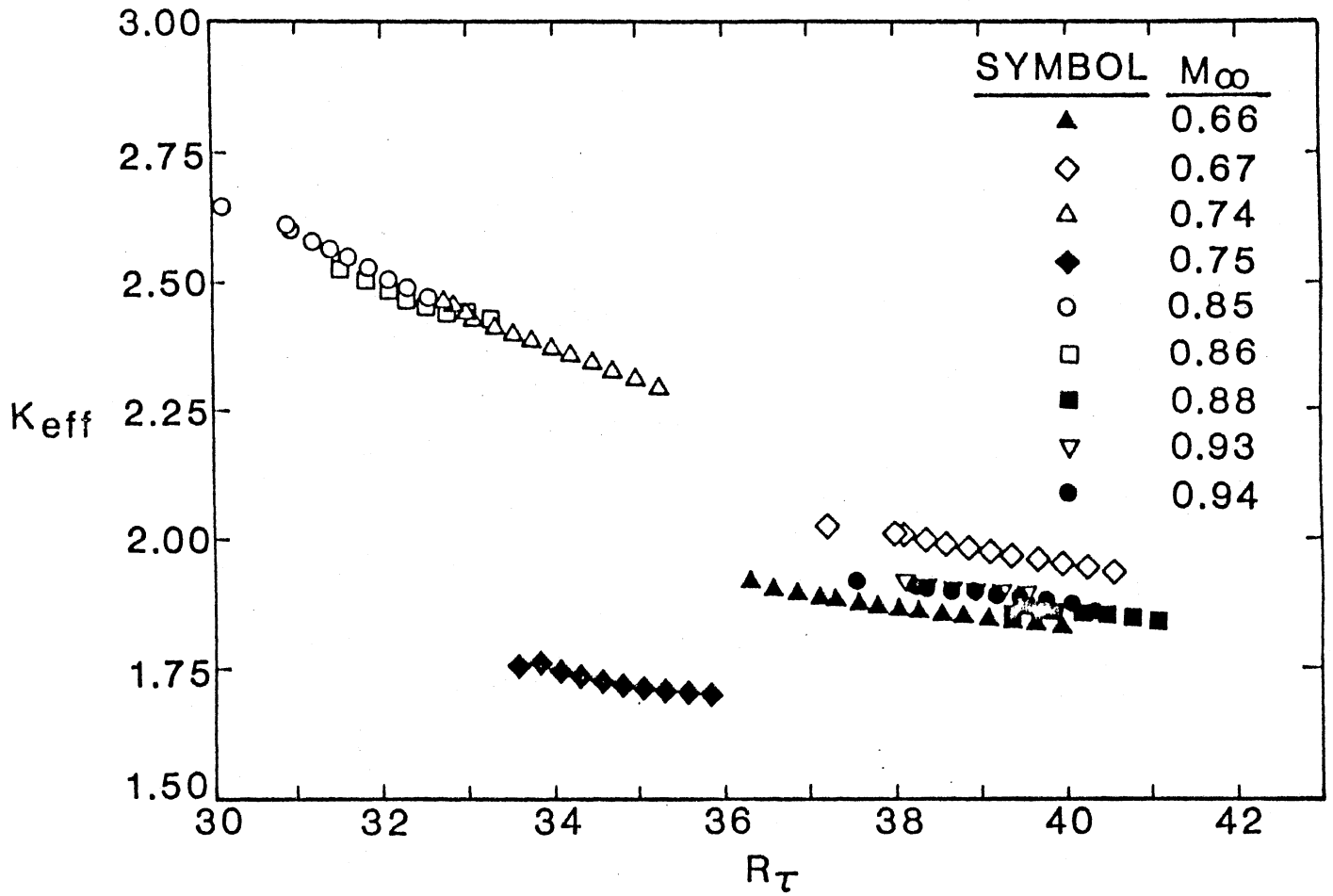

Figure 15. Distribution of Effective Probe Height as Determined from the Original Laminar Flight Data

is equivalent to different inviscid flow conditions which in turn, affect the viscous calculations.

As a check, the flight data as they are were correlated and the effective Reynolds numbers were evaluated as described before. It was found that ΔR_{eff} ($=Re_{ft,eff}/Re_{ft} - 1$) was nearly constant, viz., 6.67%, regardless of M_∞. This is inconsistent with the pattern of noise in the 11-TWT, Figure 16, which shows a peak in $C_{P,rms}$ at $M_\infty = 0.70 - 0.80$. As explained earlier, R_{eff} is expected to have a pattern similar to the noise pattern, Figure 16, since the noise effects, being unmodeled in the correlation, are suspected to be the major cause for the flight correlation being different from the wind tunnel correlation and hence allowing ΔR_{eff} to be defined. This means that a correction is needed for the flight data in order to derive meaningful effective Reynolds numbers. The author attempted to correct the flight data in two different ways:

I. If the probe is drawn out of the boundary layer and into the freestream, the value of K_{eff}, for a given M_∞, is asusmed to be the same for both wind-tunnel and flight tests. According to Becker and Brown (12), this assumption is not very accurate since freestream turbulence is found to affect the Preston-tube measurements. The assumption is equivalent to saying that as $R_\tau \to \infty$, K_{eff} for a given M goes to a value $K_o(M_\infty)$. This value will be called "the asymptotic value of K_{eff}". From the asymptotic wind tunnel equation (29), this value of K_{eff} is given by

$$K_o(M_\infty) = 0.655\ (1 - M_\infty^2)^{0.173} \qquad (31)$$

The correction procedure based on this asymptotic approach goes as follows:

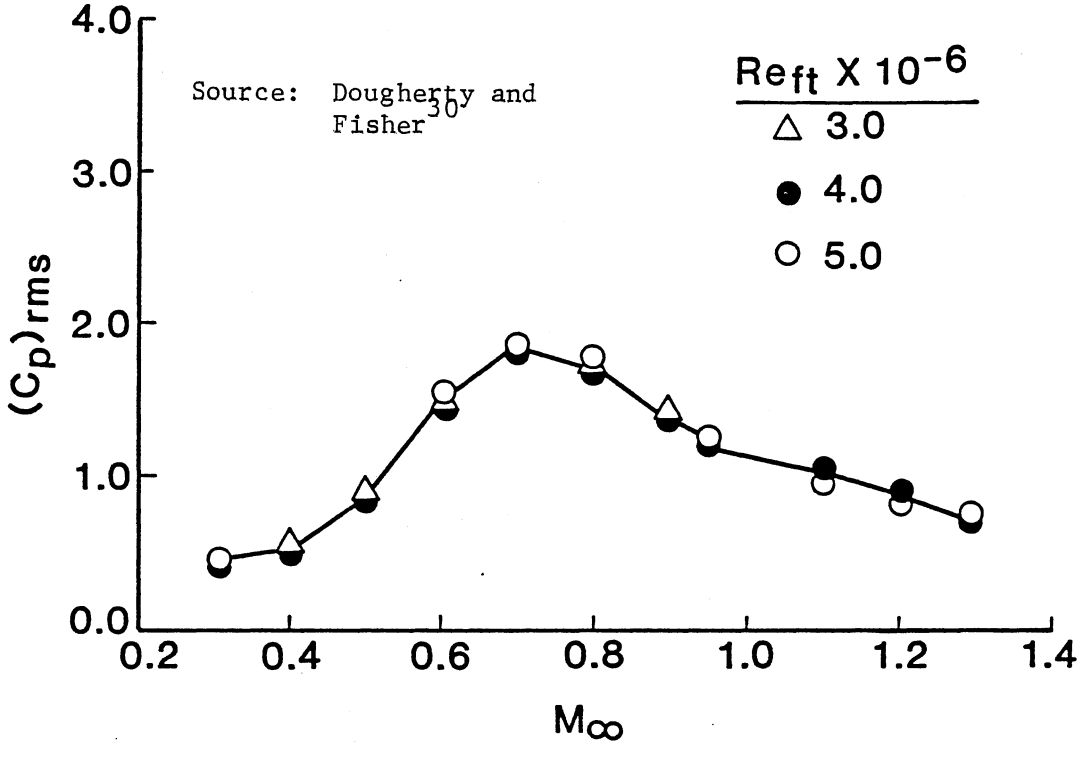

Figure 16. Noise Data on the AEDC Cone in the 11-Ft Transonic Wind Tunnel

* Calculate K_o from Equation (31) for all flight Mach numbers.
* Curve-fit the K_{eff} values for each flight in the form

$$K_{eff} = a_1 e^{-b_1 R_\tau} + c_1$$

The resulting equations are tabulated in Table III.

* As $R_\tau \to \infty$, the asymptotic values of K_{eff} for unmodified flight cases are given by the free constant C_1. The difference $K_o - C_1$ thus defines "shift errors" in the K_{eff} values in flight cases (a different increment for each flight case). This difference is therefore added or subtracted from the original K_{eff}'s of that flight case to obtain "correct" K_{eff}'s which will in the limit reach the same asymptotic values as the wind tunnel's for the given M_∞.

The result of this correction technique is much reduced K_{eff}'s, but the $K_{eff} - R_\tau$ curves do not exhibit the trend of K_{eff} decreasing with increasing M_∞ except for very large values of R_τ, see Figure 17. Besides, the theoretical total pressures corresponding to these new values of K_{eff} are nearly constant along the cone. The derived R_{eff} from a correlation based on this correction approach is plotted in Figure 18. Since, again, the distribution of ΔR_{eff} does not resemble the noise pattern, Figure 16, it was decided that this correction procedure was not helpful.

II. The second attempt to correct the flight data is based on the assumption that the measurements in Flight 349.1400 are correct. The grounds for this assumption are:

* The K_{eff} values of this case are realistic, $1.6 < K_{eff} < 1.7$.
* According to the NASA/Dryden flight report (35), several corrections were made to the measurements starting from flight #345 and on. This

TABLE III

CURVE-FITS OF EFFECTIVE PROBE HEIGHTS FOR LAMINAR FLIGHT DATA

Flight #	M_∞	Equation for K_{eff}
329.0918	0.66	$0.0510\ EXP\ [-0.4452\ (R_\tau - 38.0321)] + 1.8133$
329.1042	0.67	$0.2287\ EXP\ [-0.1293\ (R_\tau - 39.9423)] + 1.7539$
329.1035	0.74	$0.5689\ EXP\ [-0.1154\ (R_\tau - 33.8301)] + 1.8118$
349.1400	0.75	$0.0387\ EXP\ [-0.8187\ (R_\tau - 34.6364)] + 1.6866$
349.1027	0.85	$0.4787\ EXP\ [-0.1809\ (R_\tau - 31.4714)] + 2.0779$
327.0907	0.86	$0.0887\ EXP\ [-0.8263\ (R_\tau - 32.3159)] + 2.3808$
333.1353	0.88	$0.0437\ EXP\ [-0.2315\ (R_\tau - 40.0836)] + 1.8146$
332.1020	0.93	$0.0194\ EXP\ [-1.0018\ (R_\tau - 38.6302)] + 1.8922$
33.1350	0.94	$0.1090\ EXP\ [-0.1914\ (R_\tau - 39.1318)] + 1.7825$

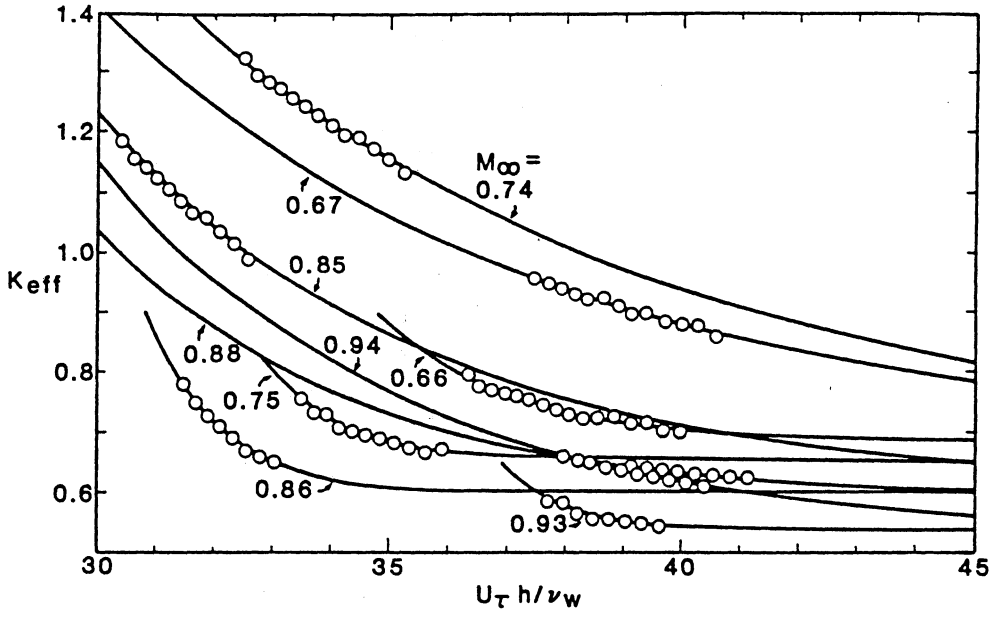

Figure 17. Distribution of Effective Probe Height of Laminar Flight Data After Asymptotic Correction

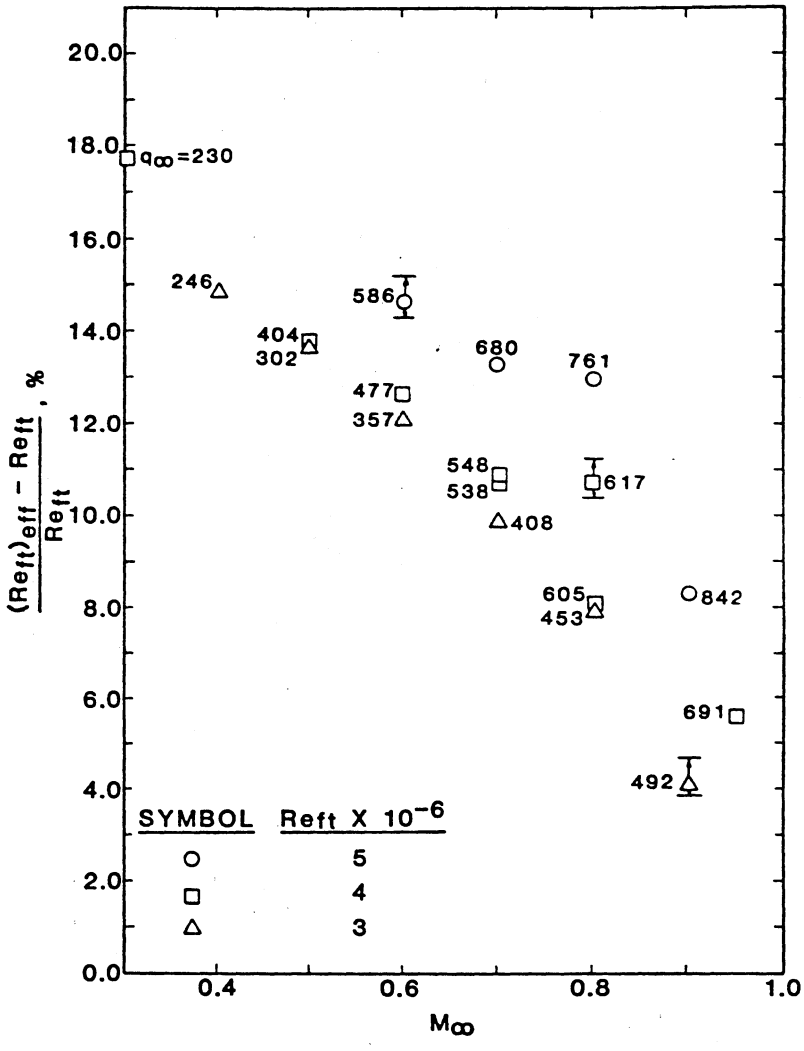

Figure 18. Distribution of Laminar Effective Reynolds Number Based on Asymptotically-Correlated Flight Data

means that Flight 349.1400 is at least less erroneous than the rest of the flights analyzed in this study.

Correction based on this assumption is done by rearranging the flight data, Figure 15, with Flight 349.1400 as the reference. Rearrangement is done with the aid of the wind-tunnel asymptotic equation as follows:

* Determine the spacing, Figure 15, between each flight curve and the curve for Flight 349 (the bottom curve). This spacing is defined as the difference in K_{eff} between the case to be corrected and the reference case at the point of average R_τ in the region were values of R_τ overlap. Call this spacing the "old" spacing.
* Calculate the "new" spacing between pairs of flight cases by substituting in Equation (29) the average value of R_τ used to calculate the old spacing, and the two Mach numbers of the two flights.
* The difference between the old and new spacings for a pair of flight cases determines the increment in K_{eff} to be added or subtracted from original K_{eff}'s in order to shift a flight case to its proper place with respect to the reference flight case. This procedure is outlined in Section 4.2.1.

It is important here to note that a simple shift in K_{eff} may preserve the $K_{eff} - R_\tau$ distributions, but is likely to destroy the $P_P - R_\tau$ distributions, since the theoretical total pressure used to calculate K_{eff} is generally a function of both X and Y, therefore $\partial P_o/\partial X$ is a function of Y and therefore changes as the probe moves across the boundary layer. Figure 19 clearly illustrates this effect. Therefore, it is important to decide whether the longitudinal difference in

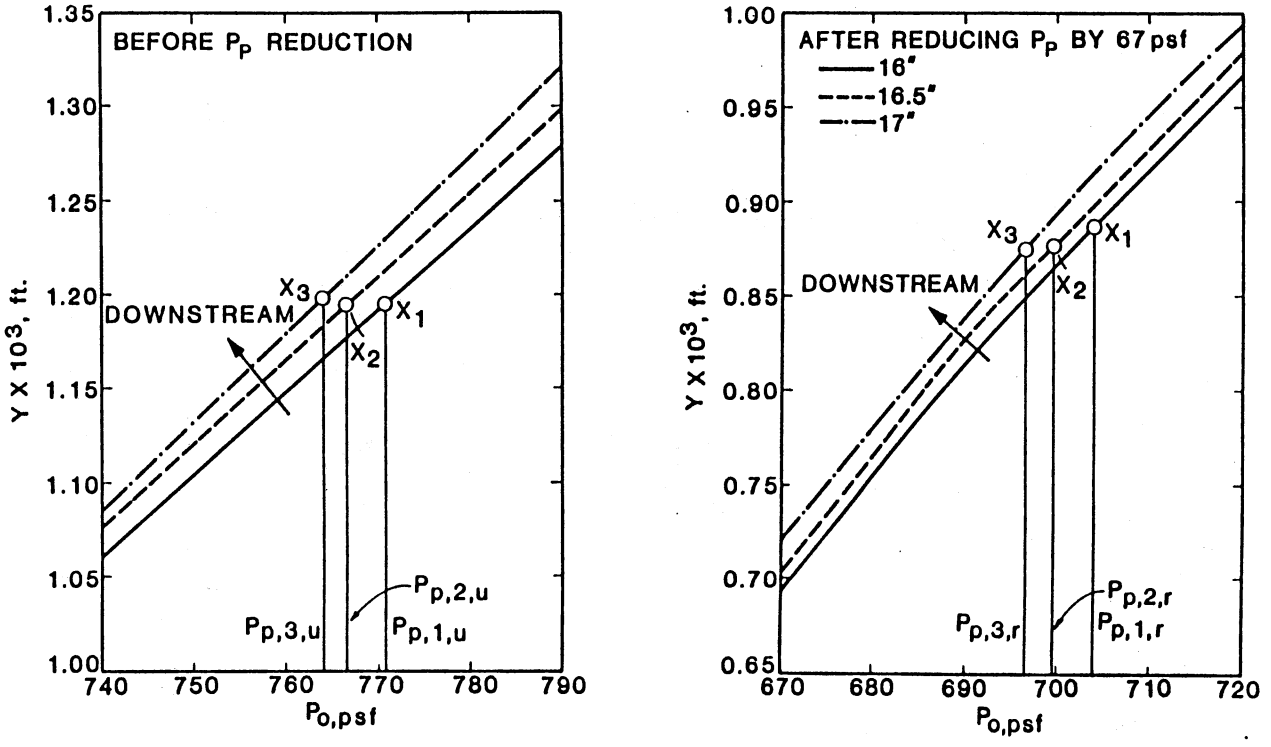

Figure 19. Effect of Changing Preston-Tube Pressure on the Effective Probe Height

measured P_p for a given traverse is valid. A zero-drift in the transducer read-out equipment is unlikely for a traverse that lasts less than a minute. The only way that such a difference may be invalid is if the probe was twisting. This may have been one of the causes of error in the measurements. But since it is impossible to trace back the pattern of twisting, there is no way to account for it. It seems logical, therefore, to preserve the longitudinal differences in measured P_p. Thus, shifting of the flight data is done on basis of theoretical total pressures that correspond to the new values of K_{eff} at the location where spacing was determined. The difference between the original P_p and the total pressure at the new K_{eff} defines the shifting increment. The rearranged flight data based on this correction procedure are shown in Figure 20.

The laminar Preston-tube correlation using the corrected flight data is given by the following equation.

$$Y^* = 0.05981(X^*)^2 - 0.1777\ X^* + 1.928,$$
$$5.6 < X^* < 6.7,\ 0.66 \leq M_\infty \leq 0.94,$$
$$2.1 \times 10^6 \leq Re_{ft} \leq 2.8 \times 10^6. \qquad (32)$$

The r.m.s. error in C_f associated with the above curve fit is only 0.37%. Figure 21 shows the correlation and the corrected data and Figure 22 shows the C_f scatter about Equation (32).

It is worth mentioning at this point that Equation (32) is, to the best of the author's knowledge, the first free-flight Preston-tube correlation in the literature.

4.2.1 Procedure for Correcting the Flight Data

a. Let $K_{eff,FD}\ (R_\tau, M_1)$ = the value of K_{eff} at R_τ for the flight case

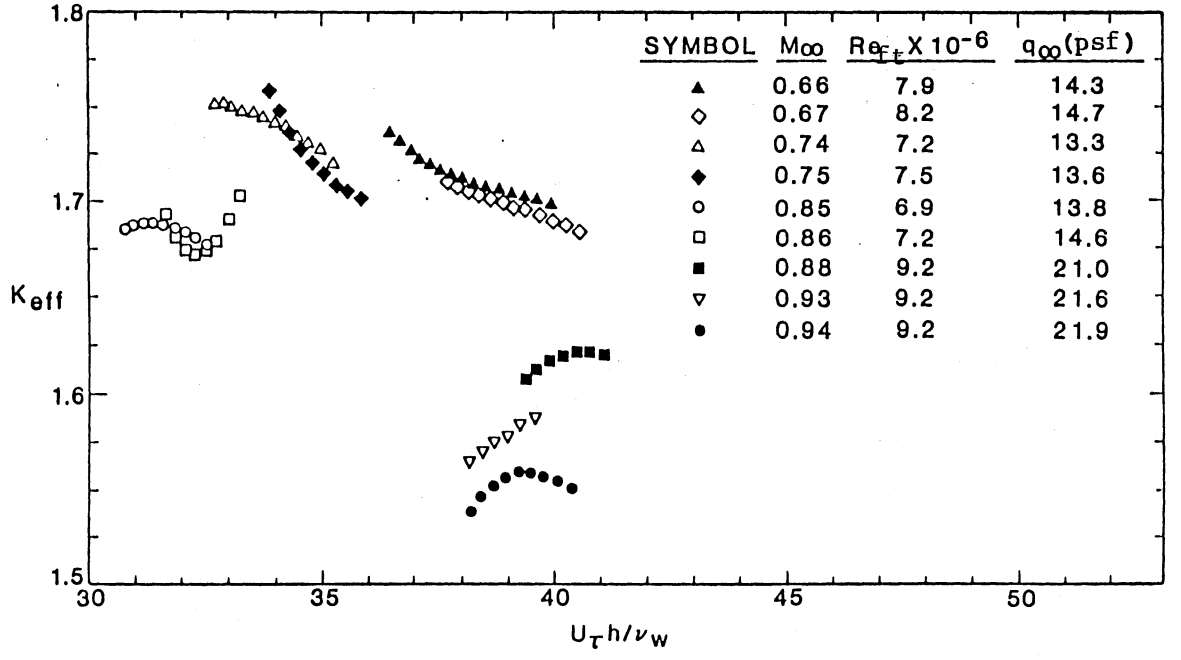

Figure 20. Distribution of Effective Probe Height as Determined from the Corrected Laminar Flight Data

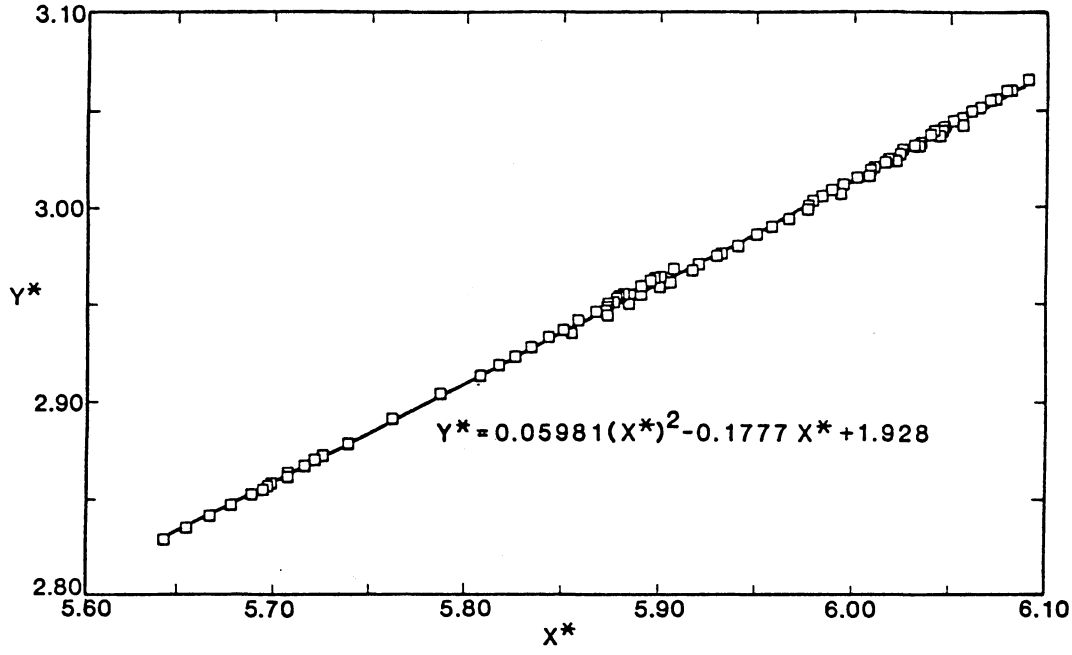

Figure 21. Laminar Correlation for Corrected Flight Data

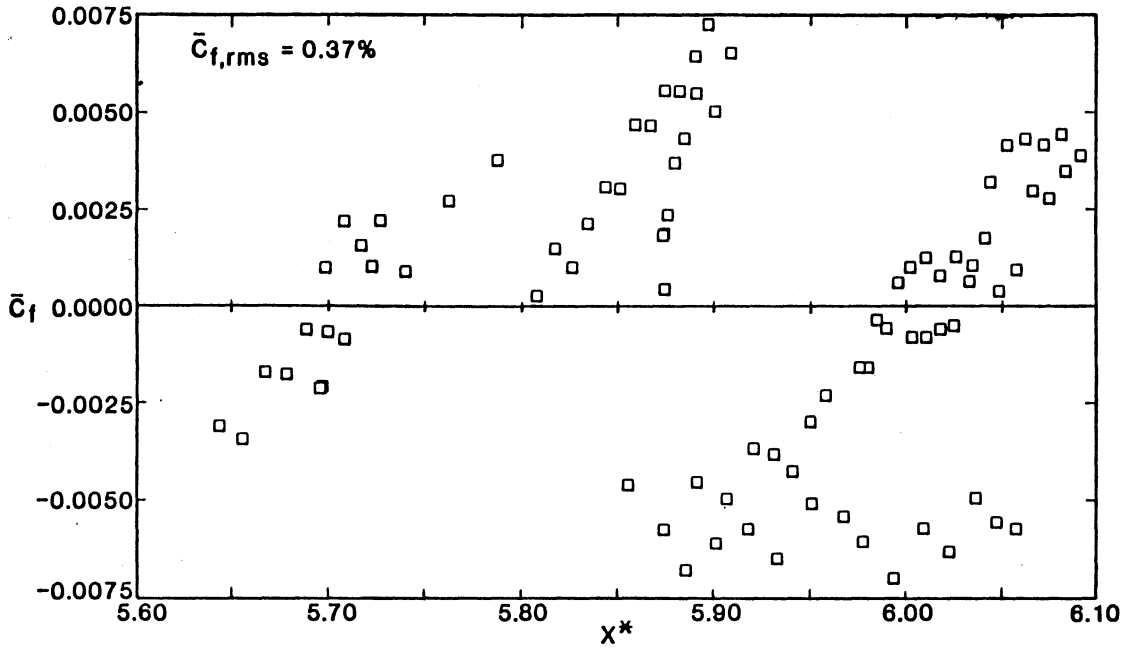

Figure 22. Scatter of Laminar Skin Friction Coefficient About Correlation for Corrected Flight Data

with $M_\infty = M_1$. Similarly define $K_{eff,WT}(R_\tau, M_1)$.

Let $\{M_1\}_{FD}$ = set of all R_τ values in the flight case with $M_\infty = M_1$.

Let $\{M_1,M_2\}_{FD}$ = set of all R_τ values common between the two flight cases whose M_∞'s are M_1 and M_2, i.e., $\{M_1,M_2\}_{FD} = \{M_1\}_{FD} \wedge \{M_2\}_{FD}$.

Let $\overline{R}_\tau(M_1,M_2)_{FD}$ = the average of all R_τ values in $\{M_1,M_2\}_{FD}$.

Let $\Delta K_{eff,FD}(M_1,M_2) = K_{eff,FD}(\overline{R}_\tau, M_1) - K_{eff,FD}(\overline{R}_\tau, M_2)$. Similarly define $\Delta K_{eff,WT}(M_1,M_2)$. Refer now to Figure 15.

b. The reference case for all flight cases is flight #349.1400, i.e. $M_2 = 0.75$. To shift a flight case $\{M_1\}_{FD}$, first determine $\{M_1, 0.75\}_{FD}$. If $\{M_1, 0.75\}_{FD} = \phi$, i.e., no R_τ values are shared by the two cases then you have one of two situations.

- $\{0.75\}_{FD} > \{M_1\}_{FD}$, in which case set $\overline{R}_\tau(M_1, 0.75)_{FD}$ to be equal to the largest R_τ in $\{M_1\}_{FD}$.
- $\{M_1\}_{FD} > \{0.75\}$, in which case set $\overline{R}_\tau(M_1, 0.75)_{FD}$ to be equal to the smallest R_τ in $\{M_1\}_{FD}$. An example of such a situation is $\{0.66\}_{FD}$, see Figure 15.

Then, go to step d below.

c. This is the case where $\{M_1, 0.75\}_{FD}$ is defined ($\neq \phi$) such as $\{0.74\}$. So, calculate $\overline{R}_\tau(M_1, 0.75)_{FD}$.

d. Find $K_{eff,FD}(\overline{R}_\tau, M_1)$ and $K_{eff,FD}(\overline{R}_\tau, 0.75)$ hence $\Delta K_{eff,FD}(M_1, 0.75)$.

e. Find $K_{eff,WT}(\overline{R}, M_1)$ and $K_{eff,WT}(\overline{R}, 0.75)$ hence $K_{eff,WT}(M_1, 0.75)$ from a curve-fit equation of K_{eff} versus R in the wind tunnel, such as Equation (29). Notice that $\overline{R}(M_1, 0.75)_{WT} = \overline{R}(M_1, 0.75)_{FD}$. Also,

$K_{eff,WT}(M_1, 0.75)$ will be <u>negative</u> if $M_1 > 0.75$.

f. Calculate $\Delta K_{eff,shift}(M_1)_{FD}$ = incremental adjustment of K_{eff} values in the flight $M_1 = \Delta K_{eff,FD}(M_1, 0.75) - \Delta K_{eff,WT}(M_1, 0.75)$.

g. From the theoretical P_o profiles for the flight case M_1, obtain $\Delta P_{o,shift}(M_1)_{FD}$ which corresponds to $\Delta K_{eff,shift}(M_1)_{FD}$ at the location where $R_T = \overline{R}_T$. This is the incremental pressure adjustment for flight case M_1.

h. For all points in $\{M_1\}_{FD}$, obtain $P_{P,shift}(M_1)_{FD} = P_P(M_{1,FD} - \Delta P_{o,shift}(M_1)_{FD}$, $P_P(M_1)_{FD}$ being the original, measured value of Preston-tube pressure.

4.3 Laminar Effective Reynolds Number

Based on Equations (30b) and (32), the effective freestream unit Reynolds number was computed and plotted versus M_∞. The plot, Figure 23, resembles the curve for noise data on the AEDC cone in the 11-TWT[1], Figure 16, and has a peak at $M_\infty = 0.70 - 0.80$, as does the noise. Actually, $\Delta R_{eff} \equiv (Re_{ft,eff} - Re_{ft})/Re_{ft}$ correlated with noise by the following equation.[2]

$$\Delta R_{eff} \simeq 6.25\ (C_{P,rms})^{0.07}.$$

This supports the thesis that environmental effects in a wind tunnel can be calibrated by a single number, i.e. $Re_{ft,eff}$. So, in order to obtain the same <u>average</u>, <u>theoretical</u> skin friction coefficient, or the same average measurement of P_P, in the tunnel as in flight, the tunnel value of freestream unit Reynolds number should be increased to $Re_{ft,eff}$. This effective Reynolds number will not necessarily equate

---

[1]These data include installation effects in addition to wall-generated noise.

[2]The accuracy of this correlation is not very good since it does not include other environmental effects such as freestream turbulence intensity. $Re_{ft,eff}$ calibrates all these effects and not only noise. It should be noted, however, that noise effects are dominant in the 11-Ft Transonic Wind Tunnel (32).

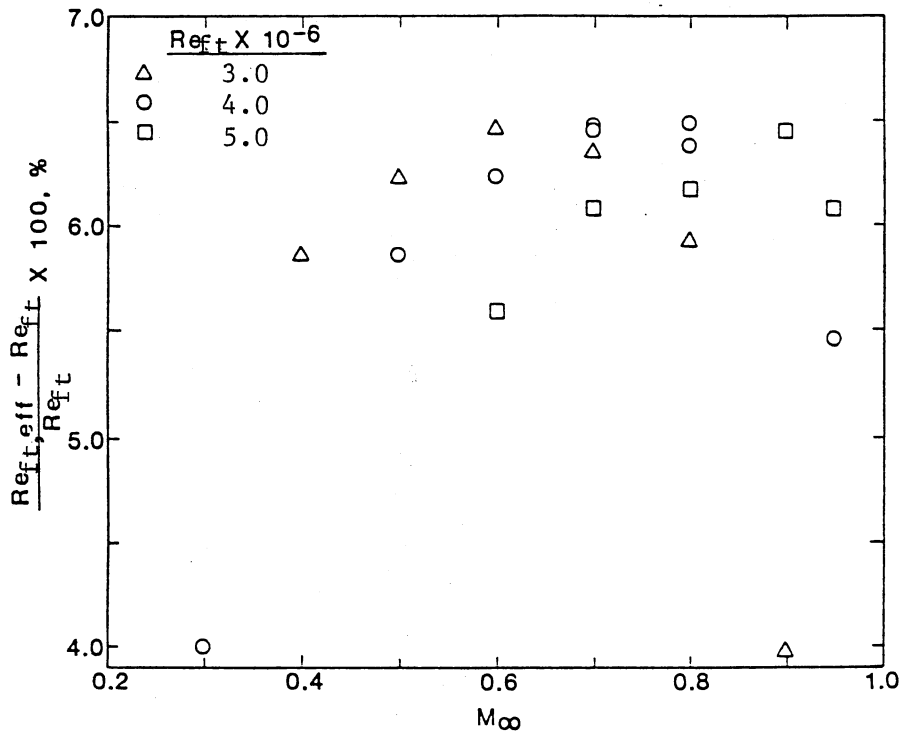

Figure 23. Distribution of Laminar Effective Reynolds Number Based on Corrected Data

the measurable value of C_f. Indeed, the effects of noise on directly measured skin friction, if any, is unknown.

4.4 The Transition Region

Recall Dhawan and Narasimha's (29) intermittency function for transitional flow:

$$\gamma(X) = 1 - e^{-A\xi^2(X)}. \tag{19}$$

In order to be able to use Equation (19), λ needs to be known for each case. Since measurements of $\gamma(X)$ are not available for this study, Equation (21) cannot be used. Another method was developed to calculate λ as will be shown now.

4.4.1 Calculation of λ

This method makes use of the available Preston-tube data. Since it is assumed that the distribution of C_f follows Preston-tube measurements (see Equation 4), one can assume that the location X_T where P_P peaks is the same location where C_f peaks. Within the transition zone, the C_f distribution is calculated using the -function in the following manner:

$$C_f = (1 - \gamma)\, C_{f,\ell} + \gamma\, C_{f,T}, \tag{33}$$

where $C_{f,\ell}(X)$ is the local laminar skin friction coefficient if it were to occur at the given location X, and $C_{f,T}(X)$ is the local turbulent skin friction coefficient if it were to occur at X. The origin of the turbulent boundary layer is determined from the fully-developed turbulent flow at or downstream from X_E, the end-of-transition location, as will be explained later. The value of X_E corresponds to $\xi = 4.0$ (or $\gamma = 0.9986$) as recommended by Dhawan and Narasimha (29).

Differentiating Equation (33) with respect to X and evaluating at X_T yields the following relation:

$$\left.\frac{dC_f}{dX}\right|_{X_T} = 0 = \left[(C_{f,T} - C_{f,\ell})\frac{d\gamma}{dX} + \left(\frac{dC_{f,T}}{dX} - \frac{dC_{f,\ell}}{dX}\right)\gamma + \frac{dC_{f,\ell}}{dX}\right]_{X_T}. \quad (34)^3$$

A following formula for calculating $C_{f,T}$ is reported by White (99) to be reasonably accurate.

$$C_{f,T} = \frac{0.455}{S^2 Ln^2\left[\frac{0.06}{S}Re_{x_v}\frac{\mu_e}{\mu_w}\left(\frac{T_e}{T_w}\right)^{.5}\right]}$$

Using Summer and Short's model for S, a compressibility factor (see Reference 30), to correct for variable properties and Tetervin's (93) correction for axisymmetric flow and making the approximation that $\frac{\sqrt{\rho_w}\sqrt{\rho'}}{\mu_w} = \frac{1}{\nu'}$ the following equation can be derived.

$$C_{f,T} = \frac{\rho'}{\rho_e}\frac{0.455}{Ln^2\left[\frac{U_e X_v}{37.8\nu'}\right]} \quad (35)$$

Here X_v = distance along cone surface measured from the virtual origin of the turbulent boundary layer. It can be written in the form

$$X_v = X - \Delta X, \quad (36)$$

where ΔX is the location of the virtual origin (see Figure 24). It is now clear that Equation (34) can be solved for λ if ΔX is known. The following section explains how this is done.

4.4.2 Calculation of ΔX

Equation (35) can be rewritten in the form

---

[3]Equation (34) is also valid as X_t, location of minimum P_p. Solving for X_B which appears in the definition of γ, it was found that $X_B \simeq X_t$. Therefore, the value of X_t is used from here on to designate the transition onset location.

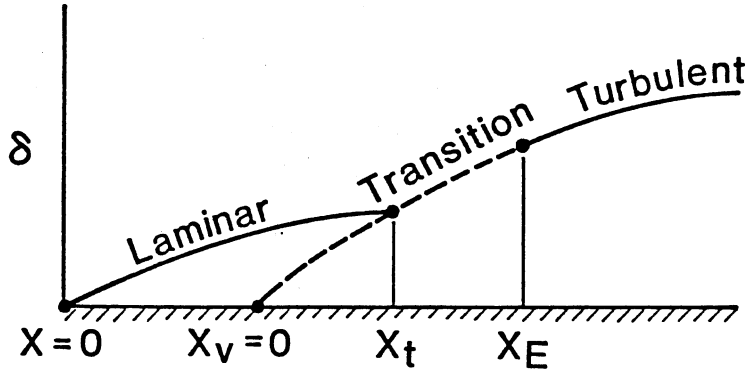

Figure 24. The Virtual Origin of a Turbulent Boundary Layer

$$X_v = X - \Delta X = \frac{37.8\nu'}{U_e} \exp\left[\frac{0.455\ \rho'}{C_{f,T}\ \rho_e}\right]^{0.5}. \tag{37}$$

So, all that is needed to calculate ΔX is a reference $C_{f,T}$ in the fully-developed turbulent flow at a location $X_{ref} \geq X_E$.

Crawford and Kays (25), who developed the STAN-5 program, state that their program's calculation of turbulent C_f agreed with extensive measurements done at Stanford University. They used the following equation to effect gradual transition.

$$A^+ = A^+_\ell + (300 - A^+_\ell)\left[1 - \sin\left(\frac{\pi}{2}\,\frac{Re_\theta(X) - Re_\theta(X_B)}{Re_\theta(X_B)}\right)\right]^2 \tag{38}$$

Here $A^+(X)$ is an effective sublayer thickness used in the Van Driest damping model

$$D = 1 - e^{-Y^+/A^+}. \tag{39}$$

Figure 25 shows a plot of Equation (38) for a typical wind tunnel case. The damping coefficient is used in the Prandtl mixing length model for turbulent boundary layer calculations near the wall as follows.[4]

$$\ell = \kappa\ Y\ D, \quad \kappa = 0.41 \tag{40}$$

And

$$A^+_\ell = \frac{\rho_w}{\mu_w\ U_\tau^3}\,\frac{dP_w}{dX} \tag{41}$$

Now, in Equation (38), it is assumed that

$$Re_\theta(X_E) = 2\ Re_\theta(X_B).$$

This was not found to be true at values of $X_E = X_B + 4\lambda$ (recommended by Dhawan and Narasimha (29)). In addition, this transition model does not

---

[4]The mixing length model is also the one used in this study to calculate the fully-developed turbulent boundary layer.

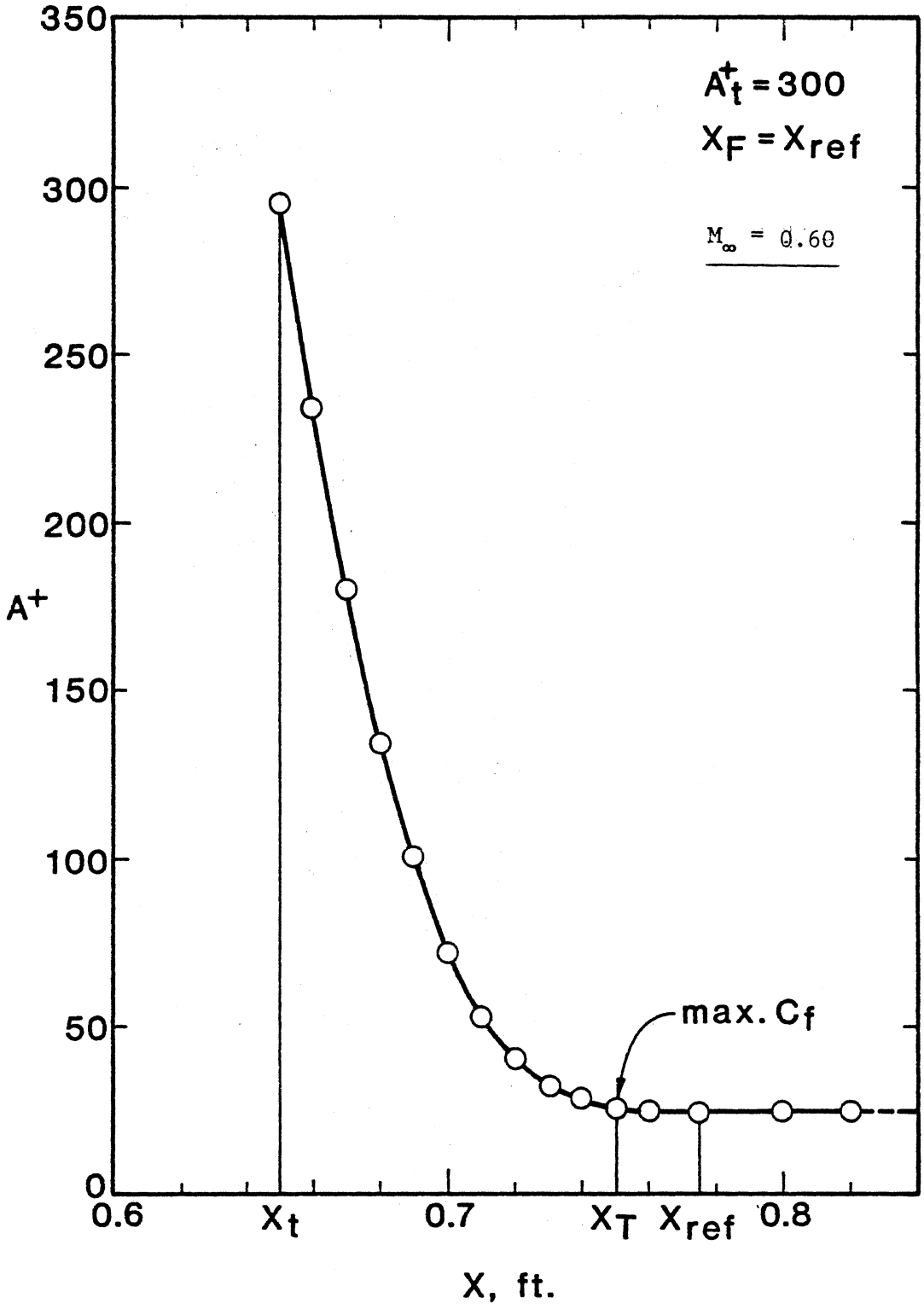

Figure 25. Distribution of Effective Sublayer Thickness for a Typical Case

produce a peak in C_f at X_T. Instead, the author used the following slightly different equation:

$$A^+ = A^+_\ell + [500 - A^+_\ell][1 - \sin(\frac{\pi}{2} \frac{Re_X - Re_B}{Re_F - Re_B})]^2, \quad (42)$$

where Re_F is the local length Reynolds number at a location X_F which is changed so that a peak in C_f occurs at X_T. This trial-and-error procedure is illustrated in Figure 26. It is important here to mention that Equation (42) is not used as a transition model. Its sole role is to effect gradual transition so that the turbulent flow downstream is accurately computed. Indeed, when either of Equations (38) or (42) was used to simulate transition, the computed skin friction was found to be greatly underestimated as compared to the Dhawan-Narasimha model.

To sum up, Equation (42) is used to prepare to compute turbulent flow, and hence obtain a good estimate of a reference value for $C_{f,T}$ at X_E or downstream. The location $X_{ref} \geq X_E$ is estimated from the Preston-tube data traces as the location downstream from X_E where the P_P measurements exhibit a slope characteristic of fully-developed turbulent flow (see Figure 27). However, this estimate of X_{ref} need not be precise, as long as it is sufficiently downstream from X_E.

Using $C_{f,T,ref}$ at X_{ref} and substituting in Equation (37), ΔX may be calculated. Hence, λ can be calculated from Equation (34). Thus, the γ-function is now fully defined, and the C_f distribution can be computed using Equation (33).

In the above argument, it is assumed that White's formula, Equation (35), accurately calculates $C_{f,T}$ and/or X_v. The author has found, by trial and error, that it does not, at least for the conditions in this study (mostly the relatively high Reynolds numbers). Best results were

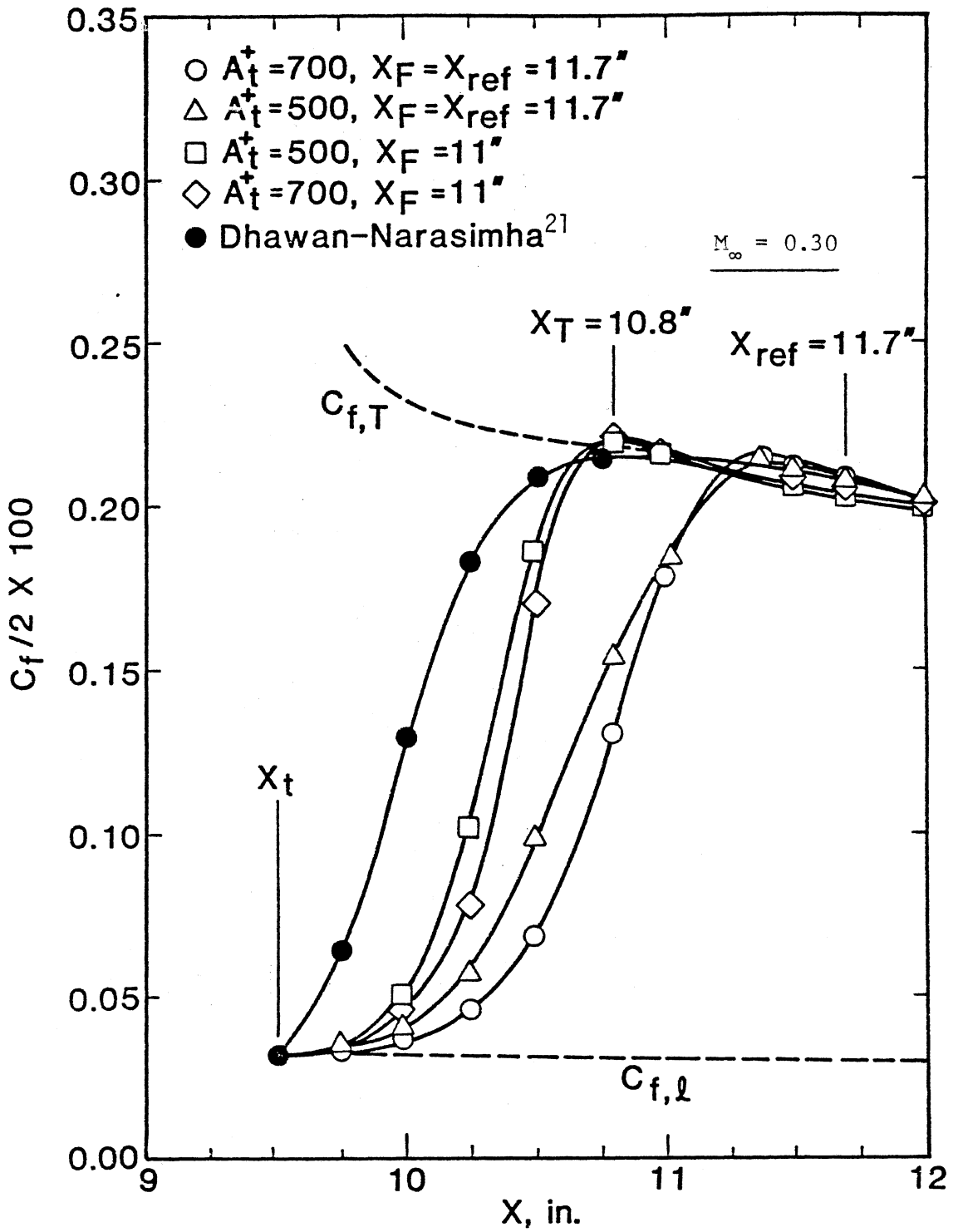

Figure 26. Effect of Sublayer Thickness Distribution on Transitional Skin Friction Coefficient

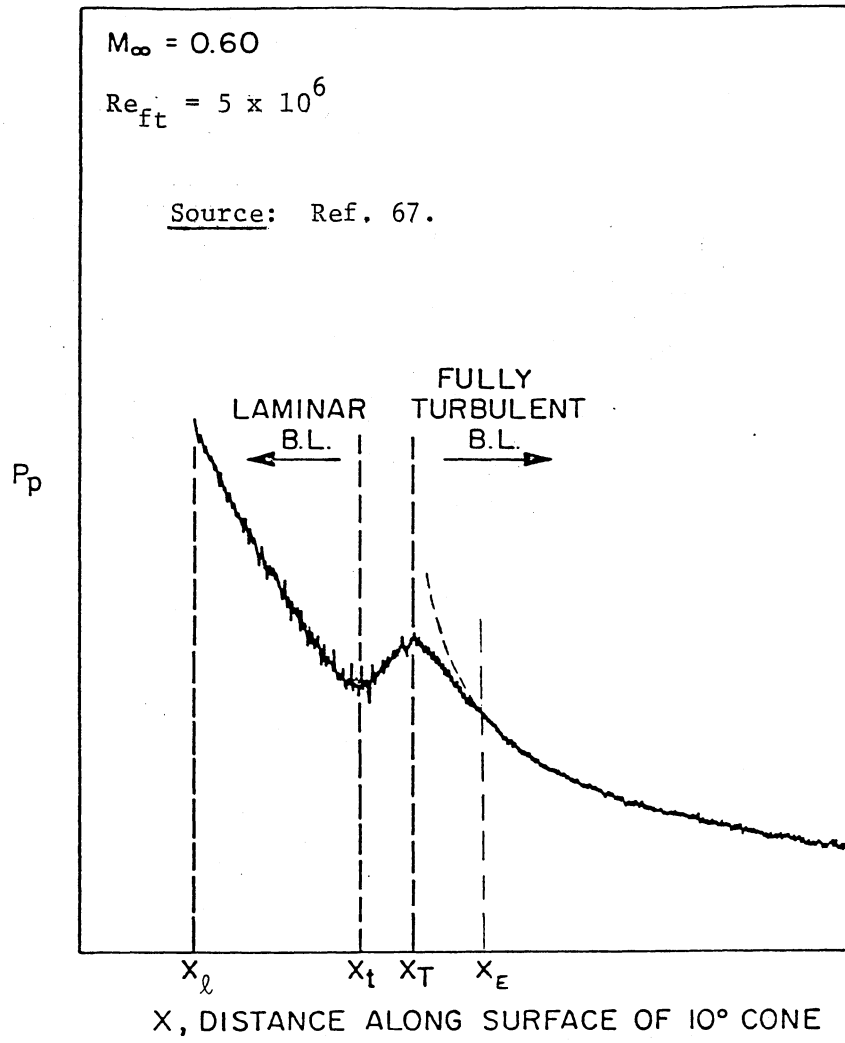

Figure 27. Pattern of Typical Preston-Tube Data Measured in the 11-Ft Transonic Wind Tunnel

obtained when the virtual origin coincided with the transition point, i.e., $X_v(0) = X_t = \Delta X$. This finding was also reported by Dhawan and Narasimha (29). Based on this finding an improved procedure to calculate λ and hence γ is described next.

The following variation of White's equation is used in place of Equation (35).

$$C_{f,T}(X) = C \frac{\rho'/\rho_e}{Ln^2 \left[\frac{U_e(X - X_t)}{\nu'}\right]}, \tag{43}$$

where C is a constant that has a different value for each case and can be directly evaluated from Equation (43) at X_{ref}.

Equation (43), then, together with its derivative with respect to X, the laminar STAN-5 calculations of $C_{f,\ell}$ and its derivative with respect to X are substituted in Equation (34) to solve for λ and hence γ.

4.4.3 The Transition Correlations

In order to completely define the correlation parameters X^* and Y^*, theoretical velocity and total pressure profiles in transition need to be computed to obtain $U_p(X)$ and $K_{eff}(X)$. These profiles may be calculated using the γ-function in a manner similar to skin friction, Equation (33).

$$U(Y) = (1 - \gamma)\, U_\ell(Y) + \gamma\, U_T(Y), \tag{44}$$

$$T(Y) = (1 - \gamma)\, T_\ell(Y) + \gamma\, T_T(Y). \tag{45}$$

From these two profiles, calculate $P_o(Y)$ as follows:

$$M(Y) = U(Y)/49.02\sqrt{T(Y)})$$

$$P_o(Y) = P_w[1 + 0.2\ M^2(Y)]^{3.5} \qquad (46)$$

Initial profiles for turbulent flow computation can be obtained by rescaling available fully-developed turbulent profiles (at X_{ref}) using edge velocity and boundary-layer thickness at the initial location which can be estimated using Musker's equation, Musker (66), as follows:

$$\delta = e^{0.41\ U_e^+ - 3.0504}\ \nu'\ U_e^+/U_e \quad \text{at } X_{initial}, \qquad (47)$$

where $U_e^+ = (\frac{C_{f,T}}{2}\frac{\rho_e}{\rho_w})^{0.5}$ at $X_{initial}$. $C_{f,T}$ at $X_{initial}$ can be calculated using Equation (35) with $X_v = X_{initial} - \Delta X$ and all properties evaluated at $X_{initial}$ which is downstream from X_t.

Values of U_P and K_{eff} can then be computed by interpolaton of measured Preston-tube pressures in velocity and total pressure profiles given by Equations (44 and 46).

Based on the above analysis the transition correlations for the original data are:

Wind Tunnel:

$$Y^* = 0.06935\ (X^*)^2 + 0.02795\ X^* + 0.9678,$$

$$5.2 < X^* < 6.3,\ 3 \times 10^6 \leq Re_{ft} \leq 5 \times 10^6,\ 0.30 \leq M_\infty \leq 0.95,$$

$$\overline{C}_{f,rms} = 2.19\%, \text{ and} \qquad (48)$$

Flight:

$$Y^* = 0.02094(X^*)^2 + 0.5988X^* - 0.7112,$$

$$5.5 < X^* < 7.1,\ 2.1 \times 10^6 \leq Re_{ft} \leq 2.8 \times 10^6, \qquad (49)$$

$$0.66 \leq M_\infty \leq 0.94,\ \overline{C}_{f,rms} = 3.64\%.$$

A plot of Equation (48) with the superimposed wind-tunnel data appears in Figure 28. Figure 29 is a plot of C_f scatter about Equation (48). Figures 30 and 31 illustrate the same for the flight data.

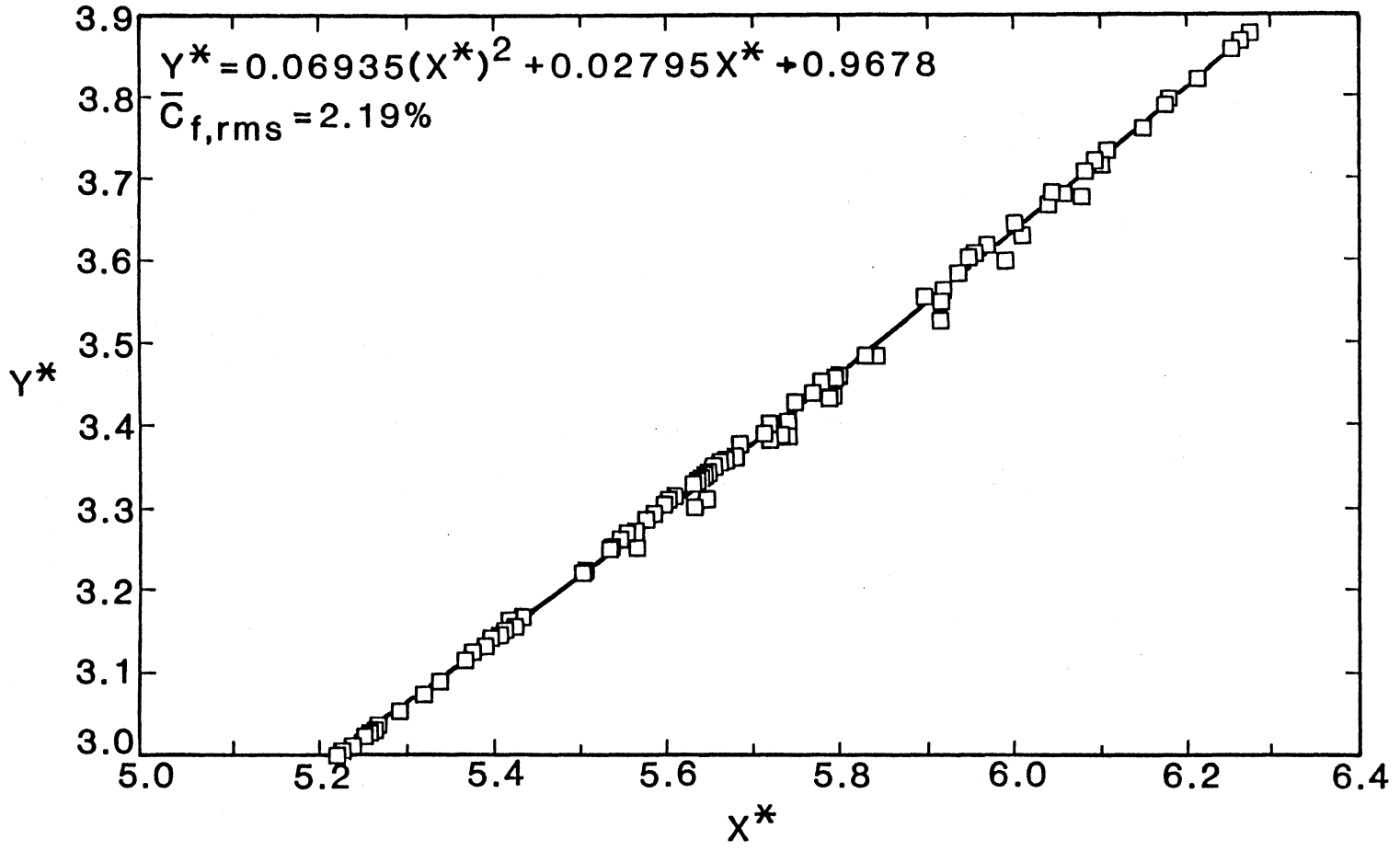

Figure 28. Transitional Correlation for Original Wind Tunnel Data

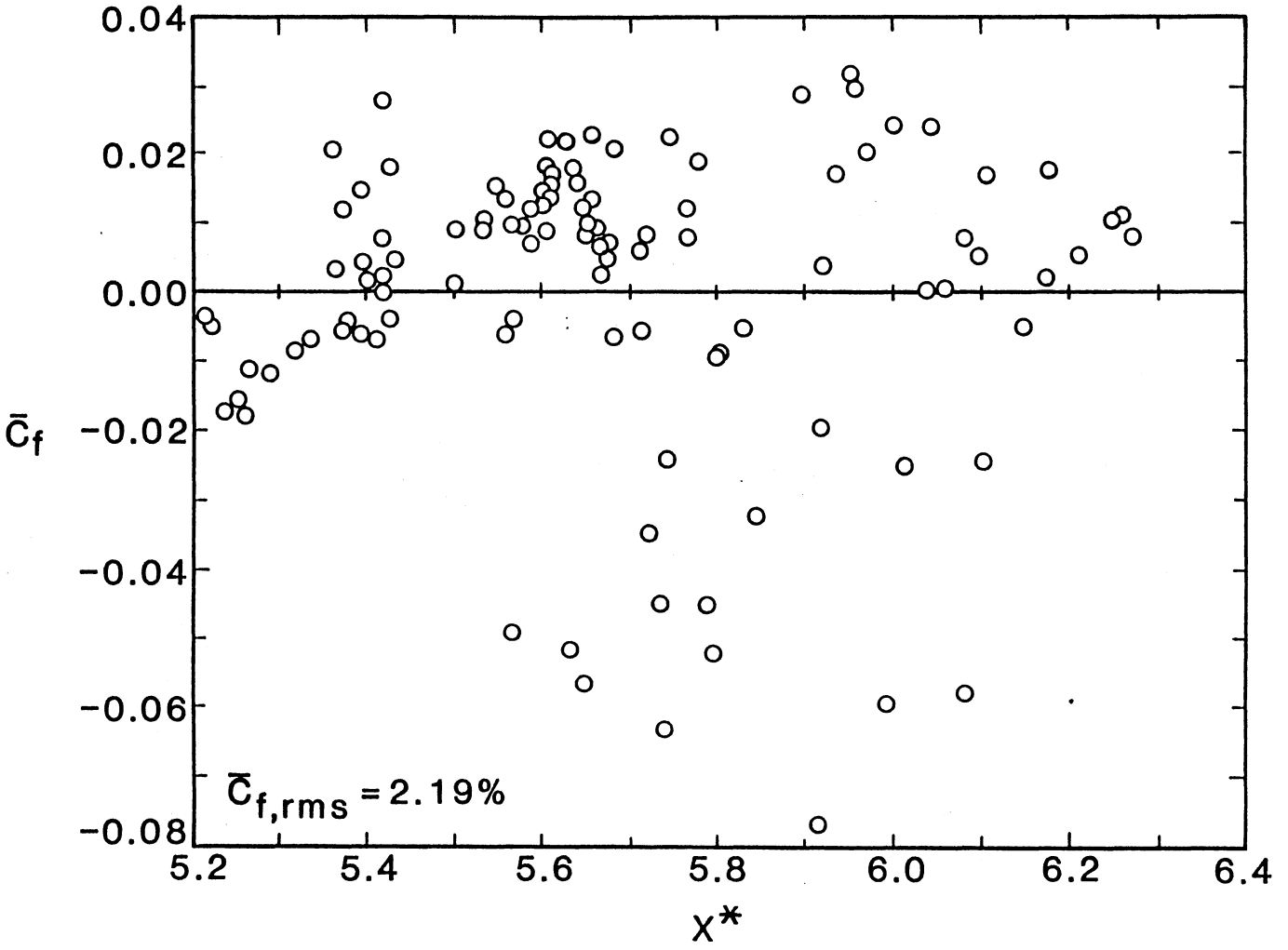

Figure 29. Scatter of Transitional Skin Friction Coefficient About Correlation for Original Wind Tunnel Data

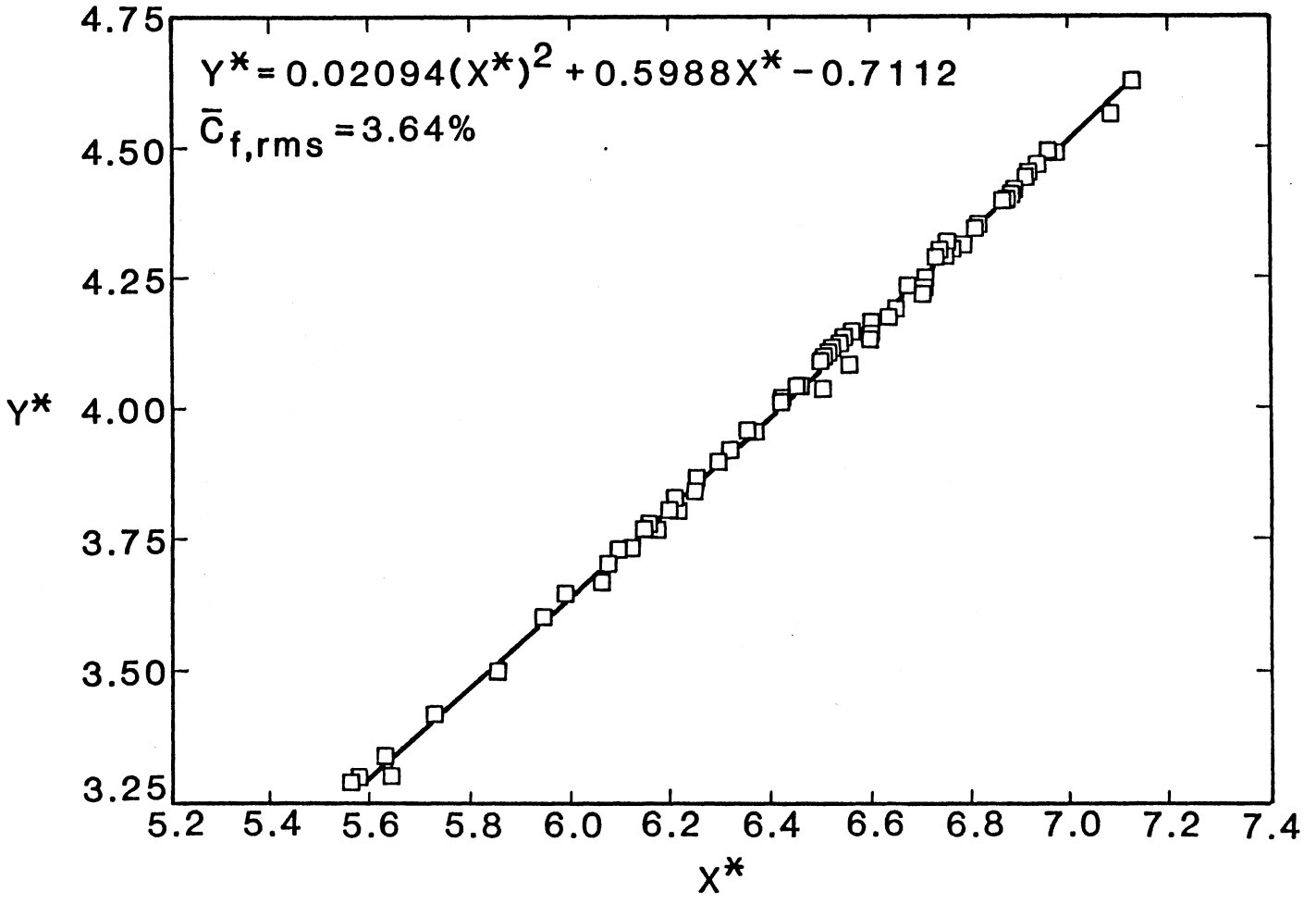

Figure 30. Transitional Correlation for Original Flight Data

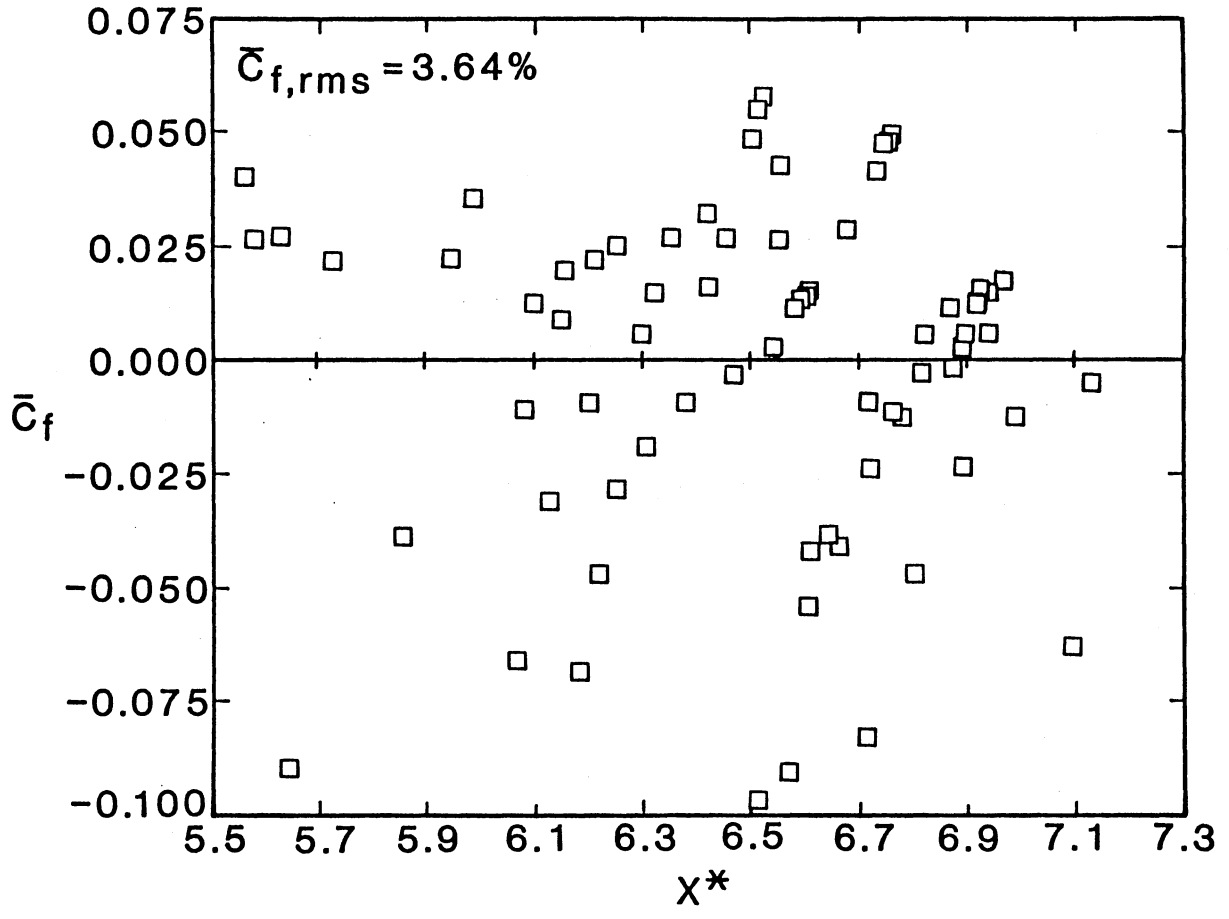

Figure 31. Scatter of Transitional Skin Friction Coefficient About Correlation for Original Flight Data

Not all the available data in trasition are included in the above correlations; only the points at which X^* and Y^* are proportional are included. (These amount to slightly more than 60% of the total number of points in the transition region.) This proportionality requirement is suggested by the basic Equation (4).

Figures 32 and 33 are plots of transitional values of K_{eff} versus R_T in the wind tunnel and flight, respectively. Notice that the data, again, indicate large errors in the flight tests. Before discussing how these errors are corrected, the author first presents the results from the analysis of turbulent data.

The effective Reynolds number distribution based on Equations (48) and (49) is shown in Figure 34. It does not correlate with noise. This situation may change after correcting the experimental data.

4.5 The Turbulent Region

The procedure, which is described in section 4.2, for estimation of a reference $C_{f,T}$ provides an accurate and complete method for theoretical computations of C_f, velocity and enthalpy profiles in the turbulent flow region. Therefore, all the information needed to define X^* and Y^* for this region is available.

The wind tunnel data are corrected in a manner similar to the laminar data, viz., by referencing all cases to case 21.318 ($M = 0.7$, $Re_{FT} = 4 \times 10^6$, $q = 548$ psf). Unlike the laminar data, the $Re_{ft} = 3 \times 10^6$ cases already form continuous curves of K_{eff} versus R, Figure 35. So, the only cases which are shifted are cases 70.726 ($M = 0.7$, $Re_{ft} = 4 \times 10^6$, $q = 538$ psf) and 72.748 ($M = 0.8$, $Re_{ft} = 4 \times 10^6$, $q = 605$).

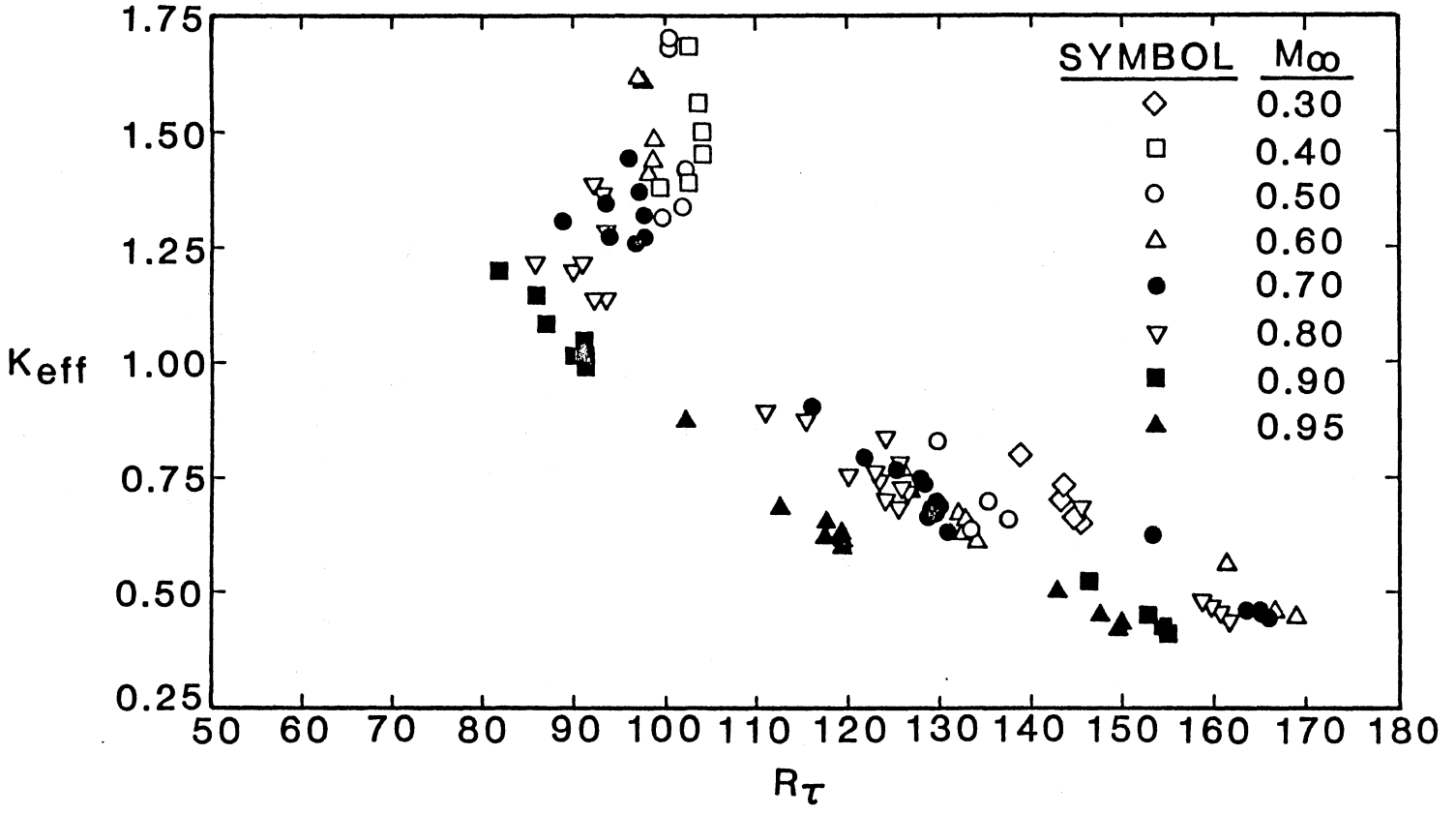

Figure 32. Distribution of Effective Probe Height as Determined from the Original Transitional Wind Tunnel Data

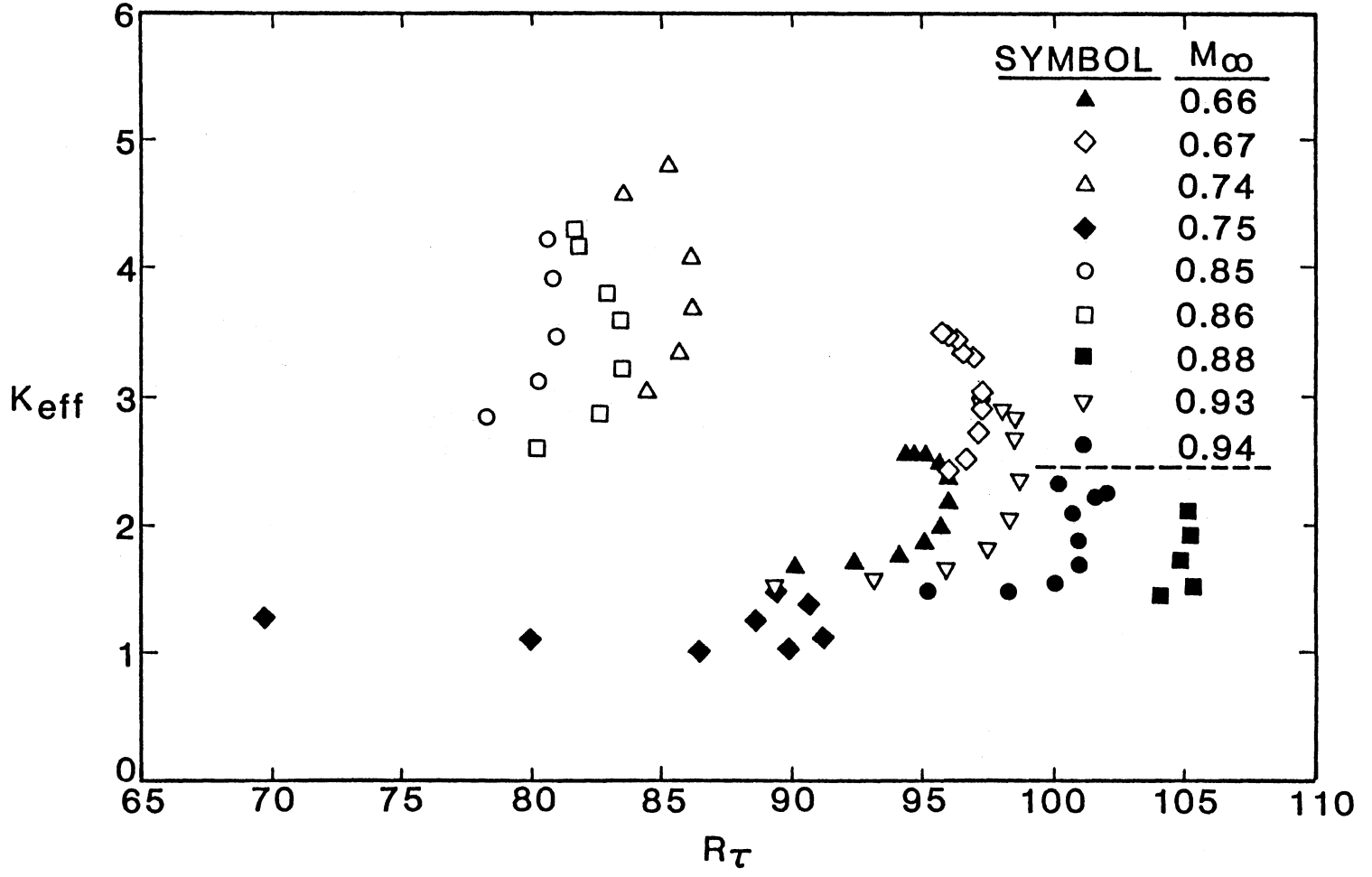

Figure 33. Distribution of Effective Probe Height as Determined from the Original Transitional Flight Data

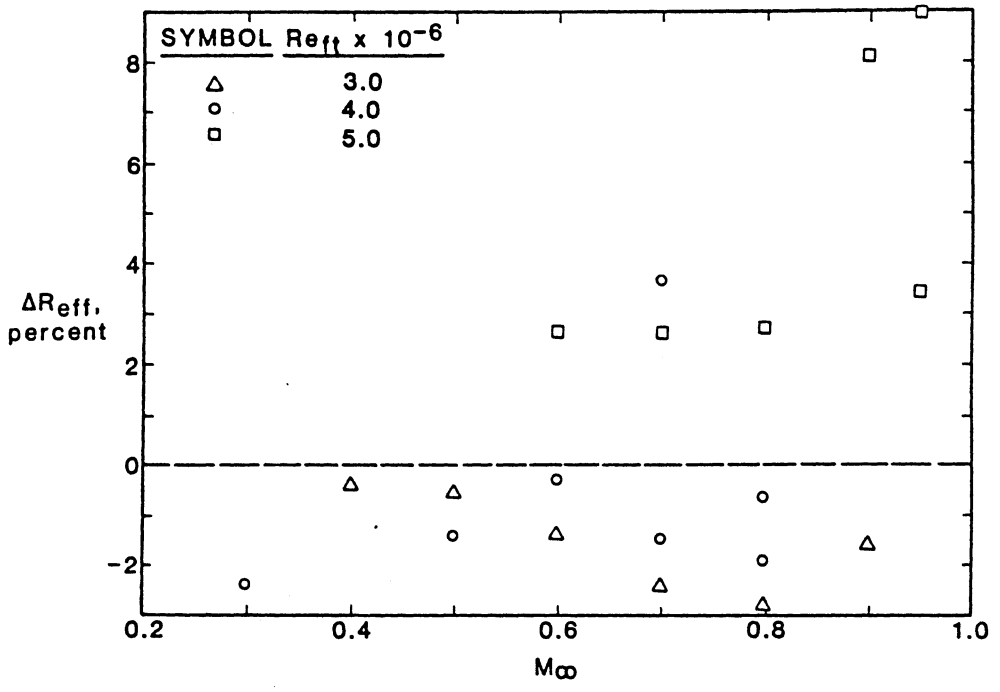

Figure 34. Distribution of Transitional Effective Reynolds Number Based on Original Data

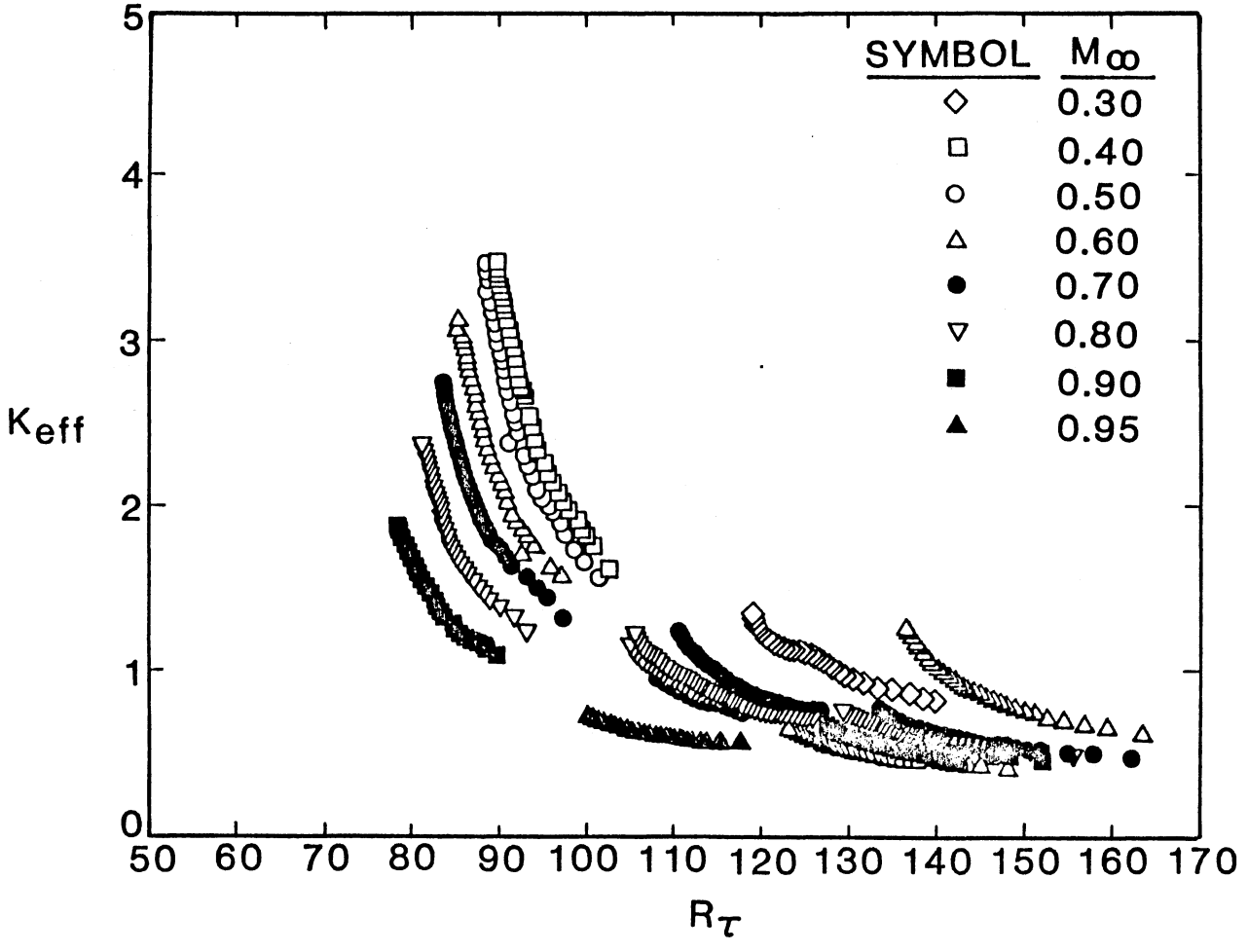

Figure 35. Distribution of Effective Probe Height as Determined from the Original Turbulent Wind Tunnel Data

Similarly, the flight data are corrected in the same manner as the laminar data, see outline at the beginning of this chapter.

The turbulent correlations without corrections are found to be:

Wind Tunnel:

$$Y^* = 0.02337\,(X^*)^2 + 0.5715X^* - 0.6202,$$

$$5.1 < X^* < 6.9.\ 3 \times 10^6 \leq Re_{ft} \leq 5 \times 10^6,\ 0.30 \leq M_\infty \leq 0.95,$$

$$\overline{C}_{f,rms} = 1.20\%, \text{ and} \qquad (50)$$

Flight:

$$Y^* = 0.007512(X^*)^2 + 0.7749X^* - 1.272,$$

$$6.0 < X^* 7.7,\ 2.1 \times 10^6 \leq Re_{ft} \leq 2.8 \times 10^6,\ 0.66 \leq M_\infty \leq 0.94,$$

$$\overline{C}_{f,rms} = 1.10\%. \qquad (51)$$

Equations (50, 51) with the data are plotted in Figures 36 and 37. The scatter of C_f is shown in Figures 38 and 39. Figures 35 and 40 show the distribution of K_{eff} versus R_T. Notice that the relative positions of different flights in Figure 40 is the same as shown in Figure 15. This suggests that the same correction procedure can be successfully applied. It was indeed as will be shown shortly.

The effective Reynolds number distribution based on Equations (50) and (51) is shown in Figure 41. Again, it does not look like the noise curve, Figure 16, which may be caused by the errors in the experimental data. The correction procedure used to correct the laminar data should result in a ΔR_{eff} distribution which is closer to the noise distribution, as can be observed in Figure 23.

4.6 Results After Data Corrections

4.6.1 The Turbulent Region

The turbulent wind tunnel data after shifting a subset of it as

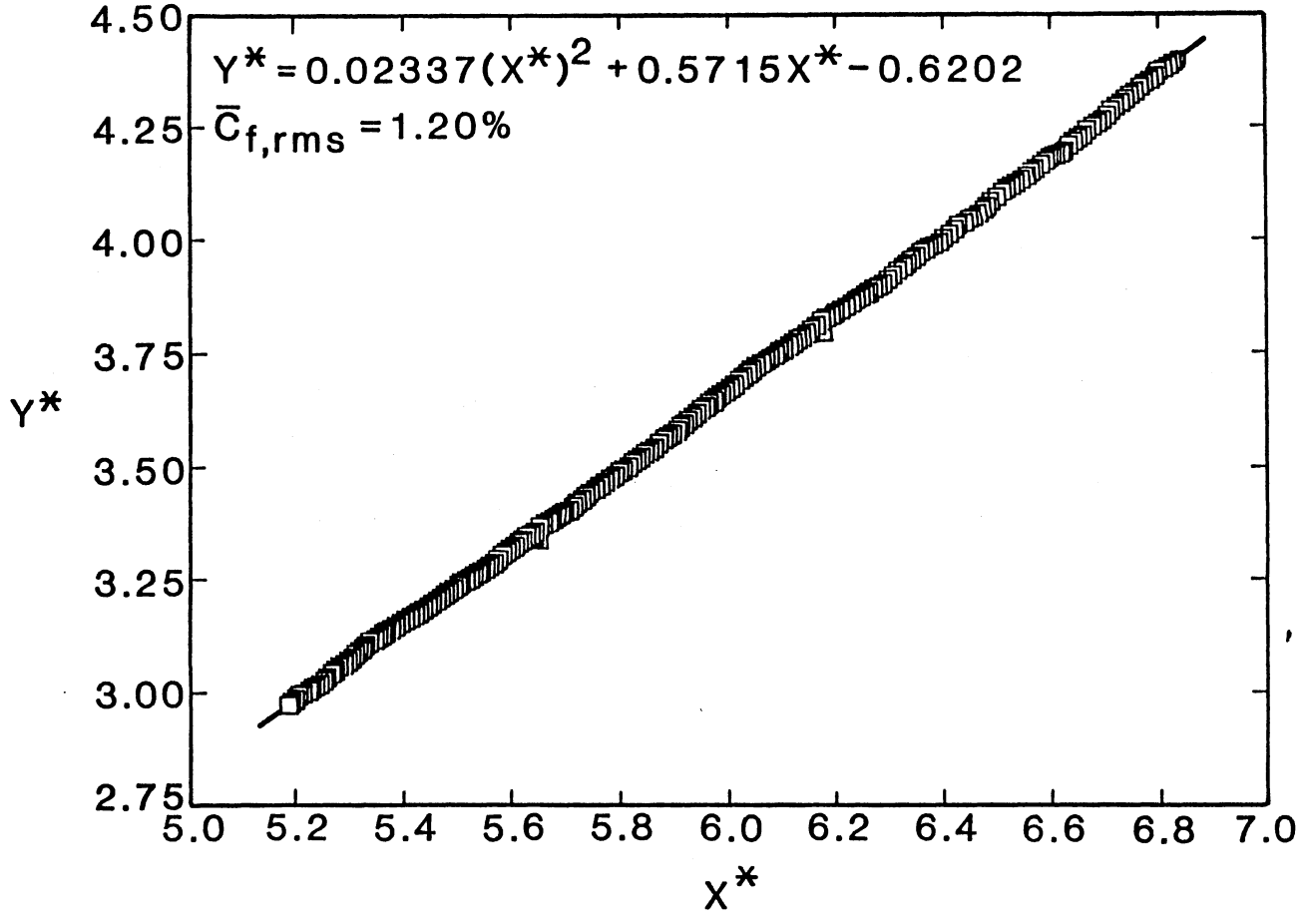

Figure 36. Turbulent Correlation for Original Wind Tunnel Data

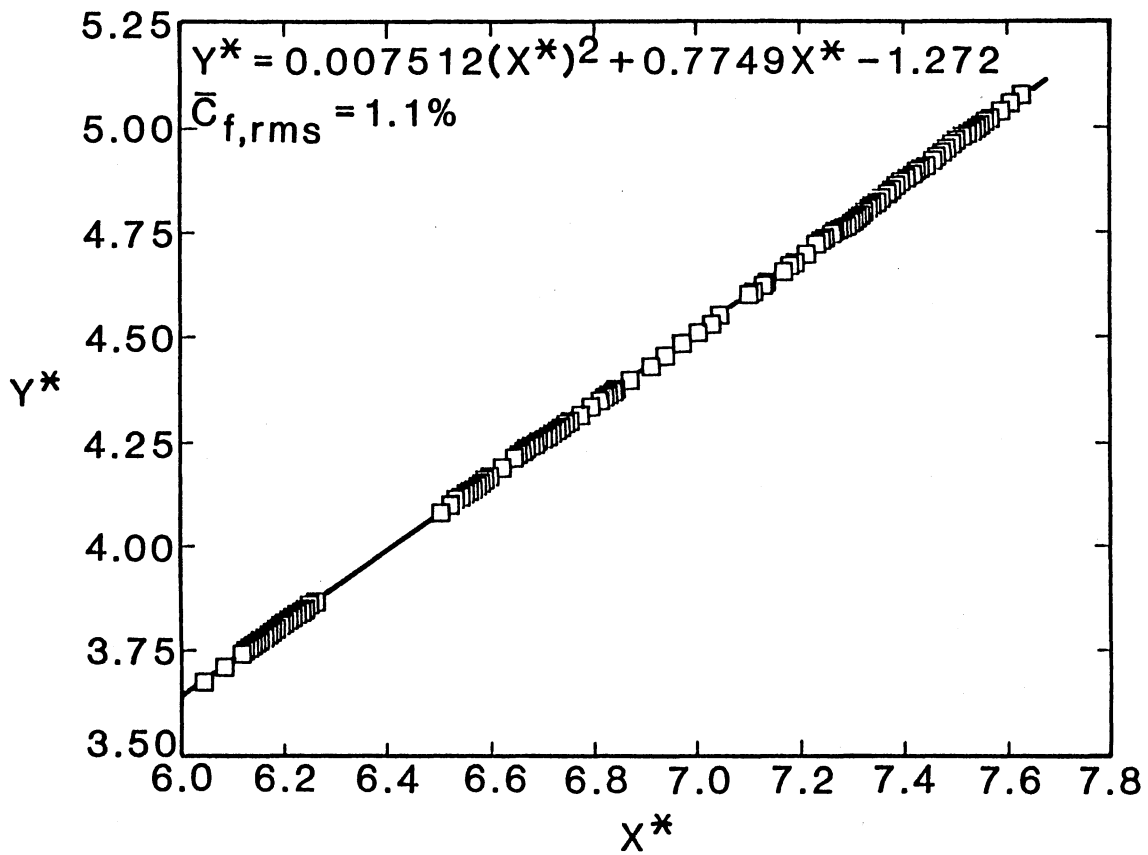

Figure 37. Turbulent Correlation for Original Flight Data

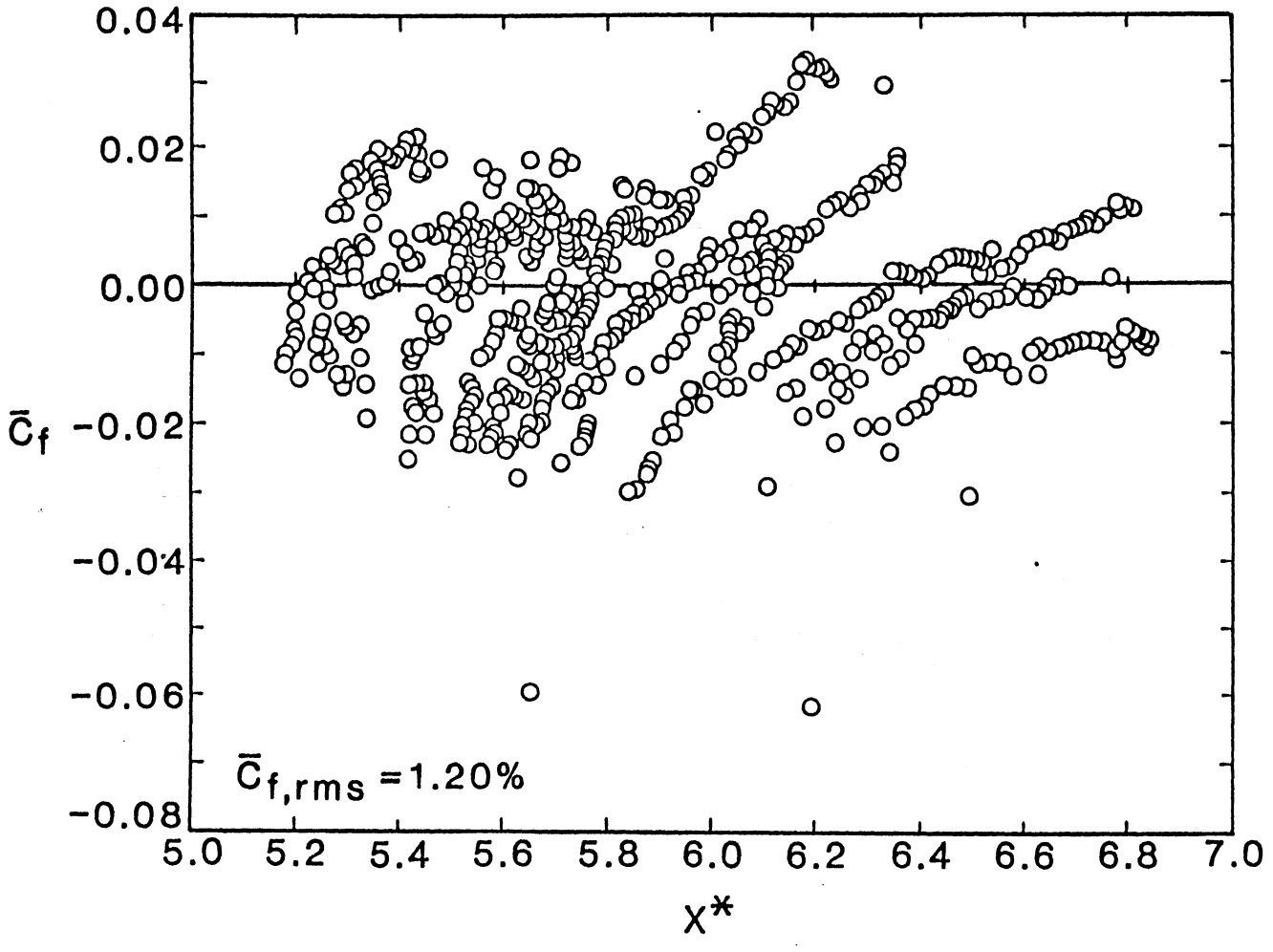

Figure 38. Scatter of Turbulent Skin Friction Coefficient About Correlation for Original Wind Tunnel Data

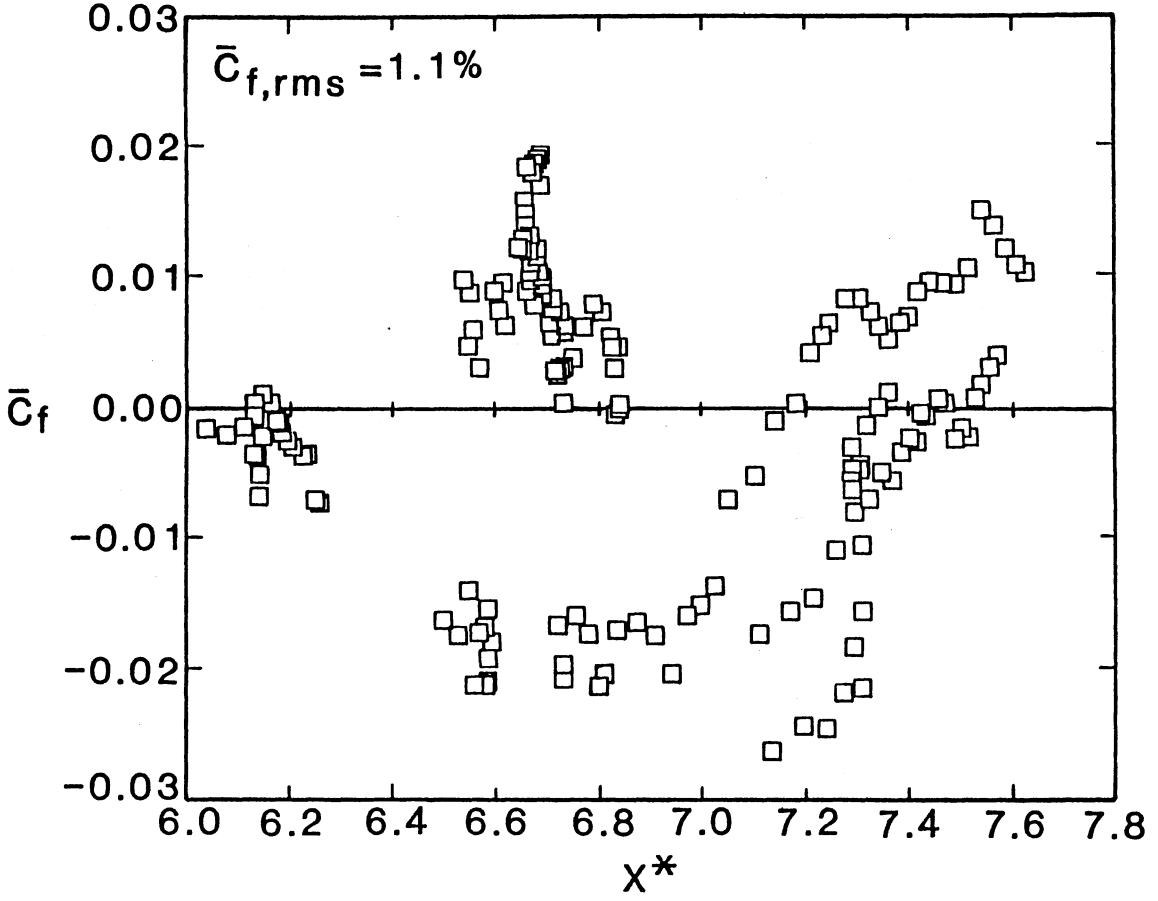

Figure 39. Scatter of Turbulent Skin Friction Coefficient About Correlation for Original Flight Data

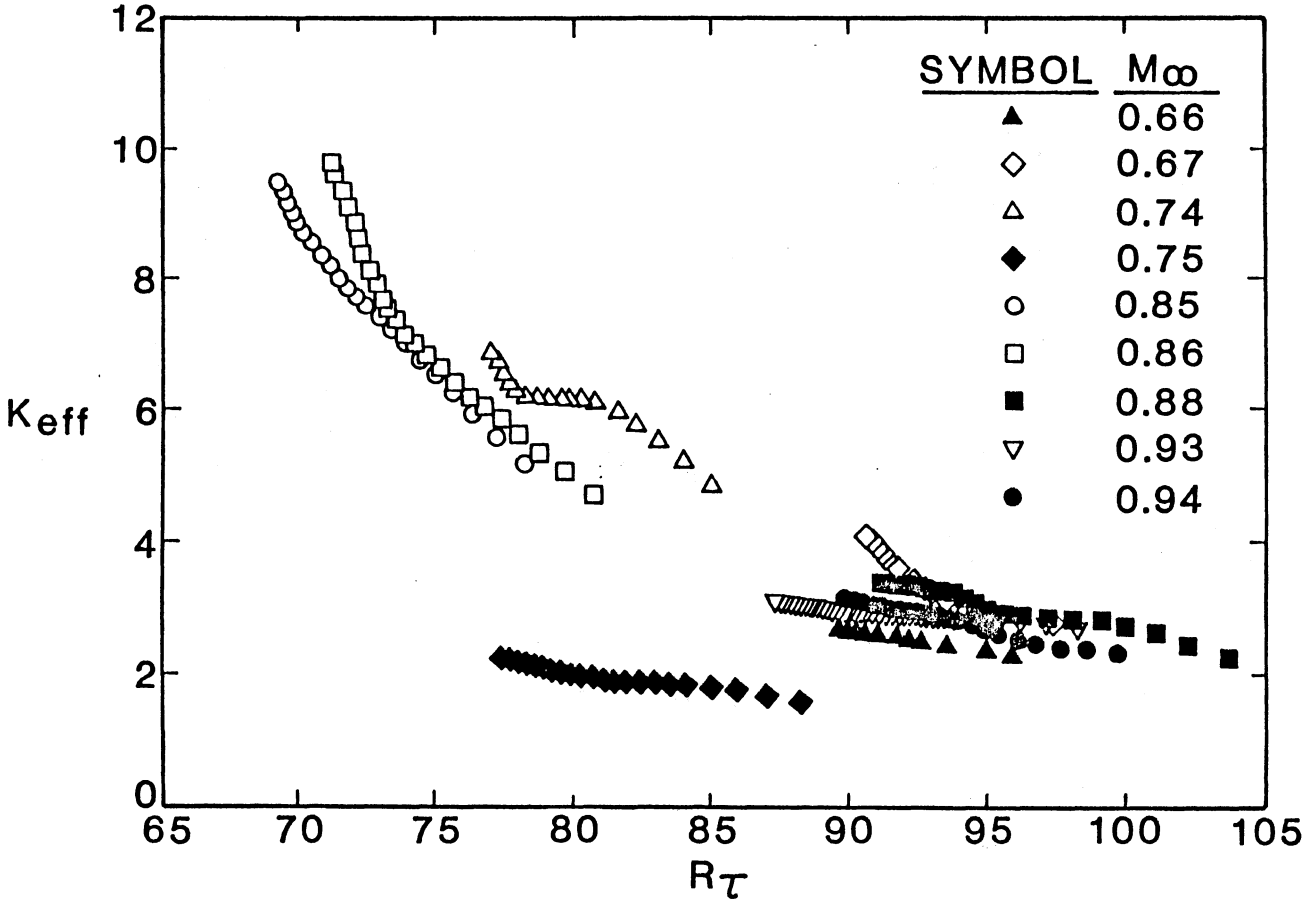

Figure 40. Distribution of Effective Probe Height as Determined from the Original Turbulent Flight Data.

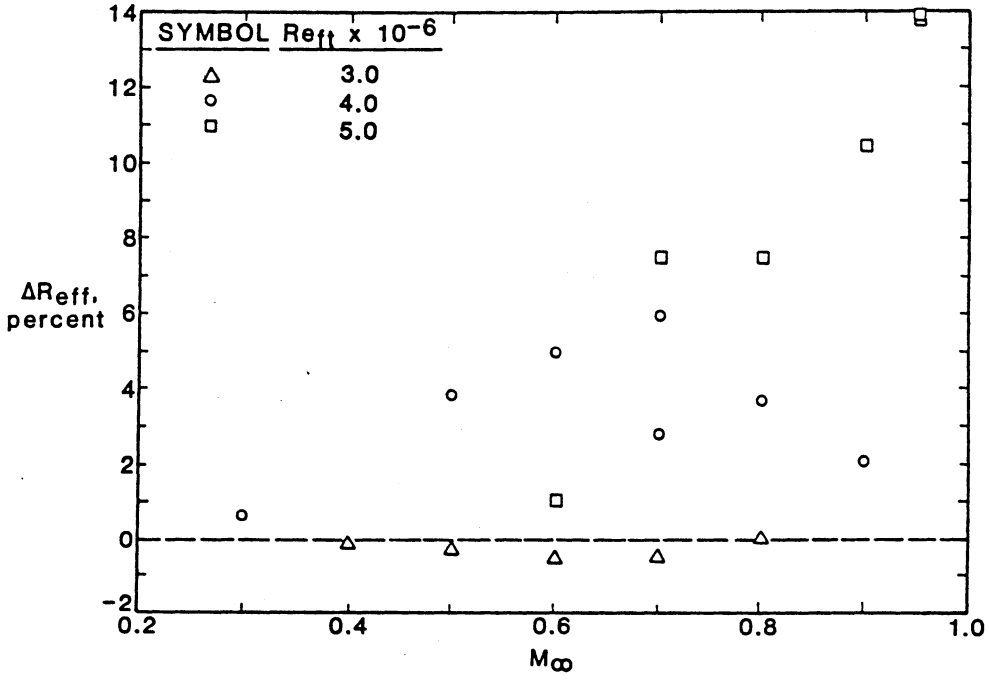

Figure 41. Distribution of Turbulent Effective Reynolds Number Based on Original Data

explained before are shown in Figure 42. The correlation is given by

$$Y^* = 0.02282(X^*) + 0.5782X^* - 0.6409,$$
$$5.1 < X^* < 6.9,$$
$$3 \times 10^6 \leq Re_{ft} \leq 5 \times 10^6, \quad (52)$$
$$0.30 \leq M_\infty \leq 0.95 \text{ and}$$
$$\overline{C}_{f,rms} = 1.20\%.$$

Notice that there is no significant change to the correlation coefficients and accuracy since the shifting was minor. Equation (52) is shown in Figure 43 with the data and the scatter of these data about Equation (52) is shown in Figure 44.

The corrected flight data appear in Figure 45. Notice, again, that the distributions of K_{eff} versus R_τ for individual cases has been altered by the corrected procedure. The flight correlation is given by

$$Y^* = 0.005586(X^*)^2 + 0.7723X^* - 1.1867,$$
$$5.45 < X^* < 6.30,$$
$$2.1 \times 10^6 \leq Re_{ft} \leq 2.8 \times 10^6 \quad (53)$$
$$0.66 \leq M_\infty \leq 0.94 \text{ and}$$
$$\overline{C}_{f,rms} = 0.65\%.$$

This equation and the corrected data are shown in Figure 46 and the data scatter is shown in Figure 47.

Based on Equations (52) and (53), the ΔR_{eff} distribution is shown in Figure 48. The distribution does not bear any resemblance to noise characteristics, Figure 16. This means that despite the data correction, the information contained in them and their correlations are not sufficient to extract the expected $Re_{ft,eff}$ information. The reason for this, it is believed, is the added complexity that was not present in the laminar analysis, namely the vorticity fluctuations, or turbulence,

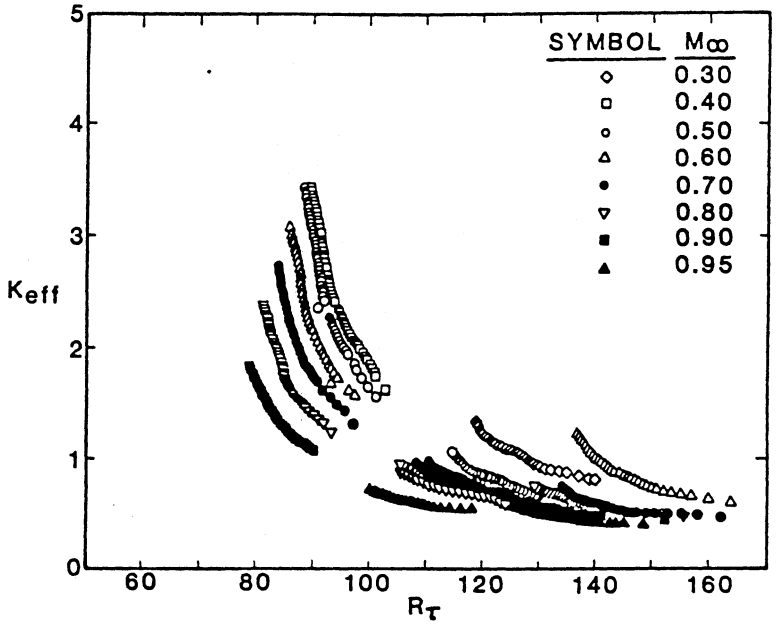

Figure 42. Distribution of Effective Probe Height as Determined from the Shifted Turbulent Wind Tunnel Data

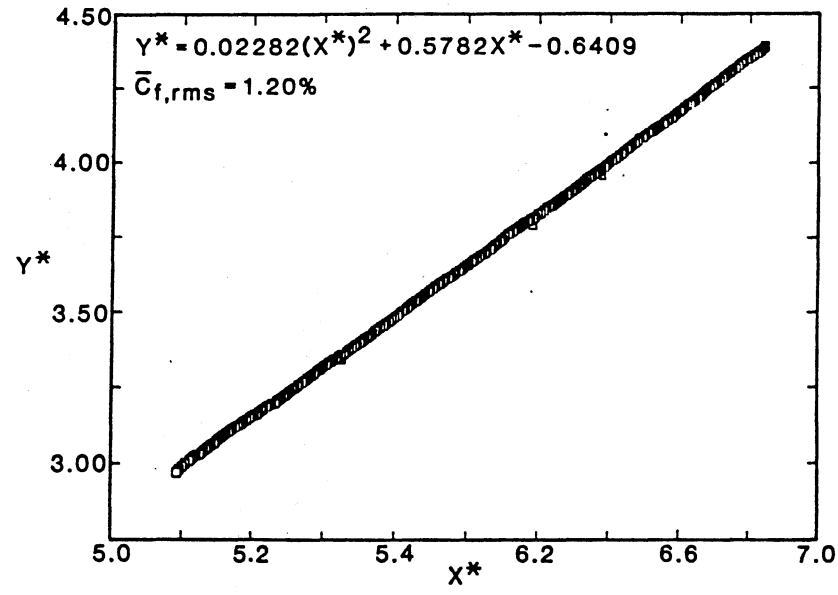

Figure 43. Turbulent Correlation for Shifted Wind Tunnel Data

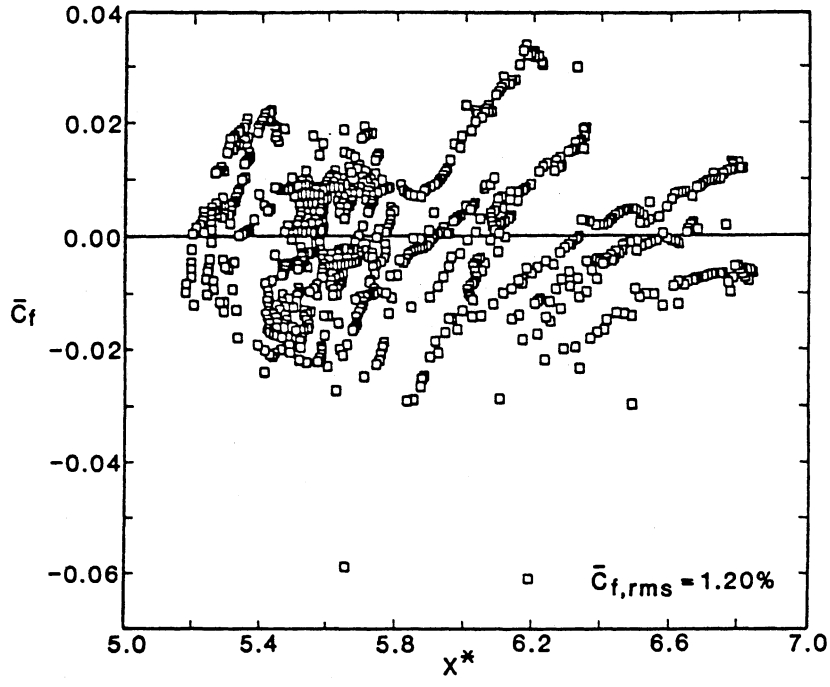

Figure 44. Scatter of Turbulent Skin Friction About Correlation for Shifted Wind Tunnel Data

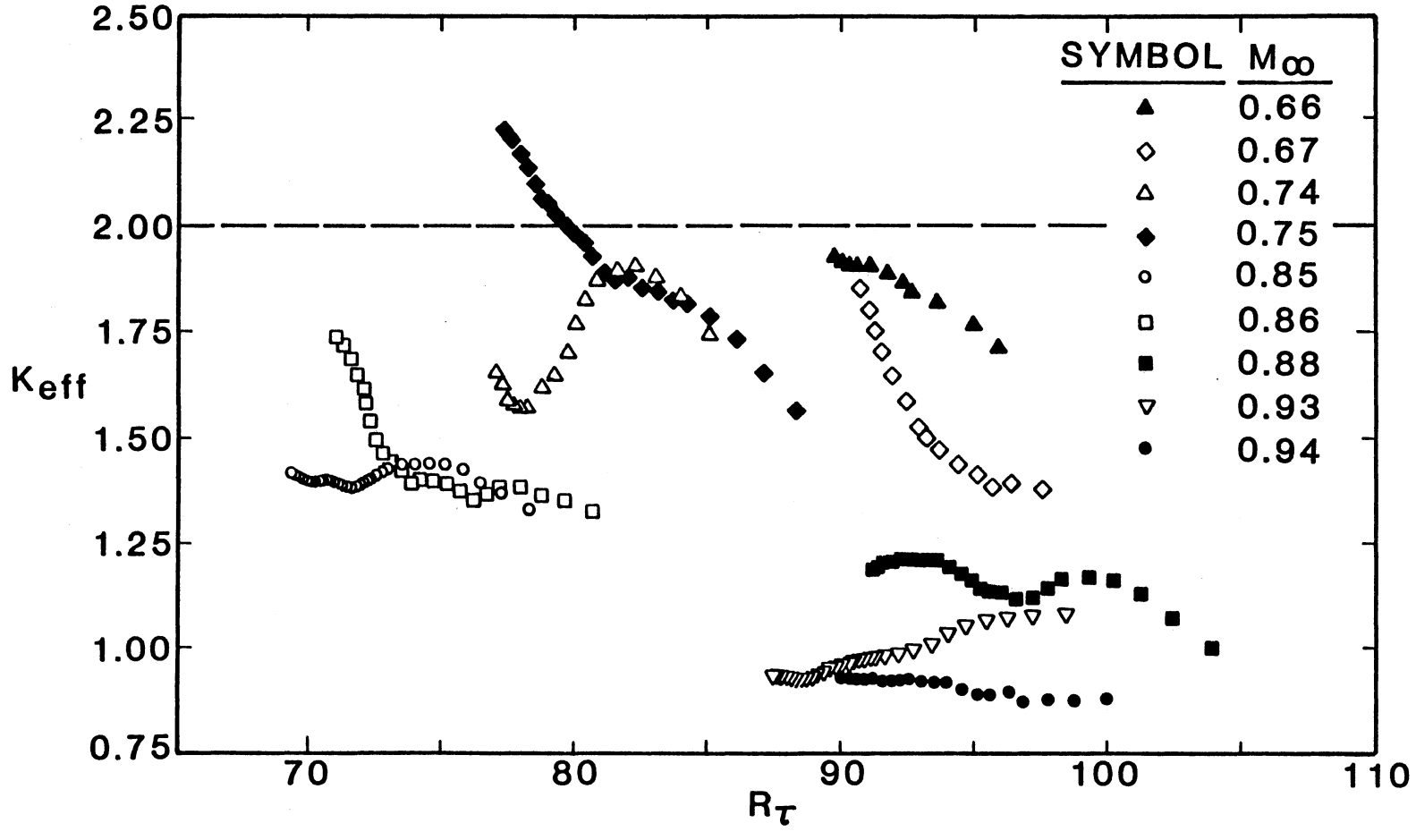

Figure 45. Distribution of Effective Probe Height as Determined from the Corrected Turbulent Flight Data

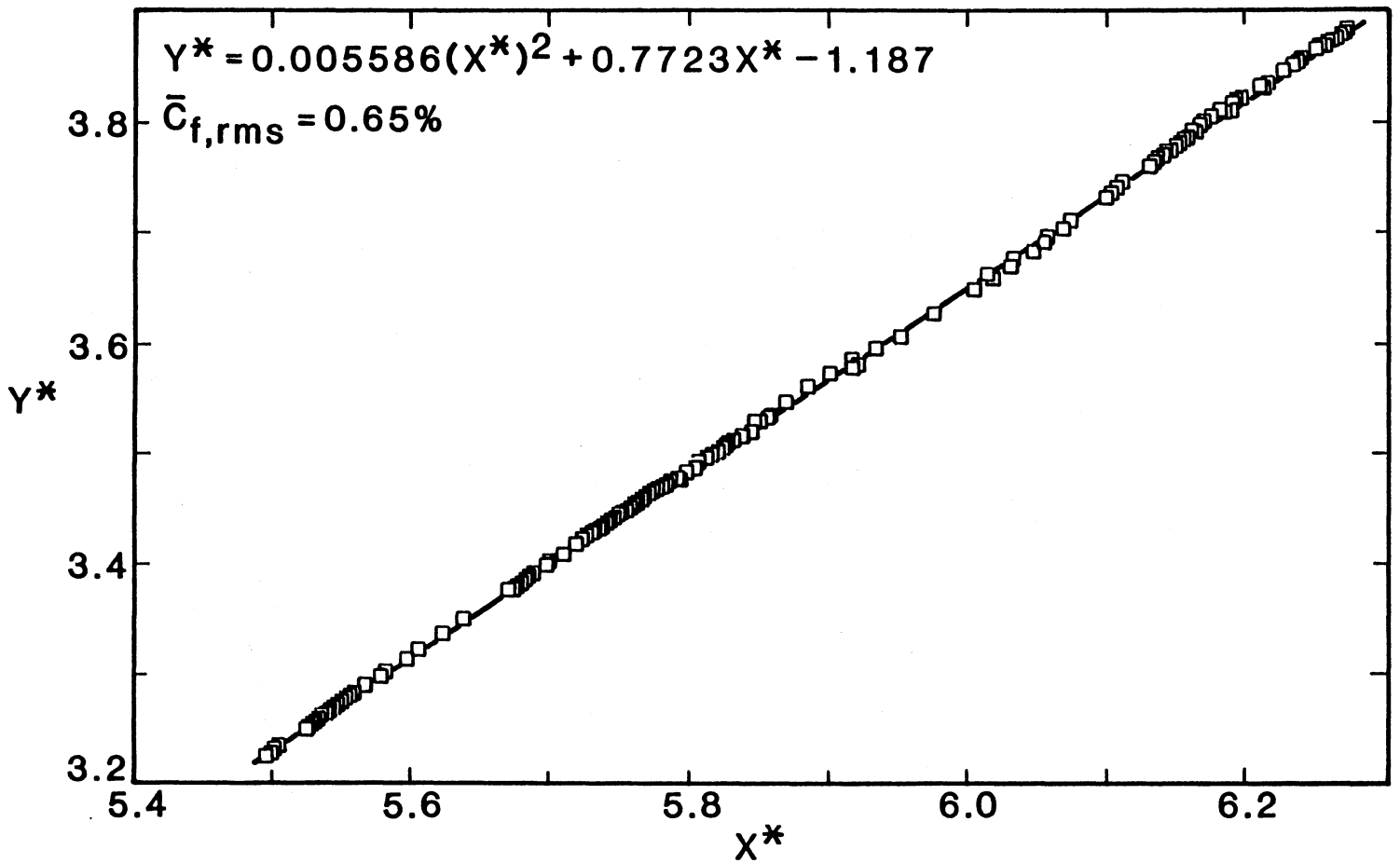

Figure 46. Turbulent Correlation for Corrected Flight Data

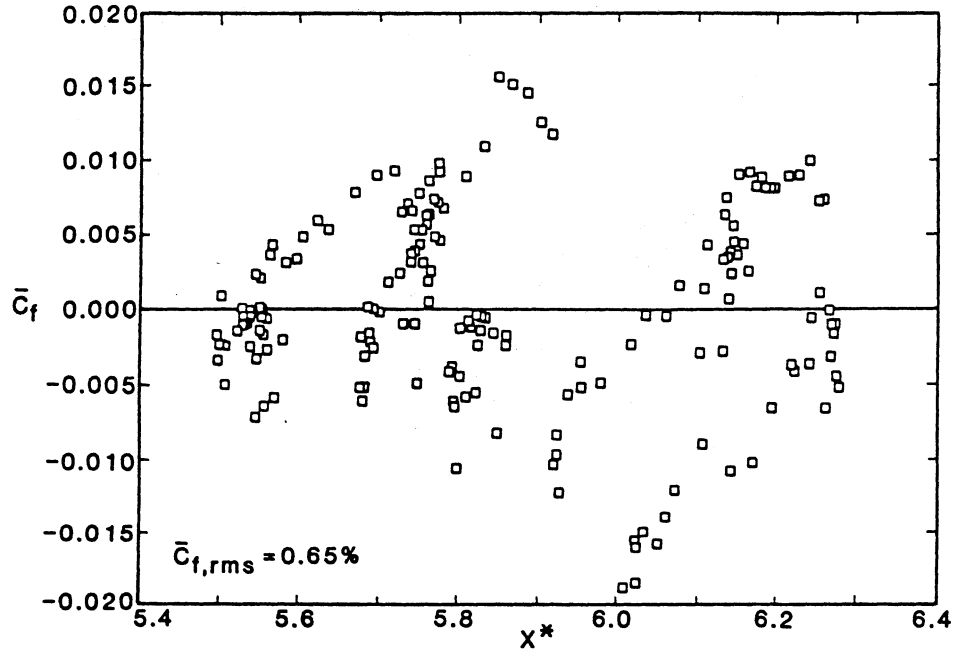

Figure 47. Scatter of Turbulent Skin Friction Coefficient About Correlation for Corrected Flight Data

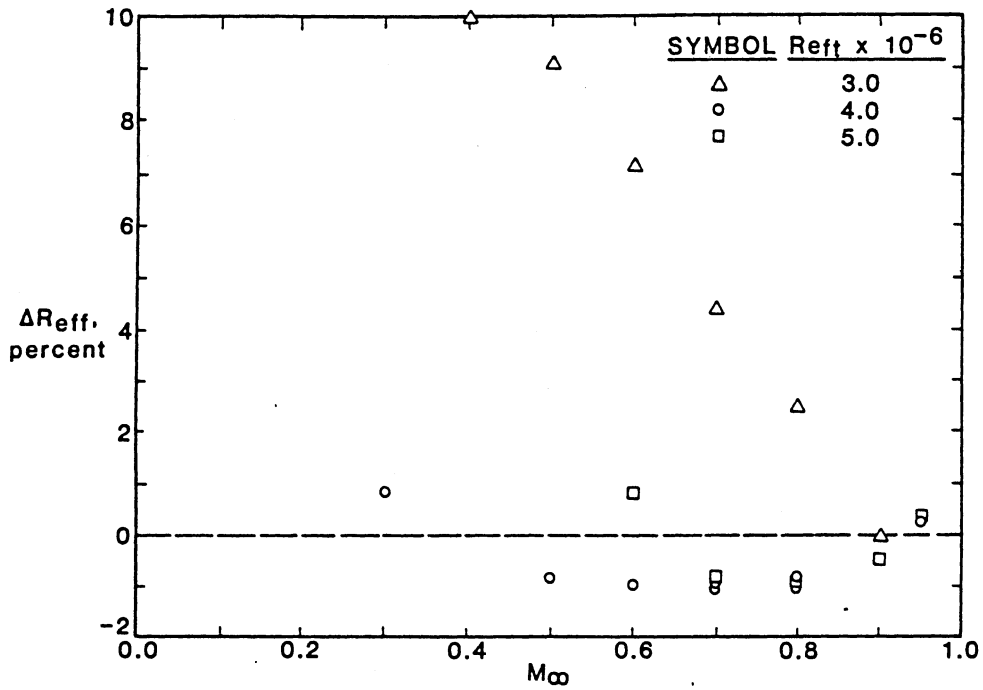

Figure 48. Distribution of Turbulent Effective Reynolds Number Based on Corrected Data

in the boundary layer. These fluctuations are so large they dominate the pressure fluctuations caused by background noise and thus eliminate their effect on Preston-tube measurements. Whitfield and Dougherty (100) reported the results of testing the effects of background noise on transitional and turbulent boundary layers on the AEDC cone in four transonic wind tunnels. They noted that each of these tunnels had an acoustic resonance near $M_\infty = 0.8$, but that the frequency components coming into resonance in these slotted-wall tunnels were so low (< approximately 200 Hz) that the cone boundary layer was insensitive to them and their influence on transition was nil. Weeks and Hodges (98) also concluded that even at noise levels up to $C_{P,rms} = 8\%$ it was not possible to identify any effect of the noise itself on the boundary layer, and they concluded that the acoustic disturbances generally found in the working sections of transonic wind tunnels are unlikely to exert measurable influence on the development of turbulent boundary layers on wind-tunnel models - at least for mild pressure gradient. Raghunathan et al., (81) showed that turbulent skin friction coefficient was hardly affected by noise levels up to $C_{P,rms} = 2\%$. Based on these findings, the value of ΔR_{eff} of turbulent data is expected to be zero for flight and wind tunnel cases with identical freestream flow conditions. Wind tunnel case #56.631 and flight case #333.1354 have similar flow conditions, and ΔR_{eff} for these conditions is indeed near zero, see Figure 46 at $M_\infty = 0.90$. As noted before, Becker and Brown (12) showed that pressure fluctuations decrease the measured Preston-tube pressure. Pressure fluctuations may be caused by background noise and/or by internal boundary layer turbulence. Since vorticity fluctuations in a laminar boundary layer are negligible, background noise and turbulence

are dominant in this region and the data analysis described in this thesis permits the calibration of these environmental effects. In transitional and turbulent boundary layers, on the other hand, internal fluctuations are dominant and background noise has no effect on the measurement of P_p and, therefore, cannot be calibrated. The $Re_{ft} = 3 \times 10^6$ data show the greatest deviation of ΔR_{eff} from zero, Figure 48. The reason is this group of data is the one suffering the greatest experimental uncertainty in the P_p measurement while it is the reference for correcting the flight data ($\overline{R}_\tau$ values at which correction is made correspond to wind tunnel $Re_{ft} = 3 \times 10^6$).

4.6.2 The Transitional Region

In order to insure the continuity of the K_{eff} distribution during transition, the $\Delta P_{o,shift}$ increments used in the correction of flight data must vary gradually from the $\Delta P_{o,shift}$ values used in the laminar correction and those used in the turbulent correction. The author used a linear variation in the following form:

$$\Delta P_{o,shift} = \Delta P_{o,shift,\ell} + \frac{X - X_t}{X_E - X_t} (\Delta P_{o,shift,T} - \Delta P_{o,shift,\ell}).$$

Figure 49 shows the continuous $K_{eff} - R_\tau$ distribution for case 19.289 in the three regions of the boundary layer. The results after shifting the wind tunnel data and correcting the flight data are as follows.

Wind Tunnel:

$$Y^* = 0.7814(X^*)^2 - 0.07967X^* - 1.2936,$$

$$5.25 < X^* < 6.30,$$

$$3 \times 10^6 \leq Re_{ft} \leq 5 \times 10^6,\ 0.30 \leq M_\infty \leq 0.95, \qquad (54)$$

$$\overline{C}_{f,rms} = 2.49\% \text{ and}$$

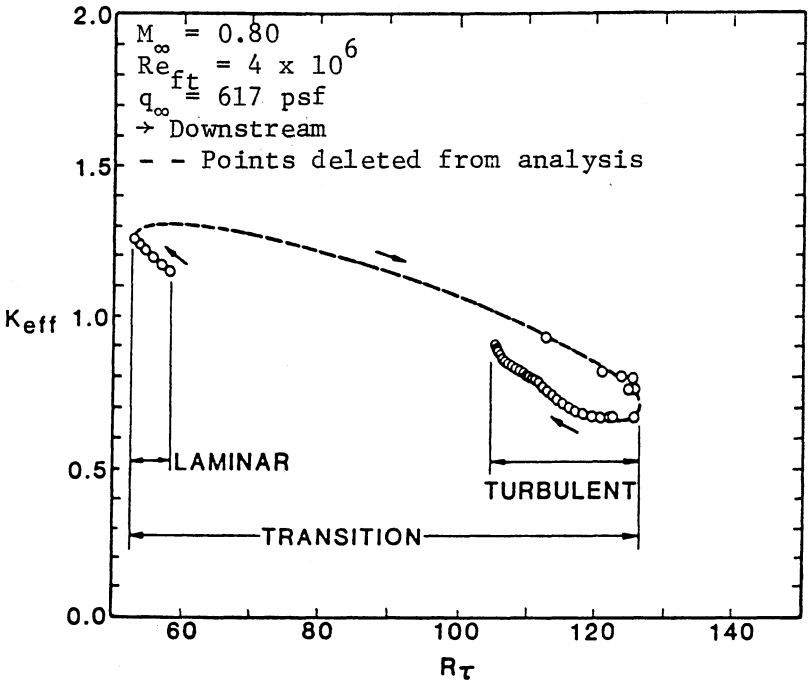

Figure 49. Distribution of Effective Probe Height for a Typical Case in the Three Boundary Layer Regions

Flight:

$$Y^* = 0.09131(X^*)^2 + 0.2596X^* - 1.9066,$$

$$5.4 < X^* < 6.4,$$

$$2.1 \times 10^6 \leq Re_{ft} \leq 2.8 \times 10^6,\ 0.66 \leq M_\infty \leq 0.94 \text{ and} \qquad (55)$$

$$\overline{C}_{f,rms} = 0.65\%.$$

Equation (54) with the wind tunnel data and their scatter are shown in Figures 50, 51. Figure 52 shows the $K_{eff} - R_\tau$ distribution. Figures 53 through 55 show the same for the flight data.

Based on Equation (54) and (55), the ΔR_{eff} distribution is shown in Figure 56. As expected the distribution cannot be correlated with noise effects for the same reason discussed in the turbulent analysis last section. Furthermore, Reed and Abu-Mostafa (82) have shown that the extent of transition, $X_E - X_t$, is larger in flight than in wind tunnel tests with the same flow conditions. This means that the transition process requires a larger distance in flight than in a wind tunnel and the rms values of P_p indicate the laminar break-down in flight is more violent and, hence, creates larger vorticity. This is the reason that ΔR_{eff}'s in Figure 56 are all negative. Indeed $C_{p'_{P,rms}}$ in flight #333.1354 is nearly <u>twice</u> that in wind tunnel case #56.631. (These are the two cases with similar freestream conditions).

The final conclusion, therefore, is that the calibration of wind tunnel environmental effects on Preston-tube measurements or theoretical skin friction by an effective freestream unit Reynolds number can only be achieved by analyzing the <u>laminar</u> data as described in this thesis.

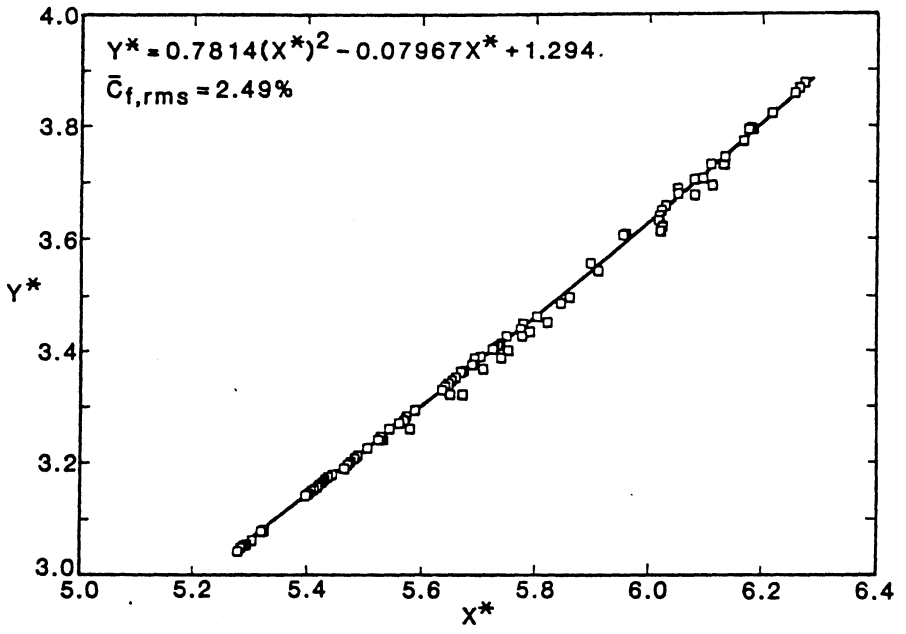

Figure 50. Transitional Correlation for Shifted Wind Tunnel Data

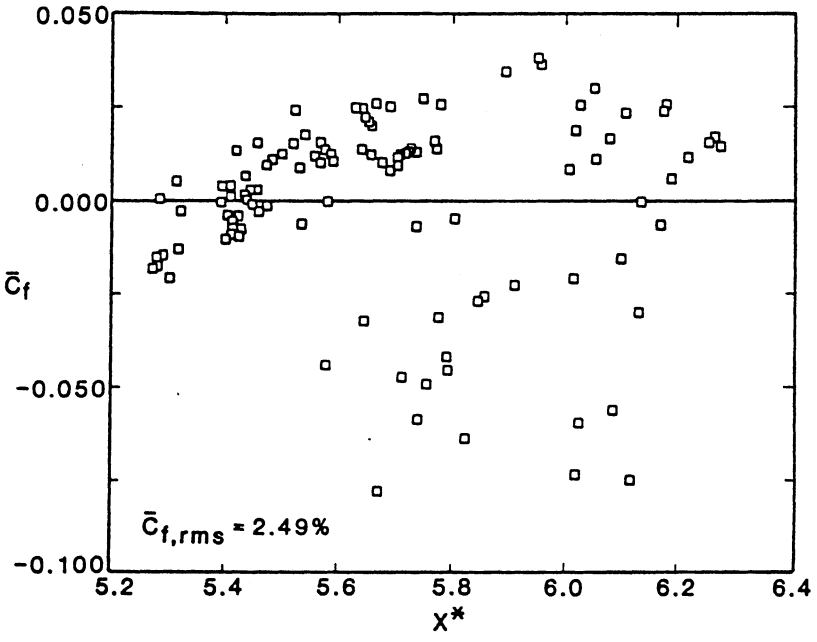

Figure 51. Scatter of Transitional Skin Friction Coefficient About Correlation for Shifted Wind Tunnel Data

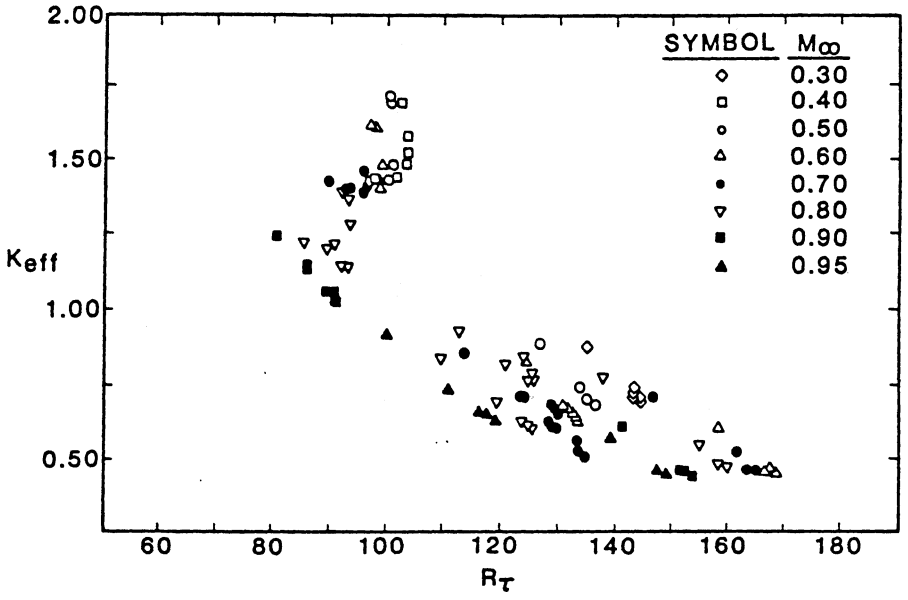

Figure 52. Distribution of Effective Probe Height as Determined from the Shifted Transitional Wind Tunnel Data

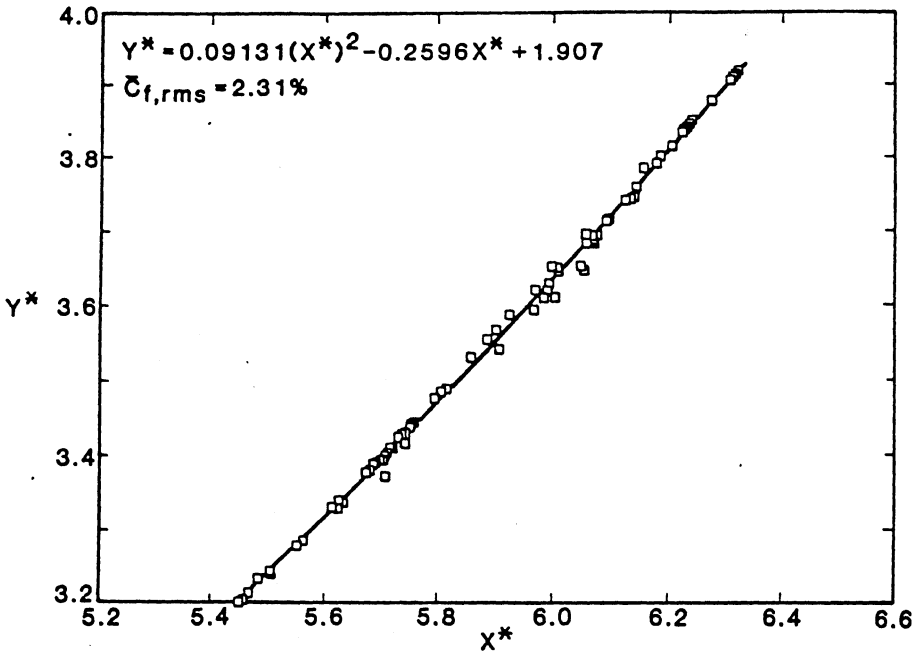

Figure 53. Transitional Correlation for Corrected Flight Data

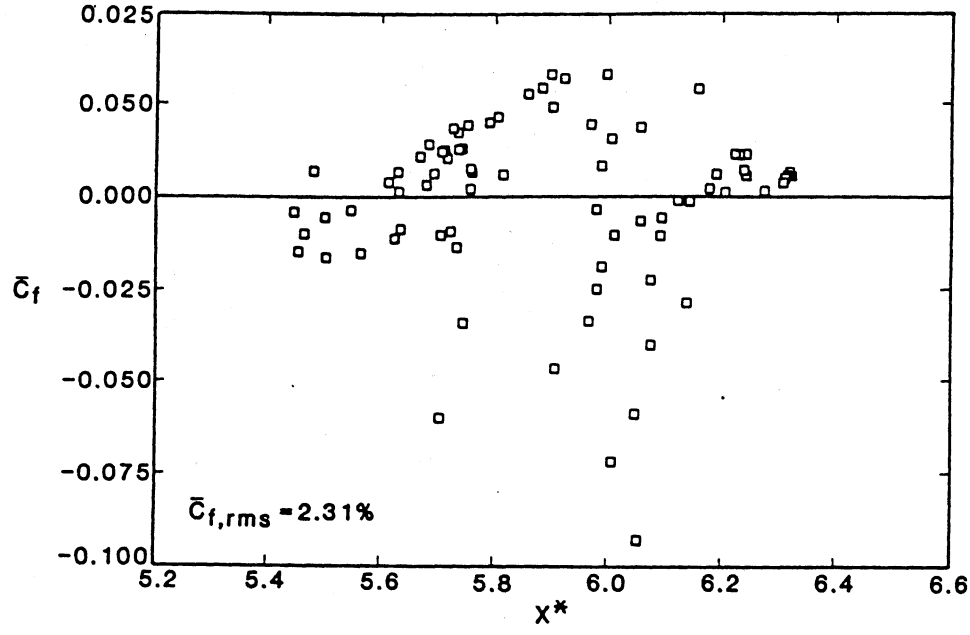

Figure 54. Scatter of Transitional Skin Friction Coefficient About Correlation for Corrected Flight Data

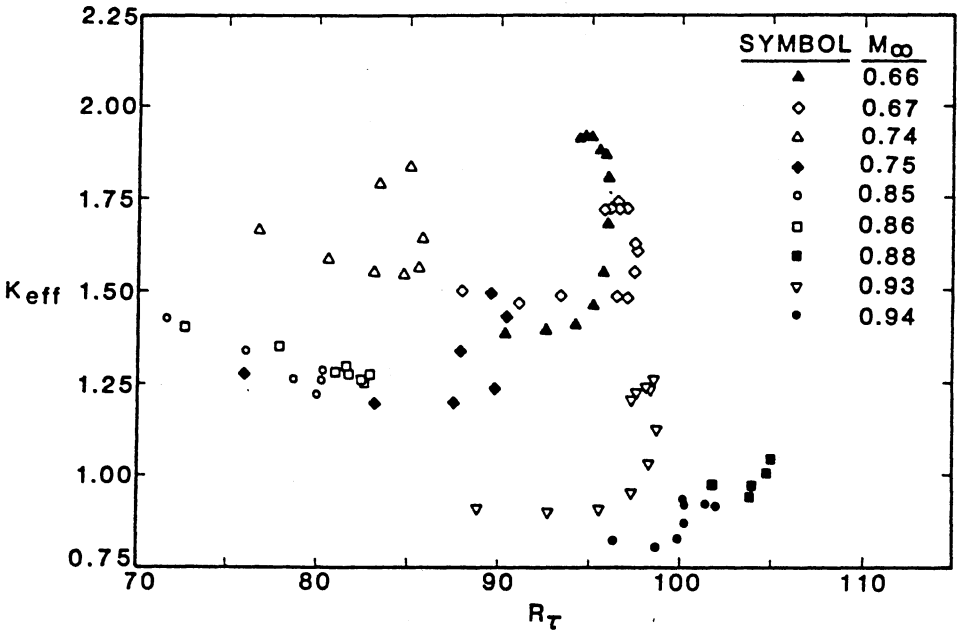

Figure 55. Distribution of Effective Probe Height as Determined from the Corrected Transitional Flight Data

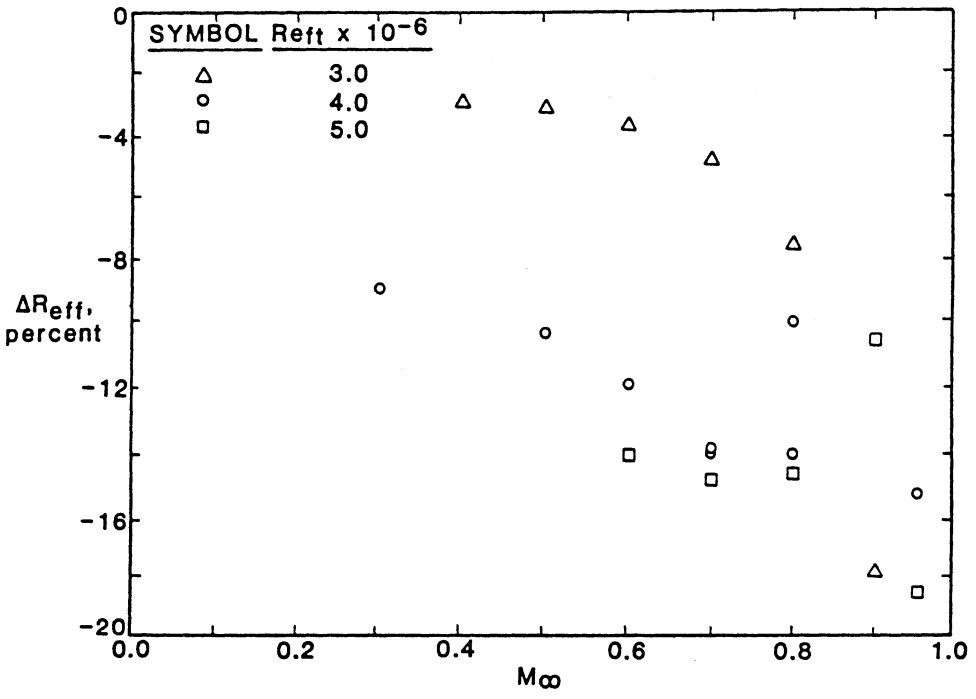

Figure 56. Distribution of Transitional Effective Reynolds Number Based on Corrected Data

CHAPTER V

SUMMARY AND CONCLUSIONS

A new procedure has been developed which uses Preston-tube data from wind tunnel and flight tests of the AEDC Transition Cone to compute an effective unit Reynolds number for transonic wind tunnels. The resulting effective Reynolds numbers are based on the requirement that the average Preston-tube pressure for a given type of boundary layer be equal in the wind tunnel and flight for a given M_∞ and q_∞ but differing Re_{ft}. The procedure has been applied to laminar, transitional, and fully-developed turbulent boundary layers by using wind tunnel data obtained in the 11-TWT. The results for laminar boundary layers indicate that noise in the 11-TWT causes Preston-tube pressures to be low compared to the values that exist in flight for the same M_∞, Re_{ft}, and q_∞. This results in the effective unit Reynolds number being higher than the reference or operating value by approximately 6.5%. Thus, in order to increase the laminar Preston-tube pressures, obtained in the 11-TWT, to match the corresponding flight data, it is necessary to increase the tunnel unit Reynolds number by 6.5%.

This unit Reynolds number trend is opposite to what is found in the technical literature on the effects of noise on boundary layer transition. In that context, transonic wind tunnel noise is known to promote early transition and is frequently viewed as being analogous to an increase in unit Reynolds number. With this perspective of matching

the location of transition, transonic tunnels are thought to have "effective" Reynolds numbers that are somewhat higher than the operating value selected by the tunnel operators. However, if for example a transonic tunnel is operated at a lower unit Reynolds to achieve matching of flight values of transition location on the AEDC cone, one would not expect a match in drag values. In fact, the lower tunnel Reynolds number would result in lower skin friction within both the laminar[1] and turbulent portions of the boundary layer.

Unfortunately, actual measurements of skin friction were not performed in either the wind tunnel or flight tests. Thus, the author was unable to reach any definitive conclusions as to the effects of noise on skin friction measurement per se.

The basic achievements of this study are summarized below.

1. The law-of-the-wall is a valid way to correlate Preston-tube data in the form of Equation (4) or Equation (23).
2. The effective height of a Preston tube is not fixed. It varies with $U_\tau h/\nu_w$, M_∞, aspect ratio and the position of the probe with respect to the wall, Section 2.1.
3. Including a variable K_{eff} in the correlation substantially improves its accuracy, Section 4.1.
4. Plotting K_{eff} versus R_τ permits the detection of errors in experimental data, Section 4.1.
5. Wind-tunnel data can be used to correct errors in P_p measurements in the flight tests. A systematic correction procedure was

---

[1]This assumes that noise does not change the steady-state laminar skin friction in any significant amount.

developed and successfully applied to the flight data, Section 4.2.

6. Preston-tube correlations for laminar, transitional and turbulent data were obtained both for the wind-tunnel and free-flight tests. The flight correlations, Equations (32), (53), and (55) are the first of their kind in the literature.

7. A semi-empirical method has been developed to define and calculate an effective Reynolds number which calibrates environmental effects on Preston-tube measurements in wind tunnels, Section 3.3 and Figure 23.

8. A computational model for the transition zone can be devised using fully-developed turbulent calculations (or measurements) of C_f and transitional Preston-tube pressure measurements without the need for hot-wire measurements of the intermittency factor, γ, Section 4.4.1.

9. The virtual origin of the turbulent boundary layer on the AEDC cone coincides with the onset of transition which is found to occur at the location of minimum P_p, viz., X_t, Section 4.4.

10. Experimental Preston-tube pressure measurements appear to have smaller errors in the turbulent portion of the boundary layer than in the other two portions, compare Figures 11, 33 and 35.

11. The effective freestream unit Reynolds number distribution obtained from the analysis of laminar data is easily correlated with noise data on the AEDC cone, Section 4.3. Therefore, calibration of enviornmental effects in a wind tunnel can be done by calculating ΔR_{eff} using <u>laminar</u> measurements of Preston-tube pressure. Best results are obtained when the freestream flow parameters, M_∞, Re_{ft}, and q_∞, are the same in the tunnel and in flight.

12. The analysis of transitional and turbulent Preston-tube data cannot be used to calculate ΔR_{eff} since vorticity fluctuations in the boundary layer make it insensitive to background noise. The derived $Re_{ft,eff}$'s from these data do not calibrate the tunnel's flow quality, but rather reflect the effect of internal vorticity fluctuations on P_p measurements, Section 4.6.1.
13. Vorticity and pressure fluctuations in transitional boundary layer flow are larger in flight than in the 11-TWT for similar freestream conditions, Section 4.6.2.
14. A traversing Preston-tube is insufficient, by itself, to calibrate the effects of transonic wind-tunnel noise on skin friction measurements of wind-tunnel models. The Preston-tube data must be supplemented with direct measurements of skin friction if this objective is to be achieved.

CHAPTER VI

RECOMMENDATIONS

The calibrating procedure described in this thesis may be used to calibrate environments in other transonic wind tunnels, especially those tunnels where the AEDC cone was tested.

The author recommends that skin friction be measured directly and used in conjunction with Preston-tubes in future wind tunnel and flight tests. This will permit the described calibration procedure to reveal the effects of noise, if any, on skin friction drag.

Care should be taken in measuring Preston-tube pressure in future experiments. Every effort to prevent probe twisting and lifting will reduce experimental errors especially in the flight tests. The gain factor and the reference pressure for the transducer should be accurately recorded.

BIBLIOGRAPHY

(1) Abu-Mostafa, A.S., "Correlation of Theoretical Laminar Skin Friction with Preston Tube Measurements on a Subsonic Cone." (Unpub. M.S. Report, Oklahoma State University, School of Mech. and Aero. Eng., Stillwater, Oklahoma, 1980).

(2) Adams, J.C., Jr. and B.K. Hodge. "Extended Mixing-Length Applications to Compressible Turbulent Boundary Layer." AIAA Jour., Vol. 16, No. 7 (July 1978), pp. 643-644.

(3) Allen, J.M. "Critical Preston-Tube Size." AIAA Jour., Vol. 7, No. 3 (1970), pp. 285-287. (1970).

(4) Allen, J.M. Evaluation of Compressible-Flow Preston Tube Calibrations. NASA TN D-7190, 1973.

(5) Allen, J.M. "Evaluation of Preston Tube Calibration Equations in Supersonic Flow." AIAA Jour., Vol. 11, No. 11 (Nov. 1973).

(6) Allen, J.M. "Reply by Author to P. Bradshaw and K. Unsworth." AIAA Jour., Vol. 12, No. 9 (Sept. 1974), pp. 1295-1296.

(7) Allen, J.M. Experimental Study of Error Sources in Skin-Friction Balance Measurements. NASA TN D-8291, Oct. 1976.

(8) Allen, J.M. Reevaluation of Compressible-Flow Preston Tube Calibrations. NASA TM X-3488, 1977.

(9) Allen, J.M. "An Improved Sensing Element for Skin-Friction Balance Measurements." AIAA Jour., Vol. 18, No. 11 (Nov. 1980).

(10) Ames Research Staff. Equations, Tables and Charts for Compressible Flow. NACA Report No. 1135, 1953.

(11) Arora, R., K.K. Kuo and M.K. Razdan. "Near-Wall Treatment for Turbulent Boundary-Layer Computations." AIAA Jour., Vol. 20, No. 11 (Nov. 1982), pp. 1481-1482.

(12) Becker, H.A. and A.P.G. Brown. "Response of Pitot Probes in Turbulent Streams." Jour. of Fluid Mechanics, Vol. 62, Part 1 (1974), pp. 85-114.

(13) Benek, J.A. and M.D. High. A Method for the Prediction of the Effects of Free-Stream Disturbances on Boundary-Layer Transition. AEDC-TR-73-158, Oct. 1973.

(14) Benek, J.A. and M.D. High. "Transition Prediction Technique." AIAA Jour., Vol. 12, No. 10 (Oct. 1974).

(15) Bertelrud, A. "Preston Tube Calibration Accuracy." AIAA Jour., Vol. 14, No. 1 (Jan. 1976), pp. 98-100.

(16) Bertelrud, A. "Total Head/Static Measurements of Skin Friction and Surface Pressure." AIAA Jour., Vo. 15, No. 3 (March 1977), pp. 436-438.

(17) Bradshaw, P. and D.H. Ferriss. The Effect of Initial Conditions on the Development of Turbulent Boundary Layers. London: Aero. Research Council, C.P. No. 986, Feb. 1967.

(18) Bradsaw, P. and K. Unsworth. A Note on Preston Tube Calibrations in Compressible Flow. London: Imperial College of Science and Tech., Dept. of Aero., Report No. 73-07, Sept. 1973.

(19) Bradshaw, P. and K. Unsworth. "Comment on 'Evaluation of Preston Tube Calibration Equations in Supersonic Flow'." AIAA Jour., Vol. 12, No. 9 (Sept 1974).

(20) Bryer, D.W. and R.C. Pomkhurst. Pressure-Probe Methods for Determining Wind Speed and Flow Direction. London: National Physics Lab., 1971.

(21) Bushnell, D.M., and D.W. Alston. "Calculation of Transitional Boundary-Layer Flows" AIAA Jour. Vol. 11, No. 4 (April 1973), pp. 554-556.

(22) Cebeci, T. and K.C. Chang. "Calculation of Incompressible Rough-Wall Boundary-Layer Flows." AIAA Jour., Vol. 16 (July 1978), No. 2, pp. 730-735.

(23) Chew, Y.T. "Two-Parameter Skin-Friction Formula for Adiabatic Compressible Flow." AIAA Jour., Vol. 16, No. 2 (Feb. 1978), pp. 186-188.

(24) Chue, S.H. "Pressure Probes for Fluid Measurements." Prog. Aerospace Science, Vol. 16, No. 2 (1975), pp. 147-221.

(25) Crawford, M.E., and W.M. Kays. STAN5 - A Program for Numerical Computation of Two-Dimensional Internal/External Boundary Layer Flows. Report No. HMT-23, Dept. Of Mech. Eng., Stanford Univ. Dec. 1975.

(26) Credle, O.P. "Perforated Wall Noise on the AEDC-PWT 16-Ft and 4-Ft Transonic Tunnels." AEDC TR-71-216, Oct. 1971.

(27) Credle, O.P and W.E. Carleton. Determination of Transition Reynolds Number in the Transonic Mach Number Range. AEDC-TR-70-218, Oct. 1970.

(28) Depooter, K., E. Brundrett, and A.B. Strong. "The Calibration of Preston Tubes in Transpired Turbulent Boundary Layers." Transactions of the ASME, Vol. 100 (March 1978), pp. 10-15.

(29) Dhawan, S. and R. Narasimha. "Some Properties of Boundary Layer Flow During the Transition from Laminar to Turbulent Motion." Jour. of Fluid Mech., Vol. 3 (1958), pp. 418-436.

(30) Dougherty, N.S., Jr. and D.B. Fisher. "Boundary Layer Transition on a 10-Degree Cone: Wind Tunnel/Flight Data Correlation." AIAA Paper No. 80-0154 (Jan. 1980).

(31) Dougherty, N.S., Jr. and D.F. Fisher. Boundary-Layer Transition Correlation on a Slender Cone in Wind Tunnels and Flight for Indications of Flow Quality. AEDC-TR-81-26, Feb. 1982.

(32) Dougherty, N.S., Jr., and F.W. Steinle, Jr. "Transition Reynolds Number Comparisons in Several Major Transonic Tunnels." AIAA Paper No. 74-627 (July 1974).

(33) Emmons, H.W. "The Laminar-Turbulent Transition in a Boundary Layer - Part I." Jour. of Aero. Sci., Vol. 18 (July 1952), pp. 490-498.

(34) Fisher, M.C. and L.M. Weinstein, "Three-Dimensional Hyperosnic Transitional/Turbulent Mean Flow Profiles." AIAA Paper No. 73-635 (July 1973).

(35) Fisher, D.F., and N.S. Dougherty, Jr. In-Flight Measurements of Transition Reynolds Number on a 10-Deg Cone at Mach Numbers from 0.5 to 2.0. NASA TP-1971, June 1982.

(36) Forest, A.E. "Engineering Predictions on Transitional Boundary Layers." AGARD-CP-224, Paper No. IV-22, Oct. 1977.

(37) Franklin, R.E. and J.M. Wallace. "Errors in Measurements of Static-Hole Error Using Flush Transducers." Jour. of Fluid Mechanics, Vol. 42, Part 1 (June 1970).

(38) Graham, J.E., W.L. Hankey and J.S. Shang. "Navier-Stokes Solution of a Slender Body of Revolution at Large Incidence." AIAA Paper No. 80-0190 (Jan. 1981).

(39) Granville, P.S. "The Determination of the Local Skin Friction and the Thickness of Turbulent Boundary Layers from the Velocity Similarity Laws." International Shipbuilding Progress, Vol. 7, No. 69 (May 1960).

(40) Granville, P.S. "The Prediction of Transition From Laminar to Turbulent Flow in Boundary Layers on Bodies of Revolution." NSRDC 3900, AS 787-060 (Sept. 1974).

(41) Gupta, R.P. "New Device for Skin-Friction Measurement in Three-Dimensional Flows." AIAA Jour., Vol. 13, No. 2 (Feb. 1975), pp. 236-238.

(42) Harvey, W.D. Influence of Free-Stream Disturbances on Boundary-Layer Trasition. NASA TM-78635, April 1978.

(43) Harvey, W.D., P.C. Stainback, and F.K. Owen. Evaluation of Flow Quality in Two Large NASA Wind Tunnels at Transonic Speeds. NASA TP-1737, Dec. 1980.

(44) Hebbar, K.S. and P.A. Paranjpe. "Laminar Sublayer Thickness in Compressible Turbulent Boundary Layers." Jour. of Aircraft, Vol. 6. No. 5 (Sept. 1969).

(45) Head, M.R. and V.V. Ram. "Simplified Presentation of Preston Tube Calibration." The Aero. Quarterly (Aug. 1971), pp. 295-300.

(46) Head, M.R. and I. Rechenberg. "The Preston Tube as A Means of Measuring Skin Friction." Jour. of Fluid Mech., vol. 14, pp. 1-17.

(47) Huprikar, A.G. "Evaluation Method for Transonic Cone Boundary-Layer Transition data by Means of Computer Simulation." (Unpub. M.S. Report, Oklahoma State Univ., School of Mech. and Aero Eng., Stillwater, Dec. 1978).

(48) Jaffe, N.A., T.T. Okamura, and A.M.O. Smith. "Determination of Spatial Amplification Factors and Their Application To Predicting Transition." AIAA Jour., Vol. 8, No. 2 (Feb. 1970).

(49) Jones, B.M. "Flight Experiments on the Boundary Layer." First Wright Brothers' Lecture, Dec. 1937, Reprinted in Astro. and Aero., Feb. 1981.

(50) Karamcheti, K. Principles of Ideal-Fluid Aerodynamics. Wiley, 1966.

(51) Kays, W.M. Convective Heat and Mass Transfer. McGraw-Hill, 1966.

(52) Kim, M.D., R.R. Thareja, and C.H. Lewis. "Three-Dimensional Viscous Flowfield Computations in a Streamline Coordinate System." AIAA Paper No. 81-0401 (Jan. 1981).

(53) Lessman, R.C. "Intermittent Transition Flow in a Boundary Layer." AIAA Jour., Vol. 15, No. 11 (Nov. 1977), pp. 1656-1658.

(54) Lin, A. and S.G. Rubin. "Three-Dimensional Supersonic Viscous Flow Over A Cone at Incidence." AIAA Paper No. 81-0192 (Jan. 1981).

(55) Lin, A., S.G. Rubin and G.F. Widhopf. "A Two-Layer Model for Coupled Three Dimensional Viscous and Inviscid Flow Calculation." AIAA Paper No. 81-0118 (Jan. 1981).

(56) Loehrke, R.I. and H.M. Nagib. "Experiments on Management of Freestream Turbulence." AGARD-R-598, Sept. 1971.

(57) Mabey, D.G. "Boundary Layer Transition Measurements on the AEDC 10^0 Cone in the RAE Wind Tunnels and Their Implications." Aero. Research Council (R & M), No. 3821 (June 1976).

(58) Mack, L.M. Boundary Layer Stability Theory. NASA CR-131501, 1969.

(59) Mack, L.N. "Transition Predictions and Linear Stability Theory." AGARD-CP-224, Paper No. I-1, Oct. 1977.

(60) McCanless, G.F., Jr. and J.R. Boone. "Noise Reduction in Transonic Wind Tunnels." Jour. of Acoust. Soc. of America, Vol. 56, No. 5 (Nov. 1974).

(61) McDonald, H. and R.W. Fish. "Practical Calculations of Transitional Boundary Layers." AGARD-AG-164, Paper I-2 (April 1982), pp. 29-53.

(62) McMillan, F.A. "Experiments on Pitot-Tubes in Shear Flow." R & M Jour., No. 3028 (1957).

(63) Meier, H.U. and H-P Kreplin. "Influence of Freestream Turbulence on Boundary-Layer Development." AIAA Jour.. Vol. 18, No. 1 (Jan. 1980), pp. 11-15.

(64) Miller, D.G., and A.B. Bailey. "Sphere Drag at Mach Numbers from 0.3 to 2.0 at Reynolds Numbers Approaching 10^7." Jour. of Fluid Mech., Vol. 93 (1979), pp. 449-464.

(65) Moskovin, M.V. "On Transition Experiments at Moderate Supersonic Speeds." Jour. of Aero. Sci. (July 1957), pp. 480-486.

(66) Musker, A.J. "Explicit Expression for the Smooth Wall Velocity Distribution in a Turbulent Boundary Layer." AIAA Jour., Vol. 17, No. 6 (1979), pp. 655-657.

(67) NASA/Ames 11-Ft Transonic Wind Tunnel Preston-Tube Measurements. Ames Research Center, Moffet Field, California, March 1975.

(68) Narasimha, R. "On the Distribution of the Intermittency in the Transition Region of a Boundary Layer." Jour. of Aero. Sci., Vol. 24 (Sept. 1957), pp. 711-712.

(69) Owen, F.K., and C.C. Horstman. "Hypersonic Transitional Boundary Layers." AIAA Jour., Vol. 10, No. 6 (June 1972), pp. 769-775.

(70) Pate, S.R. "Measurements and Correlations of Transition Reynolds Numbers on Sharp Slender Cones at High Speeds." AIAA Jour., Vol. 9, No. 6 (June 1971), pp. 1082-1090.

(71) Pate, S.R. and M.D. Borwn. "Acoustic Measurements in Supersonic Transitional Boundary Layers." AEDC-TR-69-182, Oct. 1969.

(72) Pate, S.R. and C.J. Schueler. "Effects of Radiated Aerodynamic Noise on Model Boundary-Layer Transition in Supersonic and Hypersonic Wind Tunnels." AEDC TR-67-236, March 1968.

(73) Pate, V.C., "Calibration of the Preston-Tube and Limitations on Its Use in Pressure Gradients." Jour. Fluid Mechanics, Vol. 23 (1965), pp. 185-208.

(74) Penke, D.J., D.F. Fisher and D.S. McRae. "Flight Experiments With A Slender Cone at Angle of Attack." AIAA Paper No. 81-0337 (Jan. 1981).

(75) Pfeil, H. and W. Sticksel. "About the Influence of the Pressure Gradient on the Law of the Wall." AIAA Paper No. 81-0071 (Jan. 1981).

(76) Pope, A., and J.J. Harper. Low-Speed Wind Tunnel Testing. Wiley, 1966.

(77) Potter, J.L. "The Unit Reynolds Number Effect on Boundary Longer Transition." AIAA Jour., Vol. 13, No. 3 (March 1975).

(78) Preston, J.H. "The Determination of Turbulent Skin Friction by Means of Pitot Tubes." Jour. of Royal Aero. Soc., Vol. 58 (1954), pp. 109-121.

(79) Prozorov, A.G. "Determination of the Skin Friction in the Boundary Layer with a Small Pitot Probe." Fluid Mechanics - Soviet Research, Vol. 5, No. 6 (Dec. 1976).

(80) Quarmby, A., and H.K. Das. "Measurement of Skin Friction Using a Rectangular Mouthed Preston Tube." Jour. Royal Aero. Society, Vol. 73 (March 1969).

(81) Raghunathan, S., J.B. Coil and D. G. Mabey. "Flat Plate Turbulent Boundary Layers Subject to Large Pressure Fluctuations." AIAA Jour., Vol. 17, No. 1 (Jan. 1979).

(82) Reed, T.D., and A.S. Abu-Mostafa. Study of Boundary Layer Transition Using Transonic Cone Preston-Tube Data NASA CR-169130, Washington, D.C., July 1982.

(83) Reed, T.D., A.S. Abu-Mostafa and F.W. Steinle, Jr. "Correlation of Preston-Tube Data with Laminar Skin Friction." AIAA Jour., Vol. 21 (March 1983), pp. 379-380.

(84) Reed, T.D., P.M. Moretti and A.S. Abu-Mostafa. Study of Boundary-Layer Transition Using Transonic-Cone Preston-Tube Data: Semiannual Progress Report, NASA NSF-2396, June 1980.

(85) Reed, T.D., T.C. Pope and J.M. Cooksey. Calibration of Transonic and Supersonic Wind Tunnels. NASA CR-2920, Nov. 1977.

(86) Schlichting, H. Boundary Layer Theory. New York: McGraw-Hill Book Co., 1968.

(87) Schubauer, G.B., and P.S. Klebanoff. "Contributions on the Mechanics of Boundary-Layer Transition." NACA TN 3498, Sept. 1955.

(88) Somers, D.M., J.P. Stack and W.D. Harvey. Influence of Surface Static-Pressure Orifices on Boundary-Layer Transition. NASA-TM-84492, July 1982.

(89) Sommer, S.C., and B.J. Short. Free-Flight Measurements of Turbulent-Boundary-Layer Skin Friction in the Presence of Severe Aerodynamic Heating at Mach Numbers from 2.8 to 7.0. NACA TN3391 (1955).

(90) Spradley, L.W., and J.F. Stalnaker. "A Quasi-Parabolic Technique for Computation of Three-Dimensional Viscous Flows." AIAA Paper No. 81-0113 (Jan. 1981).

(91) Steinle, F.W., Jr. Personal Communication. NASA Ames Reserach Center, Moffet Field, California.

(92) Stephens, A.V. and J.A.G. Haslam. "Flight Experiments on boundary Layer Transition in Relation to Profile Drag." R & M Jour., 1800 (Aug. 1938).

(93) Tetervin, N. "A Transformation Between Axisymmetric and Two-Dimensional Turbulent Boundary Layers." AIAA Jour., Vol. 8, No. 5 (May 1970), pp. 985-987.

(94) Treon, S.L. et al. "Further Correlation of Data from Investigations of a High-Subsonic-Speed Transport Aircraft Model in Three Major Transonic Tunnels." AIAA Paper No. 74-627 (July 1974).

(95) Van Driest, E.R. "On Turbulent Flow Near A Wall." Jour. of Aero. Sco., Vol. 23 (1956), p. 1007.

(96) Vancheret, X. "Acoustic Fluctuations Generated by the Ventilated Walls of A Transonic Wind Tunnel." AGARD-CP-174, March 1976.

(97) Wazzan, A.R., C. Gazley and A.M.O. Smith. "The H-R_x Method for Predicting Transition." Rand Tech. Paper P-6581 (Jan 1981), The Rand Corp., Santa Monica.

(98) Weeks, D.J. and J. Hodges. "An Experimental Investigation Into the Influence of Acoustic Disturbances on the Development of a Turbulent Boundary Layer." R & M Jour., No. 3825, London (1978).

(99) White, F.M. Viscous Fluid Flow. New York: McGraw-Hill Book Co., 1974.

(100) Whitfield, J.D. and N.S. Dougherty, Jr. "A Survey of Transition Research at AEDC." AGARD-CP-224, No. 25 (Oct. 1977).

(101) Whitfield, J.D. and J.L. Potter. "The Unit Reynolds Number as a Parameter in Boundary Layer Stability." AEDC TN-58-77, 1958.

(102) Wilcox, D.C. "Turbulence-Model transition Predictions." AIAA Jour., Vol. 13, No. 2 (Feb. 1975).

(103) Wilcox, D.C. and R. M. Traci. "A Complete Model of Turbulence." AIAA Paper No. 76-351 (July 1976).

(104) Wu, J-M. and R.C. Lock. A Theory for Subsonic and Transonic Flow Over a Cone - With and Without Small Yaw Angle. U.S. Army Missile Command, Redstone Arsenal, Alabama, Tech. Report RD-74-2 (Dec. 1973).

(105) Young, A.D. and J.N. Maas. "The Behavior of a Pitot-Tube in a Transverse Total-Pressure Gradient." R & M Jour., No. 1770 (1937).

VITA 2

Ayman Said Abu-Mostafa

Candidate for the Degree of

Doctor of Philosophy

Thesis: CALIBRATION OF WIND TUNNEL FLOW QUALITY

Major Field: Mechanical and Aerospace Engineering

Biographical:

Personal Data: Born in Giza, Egypt, June 1, 1953, the son of Mr. and Mrs. Said S. Abu-Mostafa.

Education: Graduated from Ibrahimia High School, Cairo, Egypt, in July, 1971; received Bachelor of Science degree in Mechanical Engineering from Cairo University in 1976; received Master of Science degree in Mechanical and Aerospace Engineering from Oklahoma State University in 1980; completed requirements for the Doctor of Philosophy degree at Oklahoma State University in May, 1984.

Professional Experience: Assistant instructor, Department of Mechanical Power Engineering, Cairo University, 1978; graduate teaching assistant and research associate, School of Mechanical and Aerospace Engineering, Oklahoma State University, 1978-1983.